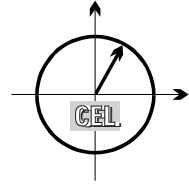*Forschungsberichte aus dem
Institut für Nachrichtentechnik des
Karlsruher Instituts für Technologie*

Ralph Tanbourgi

Diversity Combining under Interference Correlation in Wireless Networks

Band 34

Forschungsberichte aus dem Institut für Nachrichtentechnik des Karlsruher Instituts für Technologie

Herausgeber: Prof. Dr. rer. nat. Friedrich Jondral

**Forschungsberichte aus dem Institut für Nachrichtentechnik
des Karlsruher Instituts für Technologie**

Herausgeber: Prof. Dr. rer. nat. Friedrich Jondral

Forschungsberichte aus dem Institut für Nachrichtentechnik des Karlsruher Instituts für Technologie

Herausgeber: Prof. Dr. rer. nat. Friedrich Jondral

**Forschungsberichte aus dem Institut für Nachrichtentechnik
des Karlsruher Instituts für Technologie**

Herausgeber: Prof. Dr. rer. nat. Friedrich Jondral

Vorwort des Herausgebers

Der Mobilfunk spielt im täglichen Leben eine immer größere Rolle und wird in den kommenden Jahren, unter anderem getrieben durch Maschine-zu-Maschine (M2M) Kommunikation, weiter stark an Bedeutung gewinnen. Dabei ist das zur Verfügung stehende elektromagnetische Spektrum begrenzt, weshalb Mittel und Wege gefunden werden müssen, mit deren Hilfe deutlich höhere Übertragungskapazitäten als die derzeit vorhandenen nutzbar gemacht werden können. In der Forschung haben sich drei Technologien herauskristallisiert, deren Anwendungen besonders erfolgversprechend erscheinen:

- **Höhere Übertragungsbandbreiten:** Der einfachste Weg, zu höheren Funkkapazitäten zu kommen, besteht natürlich in der Zuteilung weiterer Frequenzbereiche. Solche sind aber unterhalb von 6 GHz kaum noch zu identifizieren, so dass inzwischen unter anderem untersucht wird, mit welchen Mitteln höhere Frequenzbereiche (28 GHz, 38 GHz, 90 GHz) für die Mobilkommunikation nutzbar gemacht werden können.

- **Heterogene Netze:** Ein derzeit bereits genutzter Ansatz zur Kapazitätserweiterung besteht darin, Basisstationen mit niedriger Leistung und damit Pico- bzw. Femtozellen in bestehende Netze einzufügen. Andere Untersuchungen zielen auf den Einsatz der Device-to-Device (D2D) Technologie oder von Ad-hoc Netzen ab.

- **Mehrantennentechnologien:** Die Nutzung der räumlichen Dimension durch *Multiple Input Multiple Output* (MIMO) Systeme zur Verbesserung der Verbindungsqualität oder zur Erhöhung der Datenrate wird in zukünftigen Netzen eine wichtige Rolle spielen. Je nachdem, welche Kanalzustandsinformation sende- und empfangsseitig verfügbar ist, kann hier an räumliches Multiplexing, räumliche Interferenzverringerung, Raumdiversity oder Kombinationen dieser Technologien gedacht werden.

Die vorliegende Dissertation beschäftigt sich mit Interferenzminderung durch den Einsatz von Mehrantennensystemen mit *Diversity Combining* in Ad-hoc und heterogenen zellularen Netzen. Der Schwerpunkt liegt dabei auf der Untersuchung des *Maximum Ratio Combinings* (MRC), einer Technologie bei der die von den beteiligten Empfangsantennen aufgenommenen Signale proportional zum dort vorliegenden Signal-zu-Stör- und Rauschverhältnis (*Signal-to-Interference and Noise Ratio*, SINR) gewichtet und dann addiert werden. Die zentrale Frage, die es zu beantworten gilt, ist die nach der an einem ("typischen") Empfänger innerhalb eines Netzes auftretenden Interferenz unter der Annahme, dass die von den Antennen des MRC Systems gelieferten Störsignale korreliert und somit bei der Berechnung des zugehörigen SINR diese Korrelationen zu berücksichtigen sind.

Die damit umrissene Aufgabenstellung ist offenbar komplex und die Lösung könnte beispielsweise mit Hilfe von Monte Carlo Simulationen angegangen werden. Ralph Tanbourgi hat sich aus guten Gründen dafür entschieden, dass nicht zu tun. Simulationen wären, da sie, um statistisch relevante Ergebnisse generieren zu können, über viele Netzkonstellationen mitteln müssten, extrem aufwändig. Darüber hinaus stellen solche Simulationen oft die funktionalen Zusammenhänge unvollständig oder nicht richtig dar und liefern deshalb schwer interpretierbare oder sogar fehlerhafte Ergebnisse. Hier wird bewusst der Weg über analytische Modelle auf Basis der stochastischen Geometrie (insbesondere der stationären Poisson'schen Punktprozesse mit konstanter Dichte) eingeschlagen. Aufwändige Simulationen werden dennoch zur Evaluierung der analytischen Ergebnisse herangezogen.

Karlsruhe, im Juni 2015
Friedrich Jondral

Diversity Combining under Interference Correlation in Wireless Networks

Zur Erlangung des akademischen Grades eines

DOKTOR-INGENIEURS

von der Fakultät für

Elektrotechnik und Informationstechnik

des Karlsruher Instituts für Technologie

genehmigte

DISSERTATION

von

Dipl.-Ing. Ralph Tanbourgi

geb. in

Beirut, Libanon

Acknowledgments

This thesis summarizes part of my work that I have conducted as a research associate at the Communications Engineering Lab (CEL), Karlsruhe Institute of Technology (KIT), Germany. Its present form could not have been made possible without the support from several persons, to whom I would like to express my sincere gratitude.

My utmost thanks go to my advisor Prof. Friedrich K. Jondral for all the mentoring, guidance, and confidence he put in me. The joy I feel today about doing research is mainly due to his unique leadership style, which puts a strong accent on freedom of research and autonomous working. Our interactions and discussions have profoundly contributed to my personal development and have substantially shaped my view on many things related to both academic work and personal life.

I would also like to thank my colleagues—the current ones as well as the former ones—for all the fruitful discussions we had with each other. I will certainly miss the great time we spent together, not only at work but certainly also after. Special thanks go to Dr.-Ing. Holger Jäkel for always lending me a sympathetic ear, for helping me in polishing my mathematics at times, and for proof-reading my thesis. Besides, I would also like to thank Dr.-Ing. Jens Elsner for introducing me to the interesting field of stochastic geometry and for our early collaborations. Working at CEL has always been convenient and productive for me, which is also due to the commitment of a number of people taking care of many processes in the back. In this regard, I would like to thank Brigitte Single, Beate

Dedicated to
Hannah

Abstract

Interference due to concurrent transmissions has become evermore an important issue in wireless communications systems as wireless networks continue to become increasingly dense. Moreover, trends such as limited site-planning, heterogeneous deployments, and increased user mobility, has rendered interference strongly varying and hard to predict, and it is thus appropriate to treat interference as a random variable in network analysis. A fundamental statistical property of interference is that it is correlated in space; two close-by receivers will likely experience a similar level of interference. This type of correlation, in turn, affects the performance of diversity combining, which is a well-known method to increase link reliability in communication systems. Today, many practical and mass-market receivers employ simple linear diversity-combining schemes such as maximal-ratio combining, which were primarily designed to combat channel fading. However, their vulnerability to interference correlation is not well understood, which makes it difficult for a system designer to properly choose the right scheme offering the best performance-complexity trade-off for a given scenario.

In this thesis, a theoretical framework is developed that enables a performance analysis for diversity combining under interference correlation. To reflect the quasi-random nature of the interference, an approach based on stochastic geometry is chosen, which allows taking into account the irregularity of the spatial network geometry usually encountered in practice. Within this framework, tractable stochastic models for different types of diversity combining and network architectures are presented and

used for analysis. Besides capturing the irregularity in the node locations, these models also consider performance-relevant system aspects such as network density, distance-dependent path loss, channel fading, number of antennas, and transmitter/receiver processing. The general scenarios treated in this thesis can be grouped into the following four parts.

First, wireless *ad hoc* networks with multi-antenna receivers employing diversity combining are considered. In such networks, excessive interference due to lack of centralized medium access control may occur, leading to distinct properties of the interference correlation across receive antennas. The performance under this type of correlation is analyzed for a typical multi-antenna receiver as a function of the various system parameters.

Second, the effect of interference correlation on the performance in downlink heterogeneous cellular networks with multiple antennas at both the base stations and the mobile users is analyzed. In contrast to wireless *ad hoc* networks, cellular networks have a user association mechanism, which influences the interference correlation properties at the multi-antenna receiver. In addition, the number of antennas at the interfering base stations co-influence these properties as well.

Third, a cooperative scenario involving a single-antenna source, relay, and destination node under interference is considered. In such a scenario, interference is correlated across the relay and destination, thereby influencing the performance of the cooperative transmission after diversity combining at the destination. Assuming selection decode-and-forward as the relay protocol, this influence is studied with focus on the achievable diversity.

Last, frequency-diversity reception through non-contiguous or large spectrum allocation is studied in the context of downlink heterogeneous cellular systems with single-antenna base stations and mobile users. Here, interference is correlated across different parts of the allocated spectrum and the resulting effect on data rate and probability of coverage is analyzed.

In all cases, theoretical results are derived and validated by detailed simulations, performance comparisons are presented, and valuable design insights for use of diversity combining under interference correlation are obtained.

Zusammenfassung

Als Folge der fortwährenden Verdichtung drahtloser Netze ist Interferenz aufgrund gleichzeitiger Übertragungen zunehmend zu einem bedeutsamen Problem für drahtlose Nachrichtensysteme geworden. Darüber hinaus haben Trends wie beispielsweise beschränkte Netzplanung, heterogene Netzstationierung sowie höhere Nutzermobilität Interferenz zu einer stark variierenden und schwer vorhersagbaren Größe gemacht und es ist daher in der Netzanalyse zweckmäßig, Interferenz wie eine Zufallsvariable zu behandeln. Eine grundlegende statistische Eigenschaft der Interferenz ist, dass sie räumlich korreliert ist; es ist wahrscheinlich, dass zwei benachbarte Empfänger einen ähnlichen Interferenzpegel erfahren werden. Diese Art von Korrelation wiederum beeinträchtigt die Leistungsfähigkeit von Diversity-Combining-Verfahren, welche als Mittel zur Erhöhung der Übertragungszuverlässigkeit in Kommunikationssystemen bekannt sind. Heute finden sich in vielen einfachen und massenmarkttauglichen Empfängern simple lineare Diversity-Combining-Verfahren, wie beispielweise das Maximal-Ratio-Combining-Verfahren, die vorrangig zur Bekämpfung des Kanalschwunds entwickelt wurden. Ihre Empfindlichkeit gegenüber Interferenzkorrelation wurde bislang jedoch noch nicht ganz verstanden, was eine fachgerechte Auswahl des richtigen Verfahrens für ein gegebenes Szenario, nämlich das Verfahren mit dem besten Kompromiss zwischen Leistungsfähigkeit und Komplexität, seitens des Systementwicklers erschwert.

In dieser Arbeit wird ein theoretisches Rahmenwerk, das die Analyse der Leistungsfähigkeit von Diversity-Combining-Verfahren unter Interferenz-

korrelation ermöglicht, erarbeitet. Um die quasi-zufällige Natur der Interferenz widerzuspiegeln wird ein Ansatz basierend auf der Stochastischen Geometrie gewählt, was eine Berücksichtigung der in der Praxis üblicherweise vorherrschenden Unregelmäßigkeit in der räumlichen Netzgeometrie erlaubt. In diesem Rahmenwerk werden geeignete stochastische Modelle für verschiedene Arten von Diversity-Combining-Verfahren und Netzarchitekturen vorgestellt und zur Analyse eingesetzt. Neben der Erfassung der Unregelmäßigkeit in den Positionen der Netzknoten, berücksichtigen diese Modelle auch Performance-relevante Systemaspekte wie Netzdichte, distanzabhängiger Pfadverlust, Kanalschwund, Antennenanzahl sowie Signalverarbeitung am Sender/Empfänger. Die übergeordneten Szenarien, die im Zuge dieser Arbeit betrachtet werden, können inhaltlich in die folgenden vier Teile gegliedert werden.

Zunächst werden drahtlose *ad hoc* Netze mit Multiantennen-Empfänger nach dem Diversity-Combining-Konzept behandelt. In solchen Netzen kann es aufgrund des Nichtvorhandenseins einer zentralen Medienzugriffssteuerung zu sehr hoher Interferenz kommen, was mit speziellen Eigenschaften für die Interferenzkorrelation zwischen den Empfangsantennen einhergeht. Die Leistungsfähigkeit unter Einfluss dieser Art von Korrelation wird anhand eines typischen Multiantennen-Empfängers unter Berücksichtigung der verschiedenen Systemparameter untersucht.

Anschließend wird der Effekt der Interferenzkorrelation auf die Leistungsfähigkeit in heterogenen zellularen Netzen mit Multiantennen-bestückten Basisstationen und mobilen Nutzern im Downlink untersucht. Im Gegensatz zu drahtlosen *ad hoc* Netzen besitzen zellulare Netze einen Zellzuordnungsmechanismus, welcher die Eigenschaften der Interferenzkorrelation am Mehrantennen-Empfänger beeinflusst. Ferner hat die Anzahl an Antennen an den interferierenden Basisstationen ebenfalls einen Einfluss auf diese Eigenschaften.

Danach wird ein kooperatives Szenario bestehend aus einem Quell-, Relay- und Zielknoten mit jeweils einer Antenne unter dem Einfluss von Interferenz betrachtet. In einem solchen Szenario ist die Interferenz zwischen dem Relay- und Zielknoten korreliert, was sich auf die Leistungsfähigkeit der kooperativen Übertragung nach dem Diversity-Combining am Zielknoten auswirkt. Unter Annahme, dass Selection-Decode-and-Forward als Relay-Protokoll benutzt wird, werden diese Auswirkungen mit Fokus auf die erreichbare Diversität untersucht.

Zuletzt wird der Empfang unter Frequenzdiversität, realisiert durch eine nicht zusammenhängende oder große Allokation im Frequenzspektrum, im Kontext von heterogenen zellularen Netzen im Downlink mit Basisstationen und mobilen Nutzern mit jeweils einer Antenne untersucht. Hierbei ist die Interferenz in den verschiedenen Teilen des allokierten Spektrums korreliert. Die resultierenden Auswirkungen auf die Datenrate und die Abdeckungswahrscheinlichkeit werden hier analysiert.

Zu jedem der obengenannten Teile in dieser Arbeit werden theoretische Ergebnisse erarbeitet und diese mithilfe von detaillierten Simulationen validiert, Performance-Vergleiche präsentiert und wertwolle Erkenntnisse für den praktischen Einsatz von Diversity-Combining-Verfahren unter Einfluss von Interferenzkorrelation erworben.

Contents

1

Introduction

Mobile wireless networking has continued to cover more and more of our daily life and it is a common perception that this global trend is not to decelerate in the near future. This forecast is supported by recent market studies conducted by notable industry institutions, projecting an 11-fold growth in global mobile data traffic and over 10 billion mobile-connected devices by 2018 [1]. But besides gearing up to meet these dramatically increasing capacity demands, sometimes termed as the "1000x capacity challenge" [2], future network architectures must also cope with newly emerging types of services. For instance, Machine-Type Communications (MTC), which is typically characterized by inexpensive hardware, low data-rate, and high link reliability depending on the underlying use case [3], is expected to increase at a compound annual growth rate of roughly 25%-35% between 2014 and 2018 [1, 4].

The wireless community has largely agreed on the following key technologies that hold the promise of providing the required innovation in the specific optimization direction, see [5] for an overview.

(i) **Multi-antenna techniques:** Leveraging the spatial dimension through use of Multiple-Input Multiple-Output (MIMO) to increase link reliability and/or data rate will play a key role in future networks. Depending on the number of antennas and the amount of Channel State Information (CSI) at the transmitter and receiver, spatial multiplexing, spatial interference-mitigation, spatial diversity, or combinations thereof are possible.

(ii) **Heterogeneous networks:** Deploying low-power Base Stations (BSs), i.e., pico and femto BSs, within macro coverage areas is a promising way to boost capacity in dense cellular systems [6]. Device-to-Device (D2D) communications allows mobile users to connect directly using operator-owned spectrum, which introduces an *ad hoc* component to cellular networks [7, 8]. Besides, the trend towards ubiquitous connectivity and spontaneous network formation has not lessened the importance of mobile *ad hoc* and sensor networks [9].

(iii) **Larger transmission bandwidths:** Allocating more spectrum to users allows communication at higher data rates. Carrier aggregation, where multiple frequency bands are allocated to a single user in cellular networks, is now being increasingly adopted by 3rd Generation Partnership Project (3GPP) Long Term Evolution (LTE) systems [10]. Due to spectrum scarcity in the microwave band, researchers are currently considering to move to even higher frequencies lying in the mmWave band above 6 GHz, where huge amounts of spectrum are available [11].

This thesis capitalizes on (i) and (ii) in the above list, more specifically, on multi-antenna techniques with diversity combining in *ad hoc* networks and Heterogeneous Cellular Networks (HCNs). Thereby, the main focus will be on the effect of interference created by concurrently transmitting devices on the performance of diversity combining in both types of networks. In the following, the general scenario considered in this thesis is introduced and motivated, and the main leading questions are crystallized.

1.1 Background and Motivation

The interest in using multiple antennas for communication was initiated by the early works [12–14], and was further fueled by [15–18] in the mid 90s. To date, multi-antenna communications has advanced to a well-researched technology and is covered in most common communication theory textbooks, see for instance [19, 20]. The use of multiple antennas opens up a new signaling dimension, namely *space*, in which information can be intelligently allocated and/or recovered. In (rich-scattering) fading channels, signals transmitted from or received by different antennas are subject to different channel conditions as a result of physical propagation

phenomena affecting the communication channel between each Tx-Rx antenna pair differently [20]. This introduces a certain number of so-called spatial signatures, which, if distinguishable, let the communication channel appear as having independent paths over which information can be conveyed from the transmitter to the receiver.

Multi-antenna techniques can be used for mainly three purposes: spatial diversity, spatial multiplexing, and spatial interference-mitigation. Spatial diversity uses multiple antennas at the transmitter and/or the receiver to convey the same information over the different independent paths to increase link reliability: if one path experiences a deep fade, the information may still be received successfully on another path. Spatial multiplexing, in contrast, encodes multiple information streams across antennas to increase capacity. This concept is more demanding than spatial diversity since cross-antenna interference must be resolved at the receiver [15]. If knowledge about the interfering channels is available in a multi-antenna system, spatial interference-mitigation can remove undesirable interference created by other transmissions in the same band to improve link performance. There exists a multitude of techniques that realize one or a combination of the above three multi-antenna concepts, see for instance [21]. These techniques can be roughly divided into closed-loop and open-loop based. Closed-loop techniques exploit CSI, i.e., (some) knowledge of the spatial signatures, at both the transmitter and receiver to optimize antenna parameters in some specific way. For instance, maximal-ratio transmission uses a channel-matched pre-coding at the transmitter to maximize the received useful signal power.

Among the different possibilities outlined above, *diversity combining* at the receiver is a popular multi-antenna approach [22, Sec. 9]. By linearly combining the desired signal received at the different Rx antennas under CSI-Rx, diversity combining offers Rx diversity independent of the particular signaling scheme employed by the transmitter. Its popularity is mainly due to its relatively good trade-off between performance and complexity. For instance, while comparable open-loop based Tx-diversity schemes suffer a power penalty [22, Sec. 14.3], this is not the case for diversity combining. Moreover, availability of reliable CSI-Tx may sometimes not be possible [23, Sec. 11.2.1] due to, e.g., a noisy CSI feedback link to the transmitter in Frequency Division Duplexing (FDD) systems or high user mobility, in which case diversity combining becomes a viable fallback option. It is known that, under ideal conditions, interference-mitigating

multi-antenna receivers are more powerful than simple diversity combining in the presence of interference. However, the picture changes when accounting for real-life impairments such as imperfect interference-channel estimation, finite dynamic range of analog-to-digital converters in receiver front-ends, and residual (non-canceled) interference [24, 25].

Besides, the emergence of *heterogeneous networks* has assigned evermore importance to the problem of interference, which affects also the performance of diversity-combining receivers. Depending on the particular scenario, characteristics of heterogeneous networks include multi-tier deployment, high transceiver density, limited site-planning, opportunistic roll-out, and dynamic network topology. In HCNs, for instance, small-cell BSs are deployed within macro-cell coverage areas to serve wireless-traffic hotspots in the same band, which introduces inter-tier interference in addition to intra-tier interference [6]. Mobile or vehicular *ad hoc* networks, in contrast, are infrastructure-less and highly dynamic, which renders tight interference and power control difficult [19, Sec. 16]. In such networks, harmful interference situations may thus occur sometimes unpredictably fast.

Interference is the inevitable result of the *spatial reuse* concept, which originally laid the foundation for cellular network design in the late 70s [26] and is now imperatively followed due to today's spectrum scarcity. By reusing radio resources in the same geographical area and noting that signal power decays with distance according to some path loss law [19, 27], it follows that the interference experienced at a certain location depends upon the *spatial network geometry*. Now, taking into account the nature of heterogeneous networks and that, in addition, the fading on the interfering channels co-influences the interference shape, it becomes evident that interference itself is essentially a hard-to-predict quantity in practice. As the reader may already imagine, this certainly has an impact on the performance of diversity-combining receivers. In order to approach this key point from a more concrete perspective, the discussion will be continued by specializing on a particular diversity-combining scheme.

1.1.1 A Prominent Example: Maximal-Ratio Combining

Maximal-Ratio Combining (MRC) is a popular diversity scheme found in a variety of multi-antenna receivers. In a nutshell, MRC assigns more

weight to branches with good reception quality and less weight to those with poor reception quality [12]. In the absence or without knowledge of interference, MRC is known to maximize the post-combiner Signal-to-Interference-plus-Noise Ratio (SINR). MRC is the top choice for many WiFi access points with IEEE 802.11.n multi-antenna support, typically in combination with 2–3 antennas, and the same holds for the receiver front-end of mobile devices, see for instance [28, 29]. In 3GPP LTE systems, MRC can be used in mobile multi-antenna receivers to improve downlink performance [23, Sec. 11.1.4], e.g., as a backup solution in situations where the use of more sophisticated schemes is not practical.

Like for other diversity-combining schemes, the performance of MRC is affected by interference. More specifically, its performance depends on the spatial configuration of interfering transmitters on the one hand, and on the fading on the interfering channels on the other hand. To understand this, consider for instance the post-combiner SINR for Interference-Aware (IA) MRC, i.e., when the receiver knows the current interference-plus-noise power, with N Rx antennas, which can be expressed as

$$\mathtt{SINR}_\Sigma = \sum_{n=1}^{N} \frac{\mathsf{g}_{o,n} y^{-\alpha}}{\mathsf{I}_n + \sigma^2}, \tag{1.1}$$

where $\mathsf{g}_{o,n} y^{-\alpha}$ describes the useful power from the desired transmitter at distance y received at Rx antenna n under random fading gain $\mathsf{g}_{o,n}$ and average path loss y^α, I_n is the interference power (*hereafter and throughout this thesis, simply* interference) at Rx antenna n, and σ^2 is the power of the Rx noise, typically assumed Additive White Gaussian Noise (AWGN). The reader is referred to Appendix B for details. Due to spatial reuse, the interference I_n is created by multiple interfering transmitters at locations $\{x_i\}$ with random fading gains $\{\mathsf{g}_{i,n}\}$ to antenna n of the considered receiver, hence $\mathsf{I}_n = \sum_{x_i \in \varphi} \mathsf{g}_{i,n} \|x_i\|^{-\alpha} \Rightarrow \mathsf{I}_n(\varphi)$, where $\varphi = \{x_i\}$ is the spatial configuration of interfering transmitters or simply, the *spatial network geometry*. As a result, $\mathtt{SINR}_\Sigma$ is essentially a function of φ, i.e.,

$$\mathtt{SINR}_\Sigma \Rightarrow \mathtt{SINR}_\Sigma(\varphi) = \sum_{n=1}^{N} \frac{\mathsf{g}_{o,n} y^{-\alpha}}{\mathsf{I}_n(\varphi) + \sigma^2}. \tag{1.2}$$

Obviously, the interference-plus-noise power $\mathsf{I}_n(\varphi) + \sigma^2$ inside the addends in (1.2), i.e., in the per-antenna SINRs, may have different levels across the N Rx antennas, *depending on the spatial network geometry φ and*

the fading gains $\{\mathbf{g}_{i,n}\}$. This kind of branch imbalance may significantly affect the performance of MRC as reported in [30–32] for a fixed number of interferers, a specific spatial network geometry φ, and exponentially distributed fading gains $\{\mathbf{g}_{i,n}\}$ (Rayleigh fading). Although this is a material finding, it does not help answering a system designer's question whether or not to bank on MRC in a dynamic interference environment. More specifically, while the implementation aspects of MRC do not change with the considered scenario, its performance will certainly do and thus, finding a general performance-complexity trade-off remains impossible as the performance will depend on the particular spatial network geometry. For instance in the context of 3GPP LTE, the gain of Interference Rejection Combining (IRC) over MRC varies significantly with the spatial configuration of interfering BSs [33] and for some configurations the higher complexity of IRC may not be justified. It thus becomes evident that many spatial network geometries need to be considered in order to obtain a clearer picture. In other words, one needs to *average the performance over many spatial network geometries.* Thereby, the number of network geometries that need to be considered largely depends upon the degree of spatial randomness inside the network; and this degree can be considerably high in heterogeneous networks.

1.1.2 Spatial Averaging in Wireless Networks

Spatial averaging, i.e., averaging over many spatial network geometries, is necessary to *decouple* the outcome of a performance evaluation from the actual spatial network geometry φ. This is typically realized by means of Monte-Carlo simulations, where in each iteration a particular network geometry is generated according to some law, and the results obtained are finally averaged over all simulated geometries. Although popular, simulations have several shortcomings. First, despite the high processor power of today's computers, detailed simulations are often time consuming, thereby quickly wearing out a researcher's daily routine. Second, simulations fail to reveal the functional relationship and dependence of the relevant system parameters since all effects are lumped into a single number. In this sense, simulations can often provide only marginal insights and limited intuition, if any. Third, simulations may be prone to dubious or even erroneous results if no possibility for cross-validation exists.

As a viable approach to complement simulation-based methods and to overcome their shortcomings listed above, spatial averaging using analytical tools has attracted much interest recently. The basic idea behind this approach picks up on the fact that the spatial network geometry φ in heterogeneous networks typically appears random to a mobile receiver due to the characteristics of heterogeneous networks explained before. It is thus reasonable to treat φ as a particular realization of a random variable Φ, which represents all possible spatial network geometries that may occur with some probability. Following this key idea leads to the *stochastic geometry* framework [34], which formalizes the concept of assigning a certain probability law to Φ. More specifically, the locations $\{x_i\}$ of interfering transmitters are now assumed to follow a spatial point process denoted by $\Phi \triangleq \{x_i\}$. In essence, this *randomization* of locations yields a stochastic description of the spatial network geometry, which can be viewed as the equivalent to what is commonly done to model fading channels, i.e., assuming a certain stochastic model to decouple the analysis from a particular fading realization. The application of stochastic geometry to problems in wireless networks has become a notable research branch, see for instance [35–39] and the references therein.

Revisiting (1.2), the post-combiner SINR for IA-MRC can then be expressed as a function of the point process Φ, i.e.,

$$\mathtt{SINR}_\Sigma(\varphi) \stackrel{\substack{\text{spatial} \\ \text{randomization}}}{\Rightarrow} \mathtt{SINR}_\Sigma(\Phi) = \sum_{n=1}^{N} \frac{\mathsf{g}_{o,n} y^{-\alpha}}{\mathsf{I}_n(\Phi) + \sigma^2}. \tag{1.3}$$

Comparing (1.2) and (1.3), the post-combiner SINR is no longer a random variable of only the fading gains but also of the spatial network geometry Φ of interfering transmitters. Now, from a system designer's perspective, the probability distribution of $\mathtt{SINR}_\Sigma(\Phi)$ represents an informative quantity: it offers a basis for comparisons with other schemes, reveals the effect of the different system parameters, and allows deducing related key performance indicators such as the average post-combiner SINR $\mathbb{E}[\mathtt{SINR}_\Sigma(\Phi)]$. Glancing at the mathematical structure of the right-hand side of (1.3), it becomes apparent that obtaining the distribution of $\mathtt{SINR}_\Sigma(\Phi)$ is not straightforward as $\mathtt{SINR}_\Sigma(\Phi)$ is now a sum of *correlated* random variables. The correlation is induced by the interference terms $\{\mathsf{I}_n(\Phi)\}$, which themselves are correlated across the N Rx antennas due to the common locations of interferers Φ. Knowing that (fading) correlation across branches reduces diversity and hence, degrades the performance of

MRC [40], it is evident that interference correlation will do so as well; to which degree, however, is not quite clear. Unfortunately, characterizing the underlying correlation structure is difficult since, in addition, the fading gains $\{\mathbf{g}_{i,n}\}$ usually have a de-correlation effect. As a result, the interference terms $\{\mathsf{I}_n(\Phi)\}$ are neither uncorrelated nor identical across branches, which renders a mathematical analysis of $\mathtt{SINR}_\Sigma(\Phi)$ challenging. In order to obtain a better understanding on how interference correlation impacts or limits performance, it is however mandatory to approach this problem from an analytical perspective.

1.2 Main Contributions

This thesis leverages stochastic geometry tools to model and analyze the effect of interference correlation on diversity combining. Thereby, emphasis is put on multi-antenna systems with IA-MRC at the receiver, since analyzing this form of diversity combining under correlated interference has been an open problem in the research community. Using the theory of point processes, a stochastic model for two types of networks is derived, namely for wireless *ad hoc* networks and HCNs. In the former, interfering transmitters may be located close to a receiver, thereby creating excessive interference while in the latter, the strongest BS is typically the serving one. Each of the two models captures the main characteristics of the underlying network, such as transmitter/BS density, Tx power, number of antennas, fading statistics, and path loss law. Thereby, considerable effort is put in finding the optimal balance between generality and realism on the one side and analytical tractability on the other side. The models are then modified to analyze also other forms of diversity under interference correlation such as cooperative relaying and frequency-diversity based resource allocation. Numerous theoretical expressions characterizing the performance under interference correlation are obtained and turned into practical guidelines for system design. For reference, the main take-away messages are summarized below.

- Ignoring interference correlation across Rx antennas significantly overestimates the true performance of IA-MRC. In contrast, assuming the same interference level at all Rx antennas only slightly underestimates the performance. The degree of over-/underestimation thereby depends mainly on the channel characteristics.

- Interference-Blind (IB) MRC, which does not have information about the current interference-plus-noise power at the Rx antennas, performs only slightly worse than its IA counterpart. Although estimating the interference-plus-noise power is relatively simple, IB-MRC may in certain cases offer a better performance-complexity trade-off than IA-MRC. In particular, when the fluctuations on the interfering channels become weak, e.g., in Nakagami-m fading channels with large m or in Tx diversity systems, the gain of IA-MRC over IB-MRC becomes negligibly small due to the increased interference correlation across Rx antennas.

- A comparison of MRC with other schemes indicates that IA-Selection Combining (SC) may offer a better performance-complexity trade-off at certain operating points. The gain of MRC over IA-SC in terms of average post-combiner SINR is strictly lower in the presence of interference compared to without. Minimum Mean Square Error (MMSE) combining has better performance than MRC only at small SINRs and/or large path loss exponents. In the opposite regime, MRC may be more favorable than MMSE combining due to its lower complexity and almost same performance.

- Cooperative relaying using Selection Decode-and-Forward (SDF) with MRC cannot increase the spatial diversity order, i.e., the outage probability slope as the interferer density becomes asymptotically small, under Rayleigh fading. This is due to the inability of the relay to reduce the interference at the destination on the one hand, and to the interference correlation across the relay and destination on the other hand. However, without fading and assuming a perfect relay-destination link, e.g., as in distributed Single-Input Multiple-Output (SIMO) systems, the spatial diversity order increases if the relay-destination separation is large enough to let the interference appear independent across the relay and destination.

- Exploiting frequency diversity under interference correlation in systems with large and/or flexible transmission bandwidths improves performance at small target data rates. Besides, ignoring interference correlation may overestimate the true offered data rate considerably. Thereby, the degree of overestimation also depends on how much frequency diversification is realized.

1.3 Organization

Chapter 2 develops a stochastic model for slotted-Aloha based wireless *ad hoc* networks to analyze the effect of interference correlation on IA-MRC, while related results on IB-MRC are borrowed from the literature for comparison reasons. As the main result, a theoretical expression for the success probability for dual-antenna IA-MRC is derived for the general case with Rx noise and Nakagami-m fading. A more tractable and asymptotically tight expression for the general N Rx-antenna case is presented as well. The main result can be efficiently computed using a semi-numerical method proposed and discussed in the same chapter. Using the theoretical results, the gain of MRC over Single-Input Single-Output (SISO), the accuracy loss due to oversimplified correlation models for IA-MRC, the spatial throughput of MRC, and the relative performance between MRC and other linear combining schemes are studied.

Chapter 3 develops a stochastic model for analyzing the performance of MRC under interference correlation in multi-tier HCNs in the downlink. While Chapter 2 focuses on the SIMO case, the model in Chapter 3 takes into account that BSs are typically equipped with multiple antennas as well. Theoretical expressions for the coverage probability when BSs employ Orthogonal Space-Time Blockcodes (OSTBCs) using multiple Tx antennas are derived for both IB-MRC and IA-MRC at the mobile multi-antenna receivers (MIMO diversity). Using the developed model, the second-order statistics of the interference, i.e., the variance and correlation of the interference across Rx antennas, are derived in order to gain insights into how the interference properties in HCNs fundamentally limit the gains of IA-based diversity-combining schemes. The theoretical framework is then used to discuss the separate effects of Multiple-Input Single-Output (MISO) and SIMO in HCNs, the gain over SISO transmission, as well as the effect of interference correlation through comparisons with oversimplified correlation models. The chapter concludes with an exemplary performance comparison between IB/IA-MRC and IA-SC.

Chapter 4 extends the considerations made in Chapter 2 and Chapter 3, which focused on diversity combining in multi-antenna receivers, by looking at other forms of diversity reception under interference correlation. In Section 4.1, this is done for cooperative relaying, where a source and destination node communicate with the help of a relay node. Although

spatially separated, the relay and destination experience correlated interference, since interference originates from the same set of interfering transmitters. The impact of this form of spatial interference correlation is studied for the case of SDF with MRC at the destination node. In particular, the diversity order is analyzed for different assumptions about the fading statistics and the relay-destination placements. In Section 4.2, the effect of interference correlation on frequency-diversity reception in HCNs is studied. Here, information is received by a receiver in different parts of the spectrum under correlated interference, which yields a mathematical structure similar to (1.3). Theoretical expressions for the rate coverage probability are derived and used to study the gains of frequency-diversity reception in HCNs under correlated interference. Furthermore, the rate overestimation when ignoring this type of interference correlation is analyzed as well.

Chapter 5 concludes this thesis by summarizing the main findings and discussing possible future extensions.

2

Diversity Combining in Multi-Antenna Ad-Hoc Networks

Wireless *ad hoc* networks consist of wireless devices spontaneously forming a network and communicating directly with each other without the need for pre-existing infrastructure such as access points, see for instance [9,41]. Due to lack of centralized medium access coordination between the devices, strong interference may occur in such networks thereby limiting transmission reliability and throughput [42]. Another fundamental property of wireless *ad hoc* networks is the highly dynamic network geometry as a result of opportunistic deployments and node mobility, which causes the interference scenario to vary frequently and sometimes unpredictably fast [37].

Multi-antenna receivers employing diversity combining are a promising technique to increase the performance in wireless *ad hoc* networks with interference [43, 44]. Among different schemes, MRC [12, 19, 22] is a popular choice and therefore ubiquitously found in practice. While the well-known conventional MRC approach for single-user networks, i.e., channel-matched MRC or IB-MRC, is relatively well-understood for wireless *ad hoc* networks with interference, this is not the case for IA-MRC. In IA-MRC, the current interference power (*hereafter, simply* interference) is taken into account in the computation of the MRC weights and hence, the interference properties may greatly influence the resulting

performance of IA-MRC. More specifically, interference may increase (i) reception-quality imbalance as well as (ii) correlation across Rx antennas; two effects already known to decrease the performance of MRC in the interference-free case [40,45]. The objective of this chapter, which is based on [T1,T2], is thus to analyze the performance of IA-MRC in wireless *ad hoc* networks under the effect of interference using a realistic model.

2.1 Related Work

The effect of interference on the performance of MRC was first studied assuming fixed interference levels at all Rx antennas, which corresponds to assuming a fixed spatial network geometry [30, 31]. Using the notion of outage probability, these works demonstrated that interference may indeed severely degrade the expected performance of MRC, depending on the number of interferers and their signal strengths. This degradation is further amplified when interference is received with different levels across Rx antennas [32], e.g., due to different realizations of the fading gains to each Rx antenna, as a result of the increased reception-quality imbalance across Rx antennas. In a broader sense, the outage probability expressions derived in these prior works may be seen as *conditional*, i.e., being conditioned on a certain spatial network geometry creating a specific interference scenario. This narrows down the range of obtainable insights and does not offer general guidelines for system design. Clearly, to evaluate the overall performance of MRC under interference, one thus needs to average over many realizations of the interference scenario and hence, over many spatial network geometries. Due to the dynamic nature of wireless *ad hoc* networks, this task is however challenging as the spatial network geometry, and hence the interference often appears *random* to a receiver.

A promising and fairly recent approach to address the above challenge is to use stochastic geometry tools [34]. The reader is referred to [35–38,46] and the references therein for an overview on this research direction. Using such tools, the performance of IA-MRC in the presence of interference, modeled as a Poisson shot noise field, was studied in several works; mainly under two simplified interference correlation models: for instance, in [47, 48] the interference was assumed statistically indepen-

dent across Rx antennas.[1] However, interference is correlated across Rx antennas since the interference at the different Rx antennas originates from the same source of randomness, i.e., from the same set of interfering transmitters. This type of correlation is often neglected in the literature [49], which results in significantly overestimating the true diversity that IA-MRC can offer. In contrast, treating the interference as being equally strong at all Rx antennas, as done for instance in [50], can be seen as assuming full correlation of the interference across Rx antennas. This, in turn, underestimates the true diversity IA-MRC can provide as the de-correlation effect of the channel fading is not taken into account. Clearly, the true correlation structure is in between these two extremes and capturing it is important for better understanding the performance of IA-based diversity-combining receivers [51–53]. In [51,52], the interference properties measured at a multi-antenna receiver were analyzed within the continuum between complete independence and full correlation of the interference. In [53], the second-order statistics of the interference and of outage events were characterized. These works led for instance to a more realistic performance characterization of the simple retransmission scheme [54], IA-SC [55], as well as cooperative relaying [56] in wireless *ad hoc* networks.

In line with the model treated in [50], another frequent assumption in the literature is that the MRC weights do not depend on the per-antenna interference, i.e., they are proportional to only the fading gains of the desired link, see for instance [32,57–59]. This type of MRC is referred to as IB-MRC, in which the receiver is blind to the current per-antenna interference, and is suboptimal when interference varies across Rx antennas. In slight contrast, the MRC weights in [51,60] were assumed to be inversely proportional to the spatial density of interferers corresponding to the interference seen by each Rx antenna. Since the interferer density is proportional to the mean interference [38], this type of MRC essentially adapts to the long-term effects of the interference. The authors showed that such a long-term adaptation yields some improvements when interference is correlated across Rx antennas.

In summary, while IB-MRC is well researched in the context of wireless *ad hoc* networks with random interference, this is not the case for IA-MRC,

---

[1]In [47], the different Rx antennas correspond to spatially separated single-antenna receivers in a cooperative relaying scenario.

which has yet been analyzed only using simpler correlation models for tractability reasons. This may lead to a distorted performance characterization and a wrong performance-complexity trade-off of IA-MRC. For fair comparison with other linear combining schemes and to allow for proper system design, a realistic modeling and analysis of IA-MRC is hence required. This is the main objective of this chapter.

2.2 Contributions and Outcomes

The main contributions and outcomes of this chapter are summarized below.

Performance characterization of IA-MRC: Using stochastic geometry tools, the success probability (1-outage probability) for IA-MRC is derived in Section 2.4.1 for the dual-antenna case under influence of spatially-correlated interference, Rx noise and independent Nakagami fading. For the asymptotic regime (small outage probabilities), simplified expressions and a generalization to the case with more than two Rx antennas are presented in Section 2.4.2. To complement the theoretical work, a methodology for numerical evaluation of the main results is proposed and discussed in Section 2.4.3.

Comparison with simpler correlation models: In Section 2.5.1, the theoretical results for IA-MRC are used to study the validity of simpler correlation models frequently used in the literature due to their analytical tractability. It is shown that simply ignoring interference correlation (No Correlation (NC) model) across Rx antennas considerably overestimates the true performance of IA-MRC, particularly when channel fading variability is low. In contrast, assuming identical interference levels across antennas (Full Correlation (FC) model) slightly underestimates the available diversity, and hence the true performance of IA-MRC. The resulting performance gap rapidly decreases with the Nakagami parameter m_I of the interfering links and remains less than about 10% depending on the path loss exponent. This observation suggests the existence of an asymptotic equivalence between the FC model and the exact correlation model covered in Section 2.4, which is mathematically established in Section 2.5.1. One key insight is that the much simpler FC model can be used whenever the interfering links undergo a strong path loss and/or
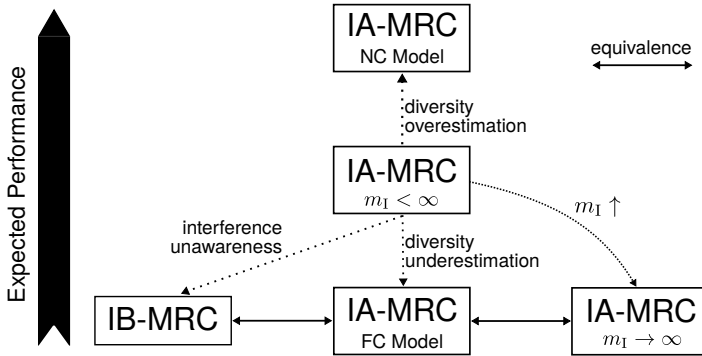
Figure 2.1: Comparison between IB-MRC and IA-MRC along with NC and FC models.

poor scattering (large m_I). Moreover, it is shown that the FC model for IA-MRC corresponds to IB-MRC in terms of post-combiner SINR. Thus, all insights obtained for IA-MRC under the FC model apply to IB-MRC as well. Fig. 2.1 illustrates the above findings.

Diversity order and spatial throughput: Exploiting the correspondence between the FC model and IB-MRC, the diversity order of IA-MRC and IB-MRC in the presence of spatial interference correlation is studied in Section 2.5.2. It is shown that both types of MRC cannot provide a diversity order gain since the diversity order is the same as for conventional SISO systems, irrespective of the number of Rx antennas. In Section 2.5.3, the improvement of MRC receivers on spatial throughput is studied, where it is found that the critical density of concurrent transmission given a target outage probability scales sublinearly in the number of Rx antennas. Thereby, the critical density gain over SISO systems scales considerably larger for IA-MRC than for IB-MRC in typical settings. For the dual-antenna case, it is further shown that MRC enables much better throughput operation points in terms of the transmission capacity metric compared to the SISO case.

Comparison with other linear combining schemes: Using the theoretical results, the performance of MRC is compared with other commonly known diversity-combining schemes in Section 2.5.4. It is found that MMSE combining, which adapts to the interference correlation across

Rx antennas, yields significant gains over MRC in terms of both success probability and average post-combiner SINR with increasing path loss exponent. For small path loss exponents, however, there is almost no benefit from estimating/exploiting the interference correlation, as MRC, although sub-optimal, achieves almost the same performance as MMSE combining. Using Jensen's inequality, the average post-combiner SINR gain of MRC over IA-SC is found to be generally smaller in wireless *ad hoc* networks than in the interference-free case, and monotonically decreasing with the path loss exponent. For typical path loss exponents, the average post-combiner SINR gain of MRC over IA-SC is about 1 dB. Especially for large path loss exponents, these observations suggest that MMSE combining and IA-SC may offer a better performance-complexity trade-of than MRC.

2.3 System Model

Consider an N-antenna receiver communicating with a single-antenna transmitter over an arbitrary distance y. In this SIMO scenario, the transmitted signal received at the N Rx antennas is corrupted by Rx noise and interference caused by other nodes concurrently transmitting over the same time-frequency resources inside the wireless network. To capture the spatial dynamics inherent to *ad hoc* networks, the locations of these interferers are modeled by a stationary Poisson Point Process (PPP) $\Phi \triangleq \{x_i\}$ on $\mathbb{R}^2$ with density λ, see Definition A.3. Here, x_i denotes the location of the i-th interferer. A realization of the point process Φ can be viewed as a single snapshot of the spatial network geometry, which typically varies over time, e.g., due to mobility. The PPP model is widely accepted for studying multiple kinds of networks, see for instance [36, 39, 61] and the references therein. Since Φ is stationary its statistics (and hence, the interference statistics) are location-invariant, see Definition A.3. Thus, the considered receiver can be placed in the origin $o \in \mathbb{R}^2$ without loss of generality.

From the *independence* property of the PPP, see (ii) in Definition A.2, it follows that there exists no spatial inhibition of interferers and hence, an interferer may be located (arbitrarily) close to any point in $\mathbb{R}^2$, including the considered receiver at o. The PPP is thus a reasonable model for networks without tight medium access coordination, e.g., slotted Aloha.
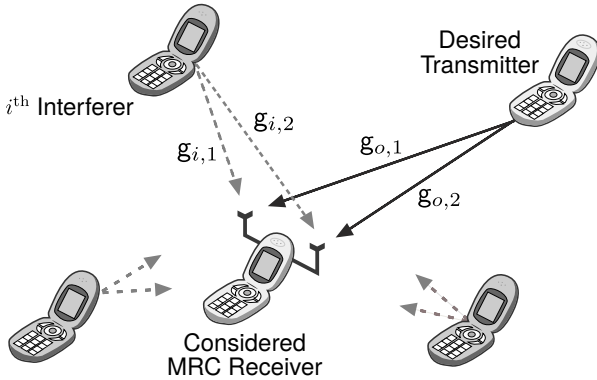
Figure 2.2: Illustration of the scenario for the example $N = 2$. The considered dual-antenna receiver communicates with the desired transmitter (solid), while experiencing interference from surrounding interferers (dashed).

All transmitted signals are subject to a distance-dependent path loss and small-scale narrowband channel fading. Large-scale or shadow fading is not modeled but can be included, e.g., using ideas from [62–65]. The path loss between the i-th interferer and the considered receiver is given by $\|x_i\|^{\alpha}$, where $\alpha > 2$ is the path loss exponent. Assuming unit Tx power for all nodes, the received power from interferer i at the n-th Rx antenna then becomes $g_{i,n}\|x_i\|^{-\alpha}$, where $g_{i,n}$ is the channel fading (power) gain on the respective link. The $\{g_{i,n}\}$ are assumed to be i.i.d. Gamma random variables with shape m_I and rate m_I, see Definition A.1. This leads to the widely used Nakagami-m fading model with parameter $m \geq 1/2$, where the fading amplitude $\sqrt{g_{i,n}}$ has Probability Density Function (PDF)

$$f_{\sqrt{g_{i,n}}}(z) = \frac{2m^m z^{2m-1}}{\Gamma(m)\bar{P}_\mathrm{r}^m} \exp\left(-\frac{mz^2}{\bar{P}_\mathrm{r}}\right), \tag{2.1}$$

where $\bar{P}_\mathrm{r}$ is the average received power, which can be set equal to one since $\|x_i\|^{-\alpha}$ already accounts for it. The Nakagami-m model is fairly general, covering rich-scattering (Rayleigh, $m = 1$), medium-scattering (Rice with fading parameter Ω, $m = (\Omega + 1)^2/(2\Omega + 1)$), and poor-scattering (pure path loss, $m \to \infty$) environments, see for instance [19].

Similarly, the fading gain between the desired transmitter and the n-th Rx antenna of the considered receiver, denoted by $g_{o,n}$, is assumed i.i.d.

Table 2.1: Notation used throughout this chapter

Notation	Description
$\Phi; \lambda$	Set of (random) interferer locations modeled as PPP; spatial density of interferers
N	Number of Rx antennas (branches)
y	Distance between considered receiver and desired transmitter
α	Path loss exponent
$\mathbf{g}_{i,n}; \mathbf{g}_{o,n}$	Power fading gain between n-th antenna of considered receiver and i-th interferer; and desired transmitter
$m_\mathrm{I}; m_\mathrm{D}; \kappa_\mathrm{DI}$	Nakagami parameter of fading on interfering links; on desired links; $\kappa_\mathrm{DI} = m_\mathrm{D}/m_\mathrm{I}$
I_n	Current interference (power) at n-th Rx antenna
SNR	Average SNR at the considered receiver
SINR_n	SINR at n-th Rx antenna
SINR_Σ	Post-combiner SINR for MRC
T	SINR threshold
P_c	Success/coverage probability
λ_ϵ	Critical density for given outage probability constraint ϵ
$\text{TC}(\epsilon)$	Transmission capacity for given outage probability constraint ϵ

Gamma distributed with shape m_D and rate m_D, where $m_\mathrm{D} \in \mathbb{N}^+$. To preserve generality, the fading parameters m_I and m_D do not need to be identical, i.e., interferers and desired transmitter may be subject to different fading statistics. The case $m_\mathrm{D} = m_\mathrm{I} = m$ is referred to as the *symmetric fading* case with parameter m while the term *asymmetric fading* is used whenever $m_\mathrm{D} \neq m_\mathrm{I}$. The short-hand notation $\kappa_\mathrm{DI} \triangleq m_\mathrm{D}/m_\mathrm{I}$ will be used throughout this chapter. By Lemma A.1, it follows that $\mathbb{E}[\mathbf{g}_{i,n}] = \mathbb{E}[\mathbf{g}_{o,n}] = 1 \; \forall n \in \{1, \dots, N\}$ and $\mathsf{x}_i \in \Phi$. Furthermore, it is easy to check from (A.2) that $\mathbf{g}_{i,n} \to 1 \; (\mathbf{g}_{o,n} \to 1)$ almost surely $\forall n \in \{1, \dots, N\}$ and $\mathsf{x}_i \in \Phi$ as $m_\mathrm{I} \to \infty \; (m_\mathrm{D} \to \infty)$. Fig. 2.2 illustrates the considered scenario.

Medium access is assumed to be slotted with a duration equal to or less than the channel coherence time. Since the receiver is interference-

aware, it can not only perfectly estimate the instantaneous fading gain of the desired link (the $\{\mathsf{g}_{o,n}\}$) but also the current interference-plus-noise power within one slot. By [12], the MRC weight in the n-th branch is then chosen proportional to the fading amplitude of the desired link and inversely proportional to the current interference-plus-noise power at the n-th antenna, see Appendix B for further details. The post-combiner SINR for IA-MRC can then be expressed as (B.7)

$$\mathtt{SINR}_\Sigma \triangleq \sum_{n=1}^{N} \mathtt{SINR}_n = \frac{\mathsf{g}_{o,1}}{\mathsf{l}_1 + \mathtt{SNR}^{-1}} + \ldots + \frac{\mathsf{g}_{o,N}}{\mathsf{l}_N + \mathtt{SNR}^{-1}}, \qquad (2.2)$$

where

$$\mathsf{l}_n \triangleq y^\alpha \sum_{\mathsf{x}_i \in \Phi} \mathsf{g}_{i,n} \|\mathsf{x}_i\|^{-\alpha} \qquad (2.3)$$

is the interference experienced at the n-th Rx antenna normalized by $y^{-\alpha}$ and $\mathtt{SNR}$ is the average Signal-to-Noise Ratio (SNR). l_n is understood as the instantaneous interference averaged over the interferer symbols within one transmission slot, and hence corresponds to the current variance of the sum interference signal at the n-th Rx antenna given that the signal is zero mean, see Appendix B for more details. Since medium access is slotted, l_n can be assumed to be constant for the duration of one slot. It can be shown that $\mathsf{l}_n < \infty$ almost surely $\forall n \in \{1, \ldots, N\}$ when $\alpha > 2$, see for instance [38]. Table 2.1 summarizes the notation used in this chapter.

Note that, although all fading gains $\{\mathsf{g}_{i,n}\}$ on the interfering links are independent across interferers and Rx antennas, the interference levels $\{\mathsf{l}_n\}$ and hence, the individual $\{\mathtt{SINR}_n\}$ are not. In fact, the $\{\mathtt{SINR}_n\}$ are correlated since the $\{\mathsf{l}_n\}$ originate from the same set of interferers, i.e., from the common point process Φ. The distribution of (2.2) can, in general, be obtained through the use of the joint PDF of the interference envelopes derived in [52] for the case of isotropic interference, i.e., by averaging the conditional distribution of the post-combiner SINR over the interference statistics. However, this approach is analytically involved since (i) the joint PDF of the interference envelopes cannot be expressed by a closed-form expression (ii) and one has to deal with the sum of *non-identical* Gamma random variables, which is analytically difficult.

2.4 Performance of IA-MRC

In this section, the success probability for IA-MRC for the setting described in Section 2.3 is derived for the special case $N = 2$ (Theorem 2.1). Then, further simplifications and a generalization to $N > 2$ for the asymptotic regime (Theorem 2.2) is presented. Finally, a semi-analytical method for evaluating some of the theoretical expressions is also discussed.

2.4.1 Dual-Antenna Case

A common way of studying the performance of diversity-combining schemes is to analyze the distribution of the post-combiner SINR. More specifically, one is interested in the probability of the post-combiner SINR exceeding a given threshold. This concept is formalized next.

Definition 2.1 (Success/coverage probability)**.** *The success or coverage probability is defined as*

$$P_c \triangleq \mathbb{P}\left(\text{SINR}_\Sigma \geq T\right) \tag{2.4}$$

for a modulation- and coding-specific threshold $T > 0$.

P_c can be seen as

   (i) the probability of the transmission between the considered receiver and the desired transmitter being *successful*.

  (ii) the complementary Cumulative Distribution Function (CDF) of SINR_Σ or $1 -$ outage probability.

 (iii) the probability of the considered receiver being *covered* by the desired transmitter.

  (iv) the average fraction of successful transmissions of the *same* type inside the network.

The alternative term *coverage probability* (iii) will be more appropriate in Chapter 3, where cellular systems with BSs *covering* the mobile users are considered. Point (iv) follows from the ergodicity of the PPP Φ [34].

The number of antennas mounted on practical wireless consumer devices, such as smartphones or WiFi devices, typically remains small due to

space limitations and complexity constraints, thereby often not exceeding $N = 2$ antennas. The following result gives the success probability for this prevalent scenario.

Theorem 2.1 (Success probability for dual-antenna IA-MRC)**.** *The success probability for dual-antenna IA-MRC ($N = 2$) in the described setting is given by*

$$
P_c^{IA} = \sum_{k=0}^{m_D-1} \frac{(-1)^{k+m_D}}{k!\,\Gamma(m_D)} \int_0^\infty z^{-1}
$$
$$
\times \frac{\partial^{k+m_D}}{\partial s^k \partial t^{m_D}} \left[\exp\left(-\frac{m_D}{\text{SNR}} \left((T-z)^+ s + zt \right) - \pi\lambda \mathcal{A}(z,s,t) \right) \right]_{\substack{s=1 \\ t=1}} dz,
$$
$$(2.5)$$

where

$$
\frac{\mathcal{A}(z,s,t)}{y^2 \kappa_{DI}^{2/\alpha} \Gamma(1-\frac{2}{\alpha})} =
\begin{cases}
s^{2/\alpha}(T-z)^{2/\alpha}\,\Gamma(2m_I + \frac{2}{\alpha}) \\
\times {}_2\mathbf{F}_1\!\left(-\frac{2}{\alpha}, m_I, 2m_I; 1 - \frac{zt}{(T-z)s}\right), & 0 \le z < T \quad (2.6a) \\
z^{2/\alpha} t^{2/\alpha} \dfrac{\Gamma(m_I + \frac{2}{\alpha})}{\Gamma(m_I)}, & z \ge T. \quad (2.6b)
\end{cases}
$$

Proof: See Section 2.7.1. ∎

The function ${}_2\mathbf{F}_1(a,b,c;z) \triangleq {}_2F_1(a,b,c;z)/\Gamma(c)$ is known as the *regularized* Gaussian hypergeometric function [66] and is implemented in most numerical software programs. A method for semi-analytical evaluation of (2.5) is presented and discussed later in Section 2.4.3. In practice, the channel fading statistics are often symmetric, i.e., $m_D = m_I = m$, in which case $\kappa_{DI} = 1$ can be assumed in (2.6).

Remark 2.1 (Integral decomposition)**.** *The integral in (2.5) over $[0,\infty)$ can be split into two integrals with limits $[0,T)$ and $[T,\infty)$ to get rid of the $(\cdot)^+$ function and to exploit the fact that the integrand of the upper integral becomes zero for all derivatives with respect to s.*

Theorem 2.1 covers only the dual-antenna case and an extension to $N > 2$ is analytically too involved unfortunately. For practical operating points, where P_c^{IA} is close to one, a possible extension to general N is presented in Section 2.4.2. Starting from the result of Theorem 2.1, simplified expressions can be obtained in certain cases as shown next.

Corollary 2.1 (Rayleigh fading $(m_D = m_I = 1)$). *When $m_D = m_I = 1$ (symmetric Rayleigh fading), the success probability for dual-antenna IA-MRC ($N = 2$) in the described setting reduces to*

$$P_c^{IA} = - \int_0^\infty z^{-1} \frac{d}{dt} \left[\exp \left(-\frac{(T-z)^+ + zt}{SNR} - \lambda \pi \mathcal{A}(z,1,t) \right) \right]_{t=1} dz, \quad (2.7)$$

with

$$\mathcal{A}(z,1,t) = \pi y^2 \frac{2}{\alpha} \csc \left(\frac{2\pi}{\alpha} \right) \frac{((T-z)^+)^{1+2/\alpha} - (zt)^{1+2/\alpha}}{(T-z)^+ - zt}. \quad (2.8)$$

The path loss exponent observed in typical urban and rural scenarios is often around $\alpha = 4$ [19, 20]. This observation motivates the following corollary, which further simplifies Corollary 2.1.

Corollary 2.2 (Rayleigh fading, $\alpha = 4$). *When $m_D = m_I = 1$ (symmetric Rayleigh fading) and $\alpha = 4$, the success probability for dual-antenna IA-MRC ($N = 2$) in the described setting reduces to*

$$P_c^{IA} = - \int_0^\infty z^{-1} \exp \left(-\frac{(T-z)^+}{SNR} \right)$$
$$\times \frac{d}{dt} \left[\exp \left(-\frac{zt}{SNR} - \frac{\lambda \pi^2 y^2}{2} \frac{((T-z)^+)^{3/2} - (zt)^{3/2}}{(T-z)^+ - zt} \right) \right]_{t=1} dz \quad (2.9)$$

Similar simplifications that allow (2.5) to be expressed through elementary functions can be obtained by invoking functional identities of the Gaussian hypergeometric function for suitable α and m_I, see for instance [66–68].

Remark 2.2 (Interference-/noise-limited performance). *The success probability for the interference-limited case can be obtained by setting $1/SNR = 0$ in (2.5). Likewise, the success probability for the noise-limited case can be recovered by setting $\lambda = 0$. In the later case, the success probability becomes $P_c^{IA} = 1 - F_{g_{o,1}+g_{o,2}}(T/SNR)$ as expected [19].*

The success probability for dual-antenna IA-MRC under poor scattering can in general be obtained by letting $m_D, m_I \to \infty$, eventually leading to the pure path loss model. However, noting that $g_{i,n}, g_{o,n} \to 1$ as $m_D, m_I \to \infty \; \forall n \in \{1, \ldots, N\}$ and $x_i \in \Phi$, $SINR_\Sigma$ for the case of N Rx antennas becomes $SINR_\Sigma = \frac{N}{SNR^{-1} + I}$, with $I = y^\alpha \sum_{x_i \in \Phi} \|x_i\|^{-\alpha}$. This, in
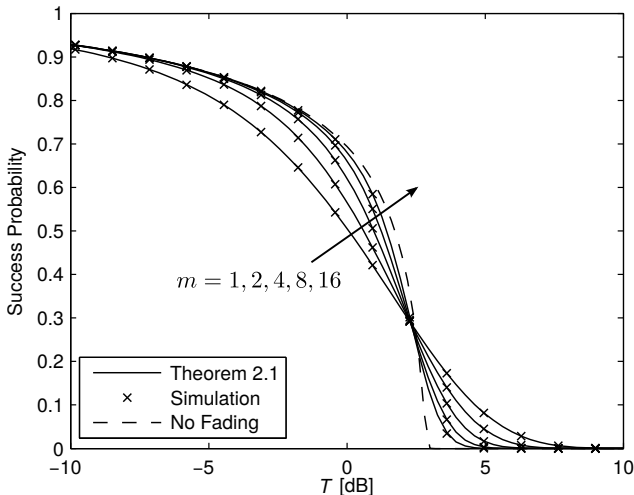
Figure 2.3: Success probability $\mathrm{P_c^{IA}}$ for different $m_\mathrm{D} = m_\mathrm{I} = m$ (symmetric Nakagami fading). Parameters: $\lambda = 10^{-3}$, $\alpha = 4$, $d = 10$, and $\mathtt{SNR} = 0$ dB. Dashed line ($m \to \infty$) was obtained using [49, Eq. (3.17)].

turn, corresponds to the SINR for the SISO case without fading and with N-fold received power increase. The success probability for this case can be obtained, e.g., by Laplace inversion [35] or using the dominant-interferer technique [42]. For $\alpha = 4$, a closed-form expression can be obtained using [49, Eq. (3.17)]. Fig. 2.3 shows the success probability $\mathrm{P_c^{IA}}$ for different $m_\mathrm{D} = m_\mathrm{I} = m$ (symmetric Nakagami fading). It can be seen that the result from Theorem 2.1 perfectly matches the simulation results. Furthermore, increasing the Nakagami parameter m has two effects on $\mathrm{P_c}$: for reasonable values of $\mathrm{P_c^{IA}} > 0.3$, a smaller channel variability ($m \uparrow$) improves transmission reliability, whereas for (non-practical) small values of $\mathrm{P_c^{IA}}$ this trend is reversed. Interestingly, all curves seem to intersect at one unique point (in this example around $T = 2.3$ dB). The success probability for $m \to \infty$ (no fading) is also shown for reference and was obtained by [49, Eq. (3.17)].

This subsection focused on the success probability for IA-MRC for general operating points. When focusing on practically relevant operating points, i.e., reasonably large success probabilities, further simplifications and a generalization to $N > 2$ are possible as shown in the following.

2.4.2 Asymptotic Analysis and Extension to N Antennas

Practical communication systems typically operate at reasonably high success probabilities in order to be energy efficient. It is therefore interesting to study the performance of IA-MRC as $T \to 0$. Another motivation for studying such an asymptotic performance is that the resulting asymptotic expression often follows a fairly simple law that can be expressed in closed-form. For instance, it would be desirable to have such a asymptotic expression for $\mathrm{P_c^{IA}}$ in (2.5) that does no longer contain an improper integral over two higher-order derivatives.

Asymptotic Analysis I: Comparison with SISO Transmission

The following corollary gives an asymptotically tight expression for the success probability for dual-antenna IA-MRC in the absence of Rx noise. A similar though more bulky expression can be derived also for the case with Rx noise, however, with no additional insights.

Corollary 2.3 (Asymptotic $\mathrm{P_c^{IA}}$ for dual-antenna case)**.** *Without Rx noise (*$1/\mathrm{SNR} = 0$*), the asymptotic success probability for dual-antenna IA-MRC in the described setting becomes*

$$\mathrm{P_c^{IA}} \sim 1 - \pi \lambda y^2 \kappa_{\mathrm{DI}}^{2/\alpha} T^{2/\alpha} \left(\frac{\Gamma(m_{\mathrm{D}} - \frac{2}{\alpha})\Gamma(m_{\mathrm{I}} + \frac{2}{\alpha})}{\Gamma(m_{\mathrm{I}})\,\Gamma(m_{\mathrm{D}})} \right.$$
$$\left. - \frac{2\,\Gamma(2m_{\mathrm{I}} + \frac{2}{\alpha})}{\alpha\,B(m_{\mathrm{I}}, m_{\mathrm{D}})} \sum_{k=0}^{m_{\mathrm{D}}-1} \frac{\Gamma(-\frac{2}{\alpha} + m_{\mathrm{D}} + k)\,C_k}{B(m_{\mathrm{I}}, k+1)(m_{\mathrm{I}} + k)} \right) \quad (2.10)$$

as $T \to 0$, where $B(x,y) \triangleq \frac{\Gamma(x)\Gamma(y)}{\Gamma(x+y)}$ is the Beta function [66] and

$$C_k \triangleq \int_0^1 u^{2/\alpha - 1 - k}\,(1 - u)^k$$
$$\times {}_2\mathbf{F}_1\!\left(-\tfrac{2}{\alpha} + m_{\mathrm{D}} + k, m_{\mathrm{I}} + k, 2m_{\mathrm{I}} + m_{\mathrm{D}} + k; 2 - \tfrac{1}{u}\right)\,\mathrm{d}u. \quad (2.11)$$

Note that (2.10) does neither contain an improper integral nor higher-order derivatives. The integral in (2.11) can be computed using standard numerical software. For the special case $m_{\mathrm{D}} = m_{\mathrm{I}} = 1$ (Rayleigh fading) and $\alpha = 4$, (2.11) becomes $C_0 = 2 + 2^{-3/2} \log(6 - 4\sqrt{2}) - 2^{-1/2} \log(2 + \sqrt{2}) \approx 0.753$ and (2.10) then reduces to

$$\mathrm{P_c^{IA}} \sim 1 - 0.2176\,\pi^2 \lambda y^2 \sqrt{T}. \quad (2.12)$$
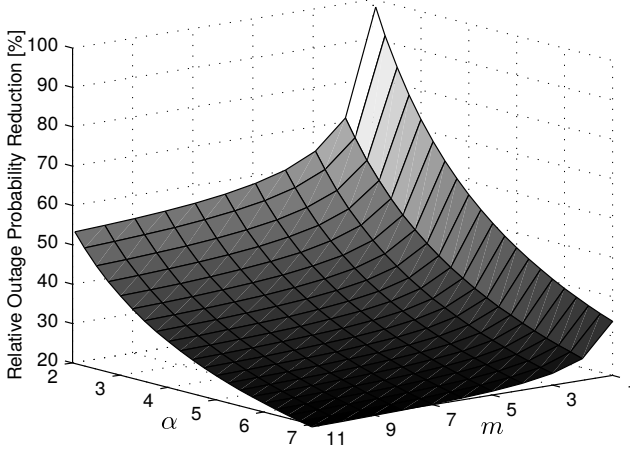
Figure 2.4: Relative outage probability reduction $\Delta^{\text{IA-MRC-SISO}}_{\mathbb{E}[\text{SINR}]}$ when switching from SISO to IA-MRC. Parameters: $m_{\text{D}} = m_{\text{I}} = m$ (symmetric Nakagami fading), no Rx noise, and $y = 10$.

Remark 2.3. *The first term inside the brackets in* (2.10) *corresponds to the asymptotic success probability for the SISO case*

$$\text{P}^{\text{SISO}}_{\text{c}} \sim 1 - \pi\lambda y^2 T^{2/\alpha}\kappa^{2/\alpha}_{\text{DI}} \frac{\Gamma(m_{\text{D}} - \frac{2}{\alpha})\Gamma(m_{\text{I}} + \frac{2}{\alpha})}{\Gamma(m_{\text{I}})\,\Gamma(m_{\text{D}})}, \qquad (2.13)$$

which was derived in [69] for symmetric Nakagami fading. Hence, the second term in (2.10) *characterizes the success probability gain due to dual-antenna IA-MRC.*

By Remark 2.3, the outage probability $(1 - \text{P}_{\text{c}})$ for the above special case $m_{\text{D}} = m_{\text{I}} = 1$ and $\alpha = 4$ is hence reduced by 56.2% when switching from SISO to dual-antenna IA-MRC in the asymptotic regime. This observation is generalized to the case of different m and α next.

Figure 2.4 shows the relative reduction in outage probability in the asymptotic regime when switching from a SISO system to dual-antenna IA-MRC. The relative reduction is defined as $\Delta^{\text{IA-MRC-SISO}}_{1-\text{P}_{\text{c}}} = (\text{P}^{\text{IA}}_{\text{c}} - \text{P}^{\text{SISO}}_{\text{c}})/(1 - \text{P}^{\text{SISO}}_{\text{c}})$ and can be obtained by leveraging Remark 2.3 and (2.13). As expected, decreasing the per-antenna SINR_n variance through increasing the Nakagami parameter m reduces the relative improvement

due to dual-antenna IA-MRC. For typical path loss exponents $3 < \alpha < 6$, the relative improvement is $20\% < \Delta_{1-P_c}^{\text{IA-MRC-SISO}} < 40\%$ for large m, and $40\% < \Delta_{1-P_c}^{\text{IA-MRC-SISO}} < 70\%$ for small m (close to Rayleigh fading).

Asymptotic Analysis II: Extension to General N

In [42], a general technique for lower bounding the outage probability $1 - P_c$ in random *ad hoc* networks was proposed, which is based on the idea of *dominant interferers*. In contrast to non-dominant interferers, the individual interference contribution from a single dominant interferer already suffices to cause outage at the considered receiver. Mathematically, this means

$$\sum_{n=1}^{N} \frac{g_{o,n}}{y^{\alpha} g_{i,n} \|x_i\|^{-\alpha} + \text{SNR}^{-1}} < T \quad \Leftrightarrow \quad \text{interferer } i \text{ is dominant.} \quad (2.14)$$

The set of dominant interferers is essentially a subset of Φ obtained by independent thinning, see Lemma A.5. This set can be expressed as

$$\mathcal{D} \triangleq \left\{ x_i \in \Phi : \sum_{n=1}^{N} \frac{g_{o,n}}{y^{\alpha} g_{i,n} \|x_i\|^{-\alpha} + \text{SNR}^{-1}} < T \right\}. \quad (2.15)$$

Note that $\mathcal{D}$ depends on the fading gains $\{g_{o,n}\}$, which can viewed as a "breathing" of the dominant-interferer set according to the actual channel quality on the desired link. Clearly, ignoring the non-dominant interferers, i.e., those from the set $\Phi \setminus \mathcal{D}$, underestimates the true interference and yields a sufficient condition for outage. Consequently, one has the inequality relation

$$P_c^{\text{IA}} \le P_{c,\text{dom}}^{\text{IA}} \triangleq \mathbb{P}\left(\mathcal{D} = \emptyset\right). \quad (2.16)$$

As explained in [42, Sec. III-D] for the no-fading case, the lower bound constructed using the dominant-interferer approach is remarkably tight for small outage probabilities, e.g., for $T \to 0$. This is due to the fact that the random variables $\{\|x_i\|^{-\alpha}\}$ follow a subexponential distribution. Using [70, Thm. 2.1], it can be shown that the latter observation extends to the model at hand with fading included, i.e., the product $g_i\|x_i\|^{-\alpha}$ is subexponential as well. Subexponential random variables satisfy the

property

$$\mathbb{P}\left(\sum_{i=1}^{\xi}\frac{\mathsf{g}_i}{\|\mathsf{x}_i\|^\alpha}>v\right)\sim\mathbb{P}\left(\max\left\{\frac{\mathsf{g}_1}{\|\mathsf{x}_1\|^\alpha},\dots,\frac{\mathsf{g}_\xi}{\|\mathsf{x}_\xi\|^\alpha}\right\}>v\right)$$

$$=\mathbb{P}\left(\bigcup_{i=1}^{\xi}\left\{\frac{\mathsf{g}_i}{\|\mathsf{x}_i\|^\alpha}>v\right\}\right) \qquad (2.17)$$

as $v\to\infty$ for some $\xi\in\mathbb{N}$, which is also referred to as the *single big-jump* principle [71, Sec. I]. Thus, (2.16) becomes an equality in the asymptotic regime, where outage events are dominated by the presence of close-by interferers. The following theorem gives the success probability bound $\mathrm{P}^{\mathrm{IA}}_{\mathrm{c,dom}}$ for arbitrary number of Rx antennas N and absence of Rx noise.

Theorem 2.2 (Success probability upper bound for IA-MRC)**.** *Without Rx noise ($1/\mathtt{SNR}=0$), the success probability for N-antenna IA-MRC is (tightly) upper bounded by*

$$\mathrm{P}^{\mathrm{IA}}_{\mathrm{c}}\lesssim\mathrm{P}^{\mathrm{IA}}_{\mathrm{c,dom}}=\exp\left(-\frac{\pi\lambda T^{2/\alpha}y^2\Gamma(m_\mathrm{D})^N}{B(m_\mathrm{D},m_\mathrm{I})^N\Gamma(2/\alpha)}\right.$$

$$\left.\times\int_0^\infty u^{2/\alpha-1}U\left(m_\mathrm{D},1-m_\mathrm{I},\frac{u}{\kappa_{\mathrm{DI}}}\right)^N\mathrm{d}u\right), \qquad (2.18)$$

where $U(a_1,a_2,x)\triangleq\frac{1}{\Gamma(a_1)}\int_0^\infty t^{a_1-1}(1+t)^{a_2-a_1-1}e^{-xt}\,\mathrm{d}t$ with $a_1>0$ is the confluent hypergeometric function (Kummer's U-function) [66].

Proof: See Section 2.7.2. ∎

In comparison with Theorem 2.1, Theorem 2.2 has three advantages for characterizing the success probability for IA-MRC;

- Arbitrary number of Rx antennas $N>1$, i.e., no longer just $N=2$.
- General Nakagami fading parameters $m_\mathrm{D},m_\mathrm{I}\geq1/2$, i.e., no need for $m_\mathrm{D}\in\mathbb{N}^+$ anymore.
- Single-integral form without higher-order derivatives.

Figure 2.5 shows the success probability bound from Theorem 2.2 along with simulation results for different number of Rx antennas N. In line with the above discussion on the subexponentiality of the $\{\mathsf{g}_i\|\mathsf{x}_i\|^{-\alpha}\}$, it can be seen that (2.18) tightly upper bounds the success probability
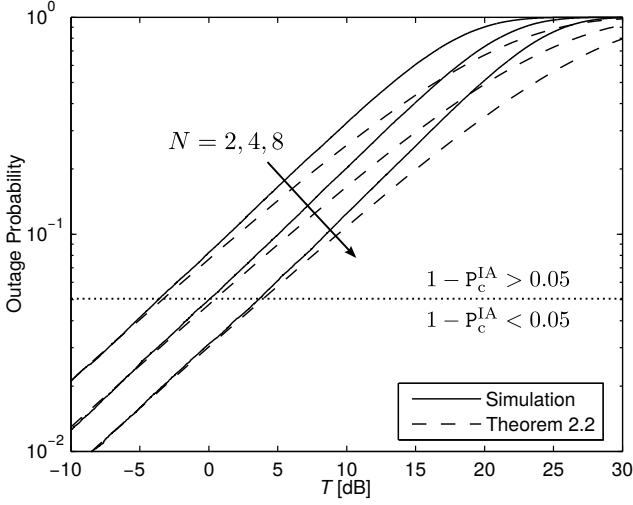
Figure 2.5: Outage probability $(1 - P_c)$ for $N = 2, 4, 8$. Dashed curves correspond to the success probability bound from Theorem 2.2. Parameters: $m_D = 3.2$, $m_I = 2.4$, $y = 10$, and $\alpha = 3.5$, no Rx noise.

for IA-MRC in the asymptotic regime; in this example, the gap becomes vanishingly small already at practically relevant outage probability values around 5%. Hence, in this regime Theorem 2.2 can be used instead of Theorem 2.1 or instead of time-consuming simulations to assess the performance of IA-MRC for different number or Rx antennas N.

2.4.3 Semi-Analytical Evaluation of Theorem 2.1

The mathematical form of (2.5) in Theorem 2.1 involves two higher-order derivatives of a composite function as well as an integral, which makes a purely analytical evaluation of the result difficult if not impossible. Thus, one has to resort to numerical tools, of which several approaches exist in the literature. In the following, a methodology for efficient and robust semi-numerical evaluation of (2.5) is proposed and discussed.

Faà di Bruno's formula and Bell polynomials for analytical t-differentiation: High-order derivatives of general composite functions of the form $f(g(x))$ can be evaluated using the well-known Faà di Bruno formula, see for instance [66, 72]. Whenever the outer function $f(\cdot)$ is an exponential function (as it is the case in (2.5)), it is useful to express Faà di Bruno's formula through Bell polynomials [73]

$$\frac{\mathrm{d}^n}{\mathrm{d}x^n} f(g(x)) = f(g(x)) \, B_n\left(g^{(1)}(x), \ldots, g^{(n)}(x)\right), \qquad (2.19)$$

where $B_n\left(x_1, \ldots, x_n\right)$ is the n-th *complete* Bell polynomial. The complete Bell polynomials can be easily constructed using the matrix determinant identity from [74]. From (2.19) it is clear that the derivatives of the inner function $g(x)$ must be computed up to order n in advance. This, in turn, means that the derivatives inside the exp-term in (2.5) need to be computed up to order m_D. This task is addressed next.

Corollary 2.4 (n-th t-derivative of $\mathcal{A}(z, s, t)$). *The n-th derivative of $\mathcal{A}(z, s, t)$ with respect to t evaluated at $t = 1$ is given by*

$$\frac{\frac{\partial^n}{\partial t^n}\left[\mathcal{A}(z, s, t)\right]_{t=1}}{z^{2/\alpha} \, y^2 \, \kappa_{\mathrm{DI}}^{2/\alpha}} = \begin{cases} \dfrac{(-1)^{n+1}}{\Gamma(m_\mathrm{I})}\Gamma(-\tfrac{2}{\alpha} + n)\,\Gamma(m_\mathrm{I} + n)\,\Gamma(\tfrac{2}{\alpha} + 2m_\mathrm{I}) \\[2mm] \quad \times {}_2\mathbf{F}_1\!\left(-\tfrac{2}{\alpha} + n, m_\mathrm{I}, 2m_\mathrm{I} + n; 1 - \tfrac{(T-z)s}{z}\right), \\[2mm] \hspace{4cm} 0 \le z < T \quad (2.20a) \\[3mm] \dfrac{2\pi\,\Gamma(\tfrac{2}{\alpha} + m_\mathrm{I})\csc(\tfrac{2\pi}{\alpha})}{\alpha\,\Gamma(m_\mathrm{I})\,\Gamma(\tfrac{2}{\alpha} - n + 1)}, \hspace{1.2cm} z \ge T. \hspace{0.8cm} (2.20b) \end{cases}$$

Using the approach described above, the derivative of the inner function with respect to t is computed analytically, i.e., without numerical difference methods. For the subsequent derivative with respect to s, however, Faà di Bruno's formula may not be the best choice since the outer function is no longer an exponential function and the derivatives of the resulting inner function are difficult to obtain. A different approach for the computation of the s-derivatives is therefore needed.

Chebyshev interpolation method for numerical s-differentiation: Before explaining this differentiation technique, first note that the $\mathrm{d}^k/\mathrm{d}s^k$ derivative in (2.5) can be moved outside the integral over z according to Leibniz's integration rule for improper integrals [66]. This step comes with the advantage of first numerically computing the integral without

caring about how to evaluate the s-derivative. Interpreting the integration result as a function of s, say $V(s)$, this function is then approximated using the Chebyshev interpolation method in some interval $[a, b]$, yielding [75]

$$V(s) \approx \tilde{V}(s) \triangleq -\frac{c_0}{2} + \sum_{i=0}^{p-1} c_\ell T_\ell \left(\frac{2s - (a+b)}{b-a} \right), \tag{2.21}$$

where $s \in [a, b]$, $T_\ell(x) \triangleq \cos(\ell \arccos x)$ is the ℓ-th Chebyshev polynomial of the first kind, p is the number of sampling points, and

$$c_\ell = \frac{2}{p} \sum_{i=0}^{p-1} V \left(\tfrac{1}{2}(b-a) \cos \left[\tfrac{\pi}{p}(i+1/2) \right] + \tfrac{1}{2}(a+b) \right)$$
$$\times \cos \left[\tfrac{\ell\pi}{p}(i+1/2) \right] \tag{2.22}$$

is the ℓ-th Chebyshev node. Differentiating $\tilde{V}(s)$ in (2.21) instead of $V(s)$ at $s = 1$ yields

$$\frac{\mathrm{d}^k}{\mathrm{d}s^k} \Big[V(s) \Big]_{s=1} \approx \frac{\mathrm{d}^k}{\mathrm{d}s^k} \Big[\tilde{V}(s) \Big]_{s=1}$$
$$= \sum_{\ell=0}^{p-1} c_\ell \frac{\mathrm{d}^k}{\mathrm{d}s^k} \left[T_\ell \left(\frac{2s - (a+b)}{b-a} \right) \right]_{s=1}$$
$$\stackrel{(a)}{=} \left(\frac{2}{b-a} \right)^k \sum_{\ell=k}^{p-1} c_\ell T_\ell^{(k)} \left(\frac{2 - (a+b)}{b-a} \right), \tag{2.23}$$

where (a) follows from the fact that $\mathrm{d}^k T_\ell(s)/\mathrm{d}s^k = 0$ if $\ell < k$ $\forall s$. It is well-known that the Chebyshev interpolation has the smallest maximum error among all polynomial approximations. This is due to the fact that end-point effects at the boundaries of the approximation interval are effectively avoided through projecting the function's domain onto the angular interval $[0, \pi]$ [75, Sec. 5.8]. As a result, the Chebyshev approximation achieves exponential convergence as p increases.

A step-by-step overview of the proposed semi-analytical method for evaluating (2.5) is shown in Fig. 2.6. All numerical results and figures in this chapter were obtained using this method.

```
 1: procedure EVALUATION OF (2.5)
 2:   w_0, ..., w_{m_D-1} ← s-DIFF(m_D)
 3:   P_c = ∑_{k=0}^{m_D-1} (-1)^{k+m_D} (w_k)/(k! Γ(m_D))
 4: end procedure

 5: function s-DIFF(m_D)                        ▷ s-derivatives up to order m_D - 1
 6:   s ← [a, ..., b]                           ▷ Chebyshev points, 0 < a < 1 < b
 7:   for ℓ ← 0, p - 1 do in parallel
 8:     V[ℓ] ← ∫_0^∞ z^{-1} t-DIFF(z, s[ℓ]) dz      ▷ Values at Chebyshev points
 9:   end for
10:   c_1, ..., c_p ← (2.22)                    ▷ Get all Chebyshev nodes
11:   for k ← 0, m_D - 1 do
12:     (∂^k)/(∂s^k) [Ṽ(s)]_{s=1} ← (2.23)         ▷ Differentiate interpolant
13:   end for
14: end function

15: function t-DIFF(z, s)                       ▷ m_D-th t-derivative for specific z, s
16:   f(x) ← e^x
17:   g^{(1)}(1), ..., g^{(m_D)}(1) ← (2.20)        ▷ Get inner t-derivatives
18:   (∂^{m_D})/(∂t^{m_D}) f(g(t)) ← (2.19)        ▷ Invoke Faà di Bruno's formula
19: end function
```

Figure 2.6: Numerical recipe for semi-analytical evaluation of (2.5).

Some comments regarding the numerical recipe in Fig. 2.6:

- Line 2: The method exploits the fact that the higher-order s-derivatives can be moved outside the integral over z. This is especially useful because this integral can be efficiently computed using powerful built-in numerical integration tools with maximum-error criterion, e.g., using the `quadgk` routine in Matlab.

- Lines 6 & 7: The value $p = m_D + 5$ was used throughout this thesis, which was found to yield a good balance between complexity and accuracy. Furthermore, the interval boundaries were chosen as $a = .8$ and $b = 1.2$.

- Lines 7–9: This *for*-loop is the most time-consuming task and can be executed in parallel whenever allowed by the employed hardware and software.

- Line 18: When $\texttt{SNR} < \infty$, the linear combination of $\mathcal{A}(z, s, t)$ *and* the $\texttt{SNR}$-related term in the exponent of (2.5) must be differentiated at $t = 1$. It is easy to check that the latter has first-order derivative $z m_D / \texttt{SNR}$ and higher-order derivatives equal to zero.

2.5 Discussion

In this section, the theoretical results developed in Section 2.4 are used for further discussions on the performance of IA-MRC.

2.5.1 Comparison with Simpler Correlation Models

For analytical tractability, it is frequently assumed in the literature that the interference across different antennas is either equally-strong or statistically independent. Certainly, such simplifications may lead to considerable accuracy losses as the true interference correlation structure across the $\{I_n\}$ and hence, across the $\{\mathtt{SINR}_n\}$ is distorted. With the exact model developed in Section 2.4.1 at hand, the validity of these simpler correlation models is verified for use with IA-MRC and accuracy losses are quantified in the following.

No-correlation model: In this correlation model, the interference levels $\{I_n\}$ are assumed statistical independent across Rx antennas. Then, (2.2) boils down to a sum of i.i.d. random variables, which is easier to handle. Note that the NC model overestimates the true diversity as it assumes that the interference originates from a separate point process for each Rx antenna.

Definition 2.2 (NC model). *In the NC model, the interference levels $\{I_n\}$ at the N Rx antennas are assumed to be statistically independent, i.e., $f_{I_n, I_m}(I_n, I_m) = f_{I_n}(I_n)\, f_{I_m}(I_m)\ \forall m, n \in \{1, \dots, N\}$. The corresponding post-combiner SINR is denoted by $\mathtt{SINR}_\Sigma^{\mathrm{NC}}$.*

For $N > 1$, one can obtain $\mathtt{P}_{\mathrm{c,NC}}^{\mathrm{IA}}$ by (numerical) Laplace inversion [35, Cor. 2.3.4] exploiting the *i.i.d.* property of the $\{\mathtt{SINR}_n\}$, provided the Laplace transform of $\mathtt{SINR}_n$ is known. However, this approach is quite involved because (i) obtaining the Laplace transform of $\mathtt{SINR}_n$ in closed-form for general α is difficult and (ii) performing the inverse Laplace transform requires solving a complex integral. For the practical case $N = 2$, the following result gives the success probability for IA-MRC under the NC model.

Proposition 2.1 (Success probability $\text{P}^{\text{IA}}_{\text{c,NC}}$ for dual-antenna IA-MRC).
*The success probability for dual-antenna IA-MRC under the NC model
has the same form as in (2.5) with $\mathcal{A}(z, s, t)$ replaced by*

$$y^2 \kappa_{\text{DI}}^{2/\alpha} \frac{\Gamma(1 - \frac{2}{\alpha}) \Gamma(\frac{2}{\alpha} + m_{\text{I}})}{\Gamma(m_{\text{I}})} \left(\left(s\,(T - z)^+ \right)^{2/\alpha} + (zt)^{2/\alpha} \right). \qquad (2.24)$$

Proof: See Section 2.7.3. ∎

In contrast to (2.6), $s\,(T - z)^+$ and zt now appear in a sum. This, in
turn, means that the integrand in (2.5) decomposes into the product
$f_{\text{SINR}_1}(T - z) f_{\text{SINR}_2}(z)$, as expected for independent SINR_1 and SINR_2.

Full-correlation model: In contrast to modeling the current interfer-
ence as being statistically independent across branches, it can be assumed
to be equally strong, i.e., $\mathsf{I}_n \equiv \mathsf{I}_m \; \forall m, n \in \{1, \ldots, N\}$. This assumption
effectively ignores the additional variability in the $\{\text{SINR}_n\}$ resulting from
the de-correlation effect of the fading on the interfering links.

Definition 2.3 (FC model). *In the FC model, the interference levels
$\{\mathsf{I}_n\}$ at the N Rx antennas are assumed equal, i.e., $\mathsf{g}_{i,m} \equiv \mathsf{g}_{i,n} \; \forall m, n \in
\{1, \ldots, N\}$ and $\mathsf{x}_i \in \Phi$. The corresponding post-combiner SINR is $\text{SINR}^{\text{FC}}_{\Sigma}$.*

Thus, in the FC model the post-combiner SINR becomes

$$\text{SINR}^{\text{FC}}_{\Sigma} = \frac{\sum_{n=1}^{N} \mathsf{g}_{o,n}}{y^{\alpha} \sum_{\mathsf{x}_i \in \Phi} \mathsf{g}_i \|\mathsf{x}_i\|^{-\alpha} + \text{SNR}^{-1}}. \qquad (2.25)$$

The next result gives the success probability $\text{P}^{\text{IA}}_{\text{c,FC}}$ under the FC model
for arbitrary $N \geq 1$.

Proposition 2.2 (Success probability $\text{P}^{\text{IA}}_{\text{c,FC}}$ for N-antenna IA-MRC).
The success probability for N-antenna IA-MRC under the FC model is

$$\text{P}^{\text{IA}}_{\text{c,FC}} = \sum_{k=0}^{Nm_{\text{D}}-1} \frac{(-1)^k}{k!} \frac{\text{d}^k}{\text{d}s^k} \Bigg[\exp \Bigg(-\frac{sm_{\text{D}}T}{\text{SNR}}$$

$$-\lambda \pi y^2 (s\kappa_{\text{DI}}T)^{2/\alpha} \Gamma(1 - \tfrac{2}{\alpha}) \frac{\Gamma(\frac{2}{\alpha} + m_{\text{I}})}{\Gamma(m_{\text{I}})} \Bigg) \Bigg]_{s=1}. \qquad (2.26)$$

Proof: See Section 2.7.4. ∎
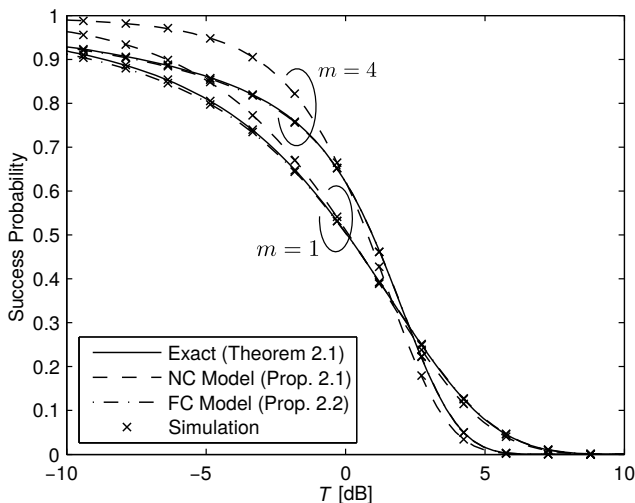
Figure 2.7: Success probability for different $m_{\mathrm{D}} = m_{\mathrm{I}} = m$ (symmetric Nakagami fading). Parameters: $\lambda = 10^{-3}$, $\alpha = 4$, $d = 10$, $\mathtt{SNR} = 0$ dB.

Note that the expression in (2.26) is much simpler than (2.5), since no convolution-type integral over z is present. When m_{I} is large, the exponent in (2.26) can be further simplified noting that $m_{\mathrm{I}}^{-2/\alpha}\Gamma(2/\alpha + m_{\mathrm{I}})/\Gamma(m_{\mathrm{I}}) \to 1$ as $m_{\mathrm{I}} \to \infty$ [66].

Remark 2.4 (Relationship between FC model and IB-MRC). *Assuming equal interference levels at all Rx antennas in IA-MRC yields the same post-combiner $\mathtt{SINR}_{\Sigma}$ as for IB-MRC, which is blind to interference. Consequently, Proposition 2.2 also characterizes the success probability for IB-MRC; this can be verified by comparing (2.26) with [50, Thm. 1 and Eq. (43)]. Thus, the following discussions on IA-MRC under the FC model apply to IB-MRC as well.*

Figure 2.7 compares the success probability for the exact model against the success probability for the NC and FC correlation model. Simulation results confirm the theoretical expressions from Proposition 2.1 and Proposition 2.2. It can be seen that the NC model considerably overestimates $\mathtt{P}_{\mathrm{c}}^{\mathrm{IA}}$ for practically relevant success probability values around 0.9. Interestingly, the gap between $\mathtt{P}_{\mathrm{c}}^{\mathrm{IA}}$ and $\mathtt{P}_{\mathrm{c,NC}}^{\mathrm{IA}}$ increases with the Nakagami

parameter m. This is due to the fact that the de-correlation effect of the channel fading is reduced as m_I increases which, in turn, increases the correlation across the $\{\texttt{SINR}_n\}$. Ignoring correlation as m_I increases hence becomes even more inappropriate as the diversity is significantly overestimated in this case.

In contrast, Fig. 2.7 suggests that the FC model yields a closer approximation to $\texttt{P}_c^{IA}$; the gap between $\texttt{P}_c^{IA}$ and $\texttt{P}_{c,FC}^{IA}$ remains fairly small for practically relevant success probability values. Furthermore, this gap virtually vanishes already for $m_D = m_I = 4$ as the curves for $\texttt{P}_c^{IA}$ and $\texttt{P}_{c,FC}^{IA}$ become indistinguishable, which is due to the smaller fading variability for larger m_I. This intuitive trend observed in Fig. 2.7 is mathematically established in the following.

Corollary 2.5 (Asymptotic equivalence of exact model and FC model for IA-MRC)**.** *The exact model and FC model for IA-MRC become equivalent in terms of success probability as $m_I \to \infty$.*

Proof: See Section 2.7.5. ∎

Corollary 2.5 is particularly useful for justifying the use of the FC model for scenarios where the interfering links undergo poor scattering. The remaining accuracy loss with respect to the exact model can be further studied by looking at the relative success probability deviation, which is defined as $\delta_{\texttt{P}_c}^{FC} \triangleq (\texttt{P}_{c,FC}^{IA} - \texttt{P}_c^{IA})/\texttt{P}_c^{IA} = \texttt{P}_{c,FC}^{IA}/\texttt{P}_c^{IA} - 1$.

Fig 2.8 illustrates the impact of different m_D and m_I on the deviation $\delta_{\texttt{P}_c}^{FC}$ for $\alpha = 3$. For reasonable operating points, e.g., $\texttt{P}_c^{IA} > 0.3$, $\delta_{\texttt{P}_c}^{FC}$ is negative due to the underestimated diversity in the FC model; assuming full interference correlation across Rx antennas reduces the gains of IA-MRC. The maximal gap, however, remains below 5%. Interestingly, $\delta_{\texttt{P}_c}^{FC}$ becomes positive for large T (practically non-relevant $\texttt{P}_c^{IA}$ values, e.g., $\texttt{P}_c^{IA} < 0.3$). This is in line with the findings in [56], where a similar behavior was observed within an interference-limited relay communication scenario. Moreover, reducing fading variance on the interfering links, i.e., increasing m_I, reduces the gap as already seen in Fig. 2.7 for symmetric fading. For asymmetric fading, though, the situation is more complex: while increasing m_I reduces $\delta_{\texttt{P}_c}^{FC}$, increasing m_D results in a larger $\delta_{\texttt{P}_c}^{FC}$. The latter effect is due to the smaller fading variance on the desired link, which renders the "modeling error" associated with the FC model more salient. Although the overall success probability deviation is fairly
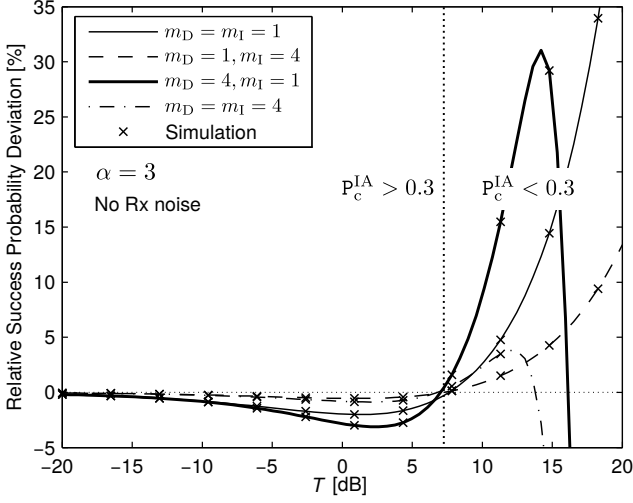
Figure 2.8: Relative success probability deviation $\delta_{\mathrm{P_c}}^{\mathrm{FC}}$ for different m_D, m_I. Parameters: $\alpha = 3$, $\lambda = 10^{-3}$, $d = 10$. No Rx noise.
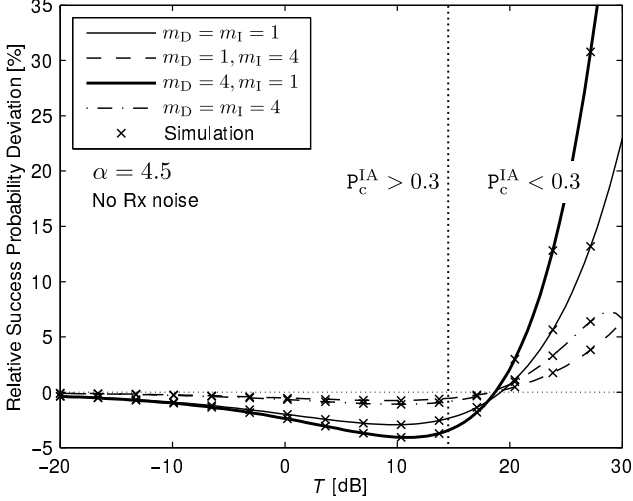
Figure 2.9: Relative success probability deviation $\delta_{\mathrm{P_c}}^{\mathrm{FC}}$ for different m_D, m_I. Parameters: $\alpha = 4.5$, $\lambda = 10^{-3}$, $d = 10$. No Rx noise.
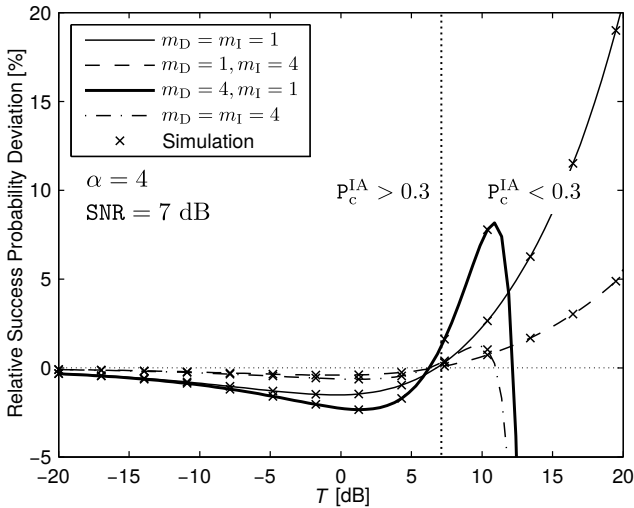
Figure 2.10: Relative success probability deviation $\delta_{P_c}^{FC}$ for different m_D, m_I. Parameters: $\alpha = 4$, $\lambda = 10^{-3}$, $d = 10$, SNR $= 7$ dB.

small, the FC model may hence be inappropriate when fading variance on the desired link is smaller than on the interfering links, e.g., when the desired transmitter pre-compensates for the fading (channel-inversion power control) or uses multiple Tx antennas to smooth out the fading. Varying α and/or including Rx noise does not change the above trends for the success probability deviation as can be seen in Fig. 2.9 and Fig. 2.10.

So far, it has been demonstrated using the exact model that the success probability deviation for the FC model is not overwhelming (still below 5%). In some cases, though, it may be desirable to quantify the performance of a communication system in terms of the complement of P_c, i.e., the *outage probability* $1 - P_c$, see for instance [19, 27]. From a wireless engineer's perspective, it is hence interesting to know in addition the relative outage probability deviation caused by the FC model. Similar to the success probability deviation, it is defined as $\delta_{1-P_c}^{FC} \triangleq (1 - P_{c,FC}^{IA})/(1 - P_c^{IA}) - 1$. The deviation $\delta_{1-P_c}^{FC}$ is shown in Fig. 2.11 and Fig. 2.12 for different α. The same parametrization as in Fig. 2.8 and Fig. 2.9 was chosen. Observe that $\delta_{1-P_c}^{FC}$ is positive in the practical regime as the outage probability is now overestimated in the FC model. While $\delta_{1-P_c}^{FC}$ and $\delta_{P_c}^{FC}$ share the same behavior in m_D, m_I, the deviation is much stronger now. For $\alpha = 4.5$,
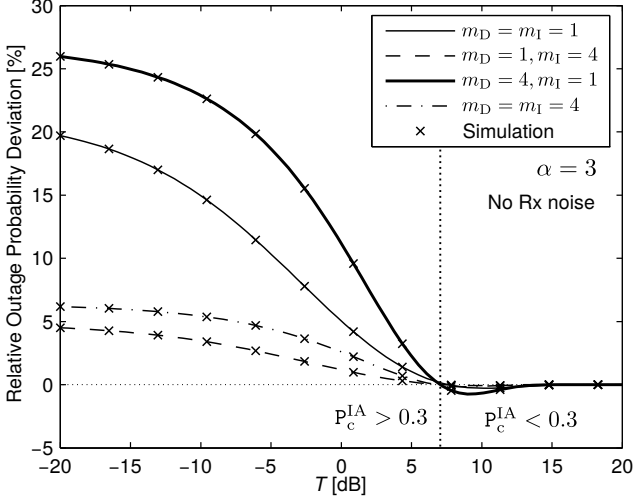
Figure 2.11: Relative outage probability deviation $\delta_{1-P_c}^{FC}$ for FC model for different m_D, m_I. Parameters: $\alpha = 3$, $\lambda = 10^{-3}$, $d = 10$. No Rx noise.
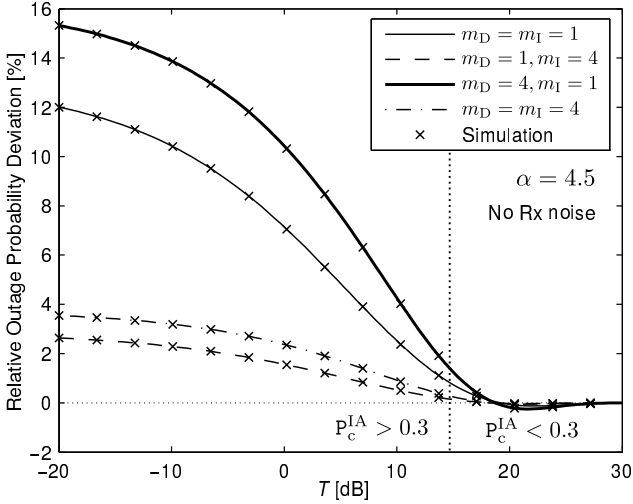
Figure 2.12: Relative outage probability deviation $\delta_{1-P_c}^{FC}$ for FC model for different m_D, m_I. Parameters: $\alpha = 4.5$, $\lambda = 10^{-3}$, $d = 10$. No Rx noise.

the deviation is between 3% and 15%, while for $\alpha = 3$ the deviation is nearly doubled, thereby suggesting that $\delta^{\mathrm{FC}}_{1-\mathrm{P_c}}$ decreases with α in the practical regime.

Recall that the FC model corresponds to IB-MRC in terms of success/outage probability, see Remark 2.4. Thus, large values for $\delta^{\mathrm{FC}}_{\mathrm{P_c}}$ and $\delta^{\mathrm{FC}}_{1-\mathrm{P_c}}$ imply a better performance of IA-MRC relative to IB-MRC.

2.5.2 Diversity Order Analysis

In addition to success/outage probability, the performance of diversity-combining schemes can be studied by analyzing also their *diversity order*, which characterizes the increase in robustness against outage events. In the single-user case without interference, the diversity order is defined as the slope of the error probability plotted against the mean SNR in a log-log fashion [20]. Assuming strong channel coding, e.g., concatenated convolutional codes or Turbo codes, the error probability is a steep function of the SNR, see for instance [76, 77], and the outage probability may then be used instead of the error probability. However, characterizing the diversity order in the multi-user case with random interference is not straightforward, since increasing the mean SINR can be realized in several ways. This problem was discussed in detail in [54], where a specific diversity order formulation was derived for the retransmission scheme. For MRC, a different formulation of the diversity order is needed, which will be the focus next.

Definition 2.4 (Diversity order)**.** *The diversity order is defined as*

$$d \triangleq - \lim_{\mathbb{E}[\mathrm{SINR}_\Sigma] \to \infty} \frac{\log \mathbb{P}(\mathrm{SINR}_\Sigma < T)}{\log \mathbb{E}[\mathrm{SINR}_\Sigma]}. \tag{2.27}$$

Starting from the general expression in Definition 2.4, $\mathbb{E}[\mathrm{SINR}_\Sigma] \to \infty$ in (2.27) can be obtained by introducing a parameter c with $c\,\mathbb{E}[\mathrm{SINR}_\Sigma] = \mathbb{E}[c\,\mathrm{SINR}_\Sigma]$ and letting $c \to \infty$. Then, (2.27) can be rewritten as

$$
\begin{aligned}
d &= - \lim_{c \to \infty} \frac{\log \mathbb{P}(c\,\mathrm{SINR}_\Sigma < T)}{\log \mathbb{E}[c\,\mathrm{SINR}_\Sigma]} \\
&= - \lim_{c \to \infty} \frac{\log \mathbb{P}(\mathrm{SINR}_\Sigma < T/c)}{\log c + \log \mathbb{E}[\mathrm{SINR}_\Sigma]} \\
&\overset{(a)}{=} - \lim_{T' \to 0} \frac{\log \mathbb{P}(\mathrm{SINR}_\Sigma < T')}{\log T - \log T' + \log \mathbb{E}[\mathrm{SINR}_\Sigma]},
\end{aligned} \tag{2.28}
$$

where (a) follows from the substitution $T' = T/c$. Hence, the diversity order d can be obtained by appropriately scaling the SINR threshold T. As an example, consider the SISO case with $N = 1$, for which the asymptotic success probability is given by (2.13). The diversity order for the SISO case is

$$d^{\text{SISO}} = \lim_{T \to 0} \frac{2/\alpha \log T + c_1}{\log T + c_2} = \frac{2}{\alpha}, \tag{2.29}$$

which can be seen as the baseline, i.e., there is no diversity gain at all.

Next, consider the asymptotic success probability for IB-MRC for general N, which is given by [51, (5.24)]

$$\mathsf{P}_c^{\text{IB}} \sim 1 - \pi \lambda y^2 T^{2/\alpha} \kappa_{\text{DI}}^{2/\alpha} \frac{\Gamma(m_{\text{I}} + \frac{2}{\alpha}) \Gamma(Nm_{\text{D}} - \frac{2}{\alpha})}{\Gamma(m_{\text{I}}) \Gamma(Nm_{\text{D}})}. \tag{2.30}$$

Note that although the term *interference-blind* is not explicitly used in [51], (2.30) applies to IB-MRC, since the combining weights depend solely on the fading gains of the desired link, see [51, Sec. 5.5.2] for further details. It can be easily verified that

$$d^{\text{IB-MRC}} = \frac{2}{\alpha}. \tag{2.31}$$

Thus, IB-MRC offers no diversity-order increase compared to the SISO case, irrespective of the number of Rx antennas N. In contrast to IB-MRC, IA-MRC takes into account the interference. However, using (2.18), the diversity order of IA-MRC is

$$d^{\text{IA-MRC}} = \frac{2}{\alpha} \tag{2.32}$$

as well, thus $d^{\text{SISO}} = d^{\text{IB-MRC}} = d^{\text{IA-MRC}}$. Hence, MRC with N Rx antennas does not increase the diversity order in *ad hoc* networks with interference.

The diversity behavior for the various MRC expressions including the NC and FC model is shown in Fig 2.13 for $N = 2$. It can be observed that the outage probability slope for both IB-MRC and IA-MRC is the same as for the SISO case, thereby validating the diversity-order results. Interestingly, while the FC model captures the true diversity order of IA-MRC (which follows from the equivalence with IB-MRC), the NC model does not; the diversity order in this case is doubled, thereby suggesting
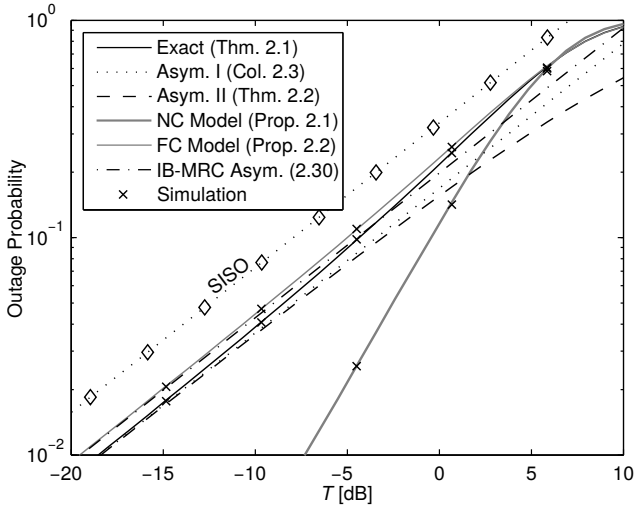
Figure 2.13: Outage probability for dual-antenna IA-MRC (exact, FC, and NC model) and IB-MRC. Parameters: $\lambda = 10^{-3}$, $N = 2$, $d = 10$, $\alpha = 3.5$, $m_D = 4$, $m_I = 1.5$. No Rx noise.

that IA-MRC achieves full diversity. However, since the NC model ignores the interference correlation across Rx antennas, the diversity that can be harvested is greatly overestimated, which explains this misleading result. This observation underlines the fact that ignoring interference correlation may significantly distort the true performance of IA-MRC.

2.5.3 Spatial Throughput

From the results obtained in the prior sections it is apparent that adding more nodes increases the interference, and hence worsens the post-combiner SINR. In wireless *ad hoc* networks it is desirable to know the number of transmissions per unit area that can be supported over a target distance y subject to a quality-of-service constraint, i.e., the spatial throughput. The target-distance assumption is known in the literature as the "dipole model" [36, Chap. 16.2] and is commonly used for studying the spatial throughput in wireless networks, see for instance [42]. Given a target outage probability $\epsilon \triangleq \mathbb{P}(\texttt{SINR}_\Sigma < T)$, the *critical density* λ_ϵ is the maximum allowable density of simultaneous transmissions over distance

y with probability of failure $\epsilon \in (0, 1)$. For $N = 2$, λ_ϵ can be obtained by numerically solving $1 - \text{P}_c^{\text{IA}}$ for λ in (2.5). For sufficiently small ϵ, the asymptotic expression from (2.18) can be used instead for an analytical solution. Note that the success probability is monotonically decreasing in λ [42].

Figure 2.14 shows the critical density gain of IA-MRC and IB-MRC over SISO systems for different N and $m_{\text{D}} = m_{\text{I}} = 1$ (symmetric Rayleigh fading). The SISO outage probability for symmetric Rayleigh fading is [42, 78]

$$1 - \text{P}_c^{\text{SISO}} = \exp\left(-\lambda \pi^2 y^2 T^{2/\alpha} \frac{2}{\alpha} \csc\left(\frac{2\pi}{\alpha}\right)\right), \qquad (2.33)$$

which is a special case of Proposition 2.2 with $N = 1$. For general $m_{\text{D}}, m_{\text{I}}$ and sufficiently small ϵ, the SISO critical density may be obtained using the first term in (2.10). Solving (2.33) for λ yields

$$\lambda_\epsilon^{\text{SISO}} = \frac{-\alpha \log(1 - \epsilon)}{2\pi^2 y^2 T^{2/\alpha} \csc(2\pi/\alpha)}. \qquad (2.34)$$

The critical density gain is then defined as $\Delta_{\lambda_\epsilon}^{\text{IA-MRC-SISO}} \triangleq \lambda_\epsilon^{\text{IA-MRC}} / \lambda_\epsilon^{\text{SISO}}$ and $\Delta_{\lambda_\epsilon}^{\text{IB-MRC-SISO}} \triangleq \lambda_\epsilon^{\text{IB-MRC}} / \lambda_\epsilon^{\text{SISO}}$ for the respective MRC expressions. As expected, multiple-antenna receivers employing MRC increase the critical density compared to SISO receivers; for the same target outage probability ϵ, more concurrent transmissions can take place simultaneously due to a higher link reliability. This gain is considerably larger for IA-MRC than for IB-MRC as the number of Rx antennas N grows. For $N = 8$ Rx antennas, IA-MRC yields an 7-fold critical density increase, while for IB-MRC the increase is approximately 4.5 in this example. Interestingly, Fig. 2.14 reveals a sublinear growth of the critical density gain in N in this example. A first-order approximation indicates that the scaling is proportional to $\sqrt{N}$ in the case of IA-MRC.

While the critical density λ_ϵ can characterize the maximal allowable number of concurrent transmissions per unit area, it cannot tell whether the parameter pair $(\epsilon, \lambda_\epsilon)$ leads to an *efficient* network operation point. The *transmission capacity* is another spatial throughput metric for wireless *ad hoc* networks, which takes into account also the probability of success. It is defined as the maximum number of concurrent transmissions that
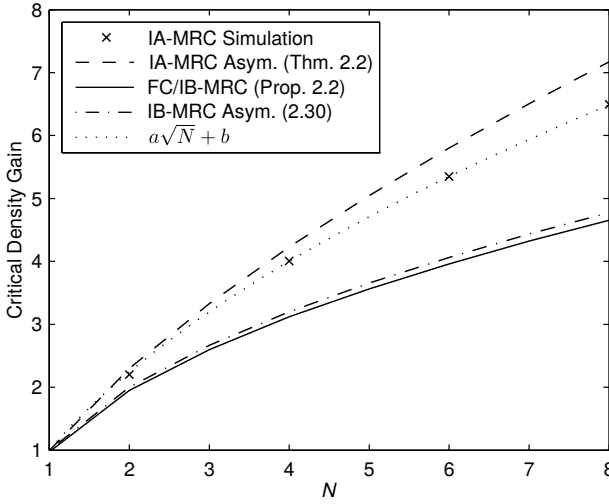
Figure 2.14: Critical density gain $\Delta_{\lambda_\epsilon}^{\text{IA-MRC-SISO}}$ and $\Delta_{\lambda_\epsilon}^{\text{IB-MRC-SISO}}$ versus N. Parameters: $\epsilon = 0.05$, $\alpha = 4$, $d = 15$, $T = 1$, $m_\text{D} = m_\text{I} = 1$ (symmetric Rayleigh fading), no Rx noise. Curve fitting coefficients are $a = 3$ and $b = -2$.
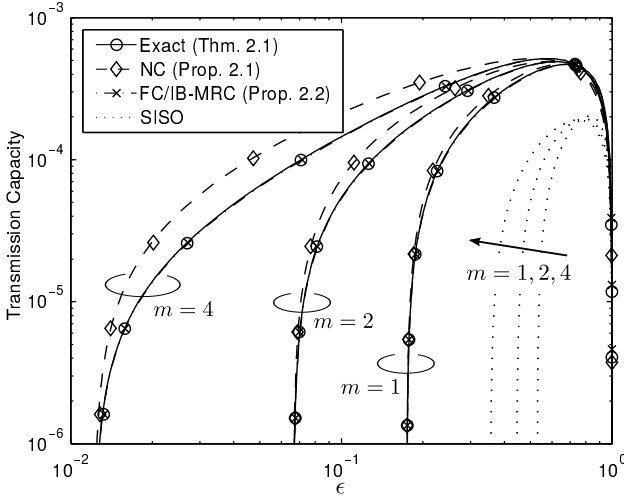
Figure 2.15: Transmission capacity $c(\epsilon)$ versus target outage probability ϵ for different $m_\text{D} = m_\text{I} = m$ (symmetric Nakagami fading). Parameters: $T = 3$, $N = 2$, $d = 10$, $\alpha = 4$, SNR $= 6$ dB. Marks represent simulation results.

can take place simultaneously subject to a target outage probability ϵ, weighted by the resulting probability of success $1 - \epsilon$ [42], i.e.,

$$\mathtt{TC}(\epsilon) \triangleq (1 - \epsilon)\lambda_\epsilon. \tag{2.35}$$

The reader is referred to [42, 46] for further discussions on the transmission capacity metric. While the effect of increasing the number of Rx antennas N on the spatial throughput was already discussed in Fig. 2.14, the influence of the Nakagami fading parameter m is studied next for symmetric Nakagami fading and $N = 2$.

Figure 2.15 shows the $\mathtt{TC}(\epsilon)$ for dual-antenna IA-MRC for different m (symmetric Nakagami fading). In agreement with the observations made in Section 2.5.1, the NC model yields a significantly optimistic result for IA-MRC while the FC model is slightly pessimistic. Interestingly, while the accuracy loss of the NC model increases with the Nakagami parameter m, as expected, the transmission capacity gap between the FC and the exact model remains fairly small even for $m = 1$. Recalling that the FC model corresponds to IB-MRC, this, in turn, means that IA-MRC and IB-MRC have similar performance in terms of transmission capacity. The SISO case is also shown for reference. As can be seen, switching from SISO to dual-antenna MRC offers the possibility to operate the network at smaller target outage probabilities ϵ as a result of the higher link reliability. This improvement further increases with the Nakagami parameter m due to higher robustness against fading induced outages.

2.5.4 Comparison with other Combining Schemes

Besides MRC there exist also other diversity-combining techniques, which differ in both performance and implementation complexity. The latter is generally dictated by system design and hardware requirements and hence, does not change with the communication environment. This, however, is not true for the performance since different assumptions about the communication environment may lead to significantly different performance outcomes. To better understand the performance-complexity trade-offs of diversity-combining techniques, it is hence essential to compare their performance under realistic model assumptions, such as correlated interference. In the following, the performance of MRC is compared with two other popular schemes, namely IA-SC and MMSE combining.

In IA-SC, only the Rx antenna providing the highest instantaneous $\mathtt{SINR}_n$ is selected among all N Rx antennas [19]. Since the incoming signals do not have to be coherently combined, IA-SC exhibits a lower complexity compared to MRC, though at the cost of lower performance. In [55], the success probability for IA-SC under PPP modeled interference was derived for symmetric Rayleigh fading ($m_\mathrm{D} = m_\mathrm{I} = 1$) and absence of Rx noise ($\mathtt{SNR} \to \infty$) as

$$\mathrm{P}_\mathrm{c}^\mathrm{SC} = \sum_{n=1}^{N} \binom{N}{n} (-1)^{n+1} \exp\left(-\lambda \pi^2 y^2 T^{2/\alpha} \frac{2}{\alpha} \csc\left(\frac{2\pi}{\alpha} \right) D_n\left(\frac{2}{\alpha} \right) \right), (2.36)$$

where $D_n(x) \triangleq \prod_{i=1}^{n-1}(1 + x/i)$ is called the *diversity polynomial*.

In MMSE combining, the weights are chosen so as to maximize the post-combiner SINR under knowledge of the interference correlation matrix. Because it maximizes the post-combiner SINR, MMSE combining is also referred to as *optimum combining* [13]. Since the interferer correlation matrix must be estimated, e.g., by decoding the pilot symbols from interfering transmitters, MMSE is more complex than MRC. The success probability for MMSE combining under PPP modeled interference with symmetric Rayleigh fading ($m_\mathrm{D} = m_\mathrm{I} = 1$) was derived in [79] as

$$\mathrm{P}_\mathrm{c}^\mathrm{MMSE} = \frac{\Gamma\left(N, \lambda \pi^2 y^2 T^{2/\alpha} \frac{2}{\alpha} \csc\left(\frac{2\pi}{\alpha} \right) + \frac{T}{\mathtt{SNR}} \right)}{\Gamma(N)}, \tag{2.37}$$

where $\Gamma(a, z) = \int_z^\infty t^{a-1} e^{-t} \mathrm{d}t$ is the upper incomplete Gamma function.

Note that similar success probability expressions for IA-SC and MMSE combining for Nakagami fading with general $m_\mathrm{D}, m_\mathrm{I}$ are currently not available in the literature.

Figure 2.16 compares the success probability for IA-MRC, IB-MRC, IA-SC, and MMSE combining for $m_\mathrm{D} = m_\mathrm{I} = 1$ (symmetric Rayleigh fading) for different path loss exponents α. The results for IB-MRC were obtained using Proposition 2.2 for the FC model, see Remark 2.4. As expected, the performance of both IA-MRC and IB-MRC is between IA-SC on the lower and MMSE combining on the upper. Interestingly, the success probabilities of MRC and MMSE combining become similar as α decreases. This result suggests that for small path loss exponents, almost no improvement is obtained from estimating the interference correlation matrix and adapting the combining weights accordingly (MMSE combining), compared to
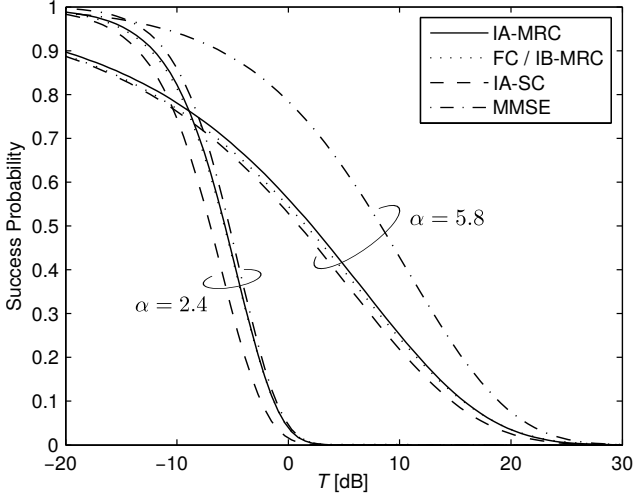
Figure 2.16: Success probability for different α. Parameters: $\lambda = 10^{-3}$, $N = 2$, $m_\mathrm{D} = m_\mathrm{I} = 1$ (symmetric Rayleigh fading), $d = 15$, no Rx noise.
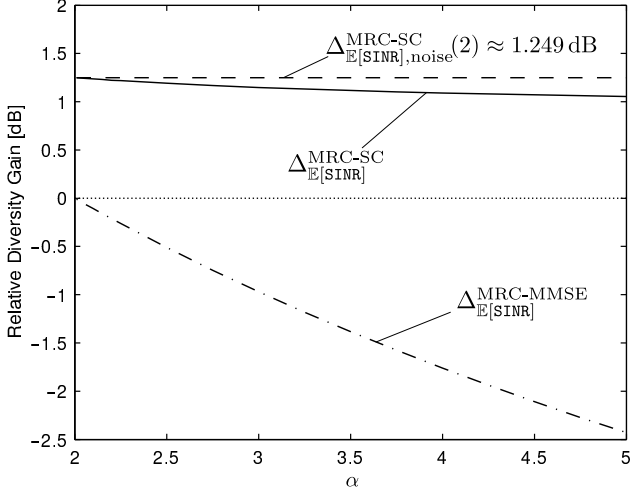
Figure 2.17: Average SINR gains $\Delta_{\mathbb{E}[\mathrm{SINR}]}^{\mathrm{MRC\text{-}SC}}$ and $\Delta_{\mathbb{E}[\mathrm{SINR}]}^{\mathrm{MRC\text{-}MMSE}}$ versus α. Parameters: $\lambda = 10^{-3}$, $N = 2$, $y = 15$, $m_\mathrm{D} = m_\mathrm{I} = 1$ (symmetric Rayleigh fading), no Rx noise.

computing the weights individually for all Rx antennas (MRC). Such a strong dependence on the path loss exponent is not observed when comparing MRC to IA-SC; the horizontal width of the success probability gap varies no more than about 1.2 dB over a wide range of SINR thresholds T independent of α. These observations are further elucidated in Fig. 2.17, which shows the gain of MRC over IA-SC and MMSE combining in terms of the post-combiner SINR, i.e., $\Delta^{\text{MRC-SC}}_{\mathbb{E}[\text{SINR}]} \triangleq \mathbb{E}[\text{SINR}_\Sigma]/\mathbb{E}[\text{SINR}_{\text{SC}}]$ and $\Delta^{\text{MRC-MMSE}}_{\mathbb{E}[\text{SINR}]} \triangleq \mathbb{E}[\text{SINR}_\Sigma]/\mathbb{E}[\text{SINR}_{\text{MMSE}}]$ versus α. The above expectations are obtained using the relation $\mathbb{E}[\mathsf{z}] = \int_0^\infty \mathbb{P}(\mathsf{z} > z)\,\mathrm{d}z$. Note that the average post-combiner SINR for IA-MRC is the same as for IB-MRC due to the *linearity* property of the expectation. It can be seen that $\Delta^{\text{MRC-MMSE}}_{\mathbb{E}[\text{SINR}]}$ plotted in dB decreases almost linearly in α. The gain of MRC over IA-SC is roughly 1.1 dB for practically relevant path loss exponents around $\alpha = 3.5$. This gain over IA-SC, however, is always smaller than in the well-studied interference-free case; in the latter, the gain for Rayleigh fading ($m = 1$) can be expressed in terms of the harmonic series as $\Delta^{\text{MRC-SC}}_{\mathbb{E}[\text{SINR}],\text{noise}}(N) \triangleq N(\sum_{n=1}^N 1/n)^{-1}$ for arbitrary number of Rx antennas N [19, Sec. 7.2.2], yielding $\Delta^{\text{MRC-SC}}_{\mathbb{E}[\text{SINR}],\text{noise}}(2) \approx 1.249$ dB for $N = 2$. The fact that $\Delta^{\text{MRC-SC}}_{\mathbb{E}[\text{SINR}]} \leq \Delta^{\text{MRC-SC}}_{\mathbb{E}[\text{SINR}],\text{noise}}(N)$ for arbitrary N can be easily verified using Jensen's inequality [80], since

$$
\begin{aligned}
\Delta^{\text{MRC-SC}}_{\mathbb{E}[\text{SINR}]} &= \frac{\mathbb{E}\left[\frac{\mathsf{g}_{o,1}}{\mathsf{I}_1} + \ldots + \frac{\mathsf{g}_{o,N}}{\mathsf{I}_N}\right]}{\mathbb{E}_{\{\mathsf{g}_{o,n}\}}\left[\mathbb{E}_{\{\mathsf{I}_n\}}\left[\max\left\{\frac{\mathsf{g}_{o,1}}{\mathsf{I}_1}, \ldots, \frac{\mathsf{g}_{o,N}}{\mathsf{I}_N}\right\}\right]\right]} \\
&\overset{(a)}{\leq} \frac{N\mathbb{E}\left[\frac{\mathsf{g}_o}{\mathsf{I}}\right]}{\mathbb{E}_{\{\mathsf{g}_{o,n}\}}\left[\max\left\{\mathbb{E}_{\mathsf{I}_1}\left[\frac{\mathsf{g}_{o,1}}{\mathsf{I}_1}\right], \ldots, \mathbb{E}_{\mathsf{I}_N}\left[\frac{\mathsf{g}_{o,N}}{\mathsf{I}_N}\right]\right\}\right]} \\
&\overset{(b)}{=} \frac{\mathbb{E}_{\mathsf{I}}\left[\mathsf{I}^{-1}\right] N \mathbb{E}[\mathsf{g}_o]}{\mathbb{E}_{\mathsf{I}}\left[\mathsf{I}^{-1}\right] \mathbb{E}_{\{\mathsf{g}_{o,n}\}}\left[\max\left\{\mathsf{g}_{o,1}, \ldots, \mathsf{g}_{o,N}\right\}\right]} \\
&= \Delta^{\text{MRC-SC}}_{\mathbb{E}[\text{SINR}],\text{noise}}(N),
\end{aligned}
\tag{2.38}
$$

where (a) follows from the fact that $\mathsf{g}_{o,1}/\mathsf{I}_1, \ldots, \mathsf{g}_{o,N}/\mathsf{I}_N$ and hence, the max function are convex in $\mathsf{I}_1, \ldots, \mathsf{I}_N$, and by Jensen's inequality, (b) follows from the $\{\mathsf{I}_n\}$ being identically distributed and independent of the $\{\mathsf{g}_{o,n}\}$. Note that the inequality in (a) applies to general fading distributions. Interestingly, it can be seen that $\Delta^{\text{MRC-SC}}_{\mathbb{E}[\text{SINR}]} \to \Delta^{\text{MRC-SC}}_{\mathbb{E}[\text{SINR}],\text{noise}}(2) \approx$ 1.249 dB as $\alpha \to 2$. This can be explained by the fact that as $\alpha \to 2$, the $\{\mathsf{I}_n\}$ degenerate to $\mathsf{I}_n \equiv \infty$ almost surely [38]; for a degenerate random variable, Jensen's inequality becomes an equality.
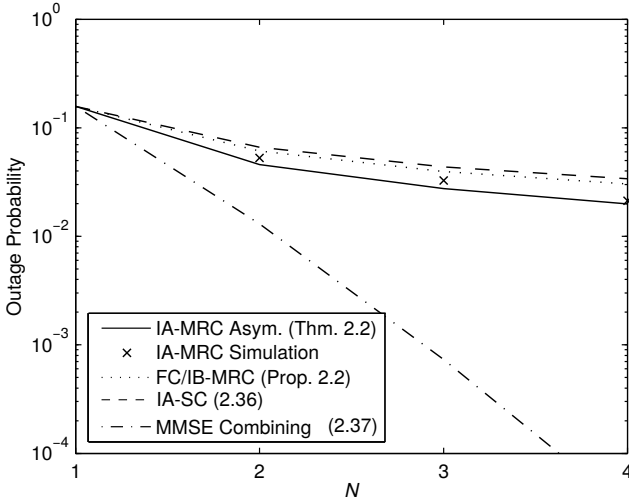
Figure 2.18: Success probability versus number of Rx antennas N. Parameters: $\lambda = 10^{-4}$, $m_{\mathrm{D}} = m_{\mathrm{I}} = 1$ (symmetric Rayleigh fading), $d = 15$, $\alpha = 3$, $T = 1$, no Rx noise.

The effect of increasing the number of Rx antennas N on the outage probability is shown in Fig. 2.18 for the considered diversity schemes. As expected, MMSE combining, which takes into account the interference correlation across Rx antennas, performs best. In contrast to MRC and IA-SC, MMSE combining can significantly decrease outage probability by using more Rx antennas, which is in line with the findings obtained in [79]. Interestingly, MRC and IA-SC follow a similar outage probability scaling law with N. This suggests that considerable gains using multi-antenna receivers can be obtained only by leveraging the interference correlation structure in the computation of the combining weights, as done in MMSE combining.

2.6 Summary

In this chapter, a theoretical framework for analyzing the performance of IA-MRC in wireless *ad hoc* networks under fairly general model assumptions was derived. The analysis led to tractable expressions, which were

further used to obtain several insights for both network modeling and network design. For instance, while the NC model leads to a considerably distorted performance evaluation of IA-MRC, the FC model provides a reasonably tight approximation to the true performance whenever the fading variance is low and/or the path loss exponent is large. This result justifies the use of the FC model and could help studying also other combining schemes, which would otherwise not be tractable when considering the exact correlation structure. Since the FC model corresponds to IB-MRC in terms of post-combiner SINR, it follows that IB-MRC may be the better choice in radio environments with poor scattering and/or high path loss exponent due to its lower complexity compared to IA-MRC. Furthermore, a performance comparison between MRC, IA-SC, and MMSE combining demonstrated that system design should factor in the particular nature of the channel before deciding which combining scheme to select in order to find the optimal performance-complexity trade-off. For instance, in scenarios with small path loss exponents, IA-MRC achieves almost the same performance as MMSE combining though with less complexity. Similarly, at large path loss exponents, IA-SC may be more favorable than MRC due to their similar performance.

2.7 Proofs

2.7.1 Proof of Theorem 2.1

Consider the random variable

$$\mathtt{SINR}_2 = \frac{\mathsf{g}_{o,2}}{\mathsf{I}_2 + \mathtt{SNR}^{-1}} \tag{2.39}$$

and condition $\mathtt{P}_{\mathrm{c}}^{\mathrm{IA}}$ on the point process Φ and $\mathtt{SINR}_2$, yielding

$$\mathtt{P}_{\mathrm{c}}^{\mathrm{IA}} = \mathbb{E}_{\Phi,\mathtt{SINR}_2}\left[\mathbb{P}\left(\mathsf{g}_{o,1} \geq (T - \mathtt{SINR}_2)(\mathsf{I}_1 + \mathtt{SNR}^{-1})\,\middle|\,\Phi,\mathtt{SINR}_2\right)\right]. \tag{2.40}$$

The conditional success probability in (2.40) can be written as

$$\mathbb{P}\left(\mathsf{g}_{o,1} \geq (T - \mathtt{SINR}_2)(\mathsf{I}_1 + \mathtt{SNR}^{-1})\,\middle|\,\Phi,\mathtt{SINR}_2\right)$$
$$= \mathbb{E}_{\mathsf{I}_1}\left[\mathbb{P}\left(\mathsf{g}_{o,1} \geq (T - \mathtt{SINR}_2)(\mathsf{I}_1 + \mathtt{SNR}^{-1})\,\middle|\,\Phi,\mathtt{SINR}_2,\mathsf{I}_1\right)\right]$$

$$\stackrel{(a)}{=} \mathbb{E}_{I_1} \left[\sum_{k=0}^{m_D-1} \frac{\psi_1^k}{k!} (I_1 + \text{SNR}^{-1})^k \exp\left(-\psi_1(I_1 + \text{SNR}^{-1})\right) \right]$$

$$\stackrel{(b)}{=} \sum_{k=0}^{m_D-1} \frac{(-1)^k}{k!} \mathbb{E}_{I_1} \left[(-1)^k Y^k e^{-Y} \right]$$

$$\stackrel{(c)}{=} \sum_{k=0}^{m_D-1} \frac{(-1)^k}{k!} \frac{d^k}{ds^k} \left[\mathcal{L}_Y(s) \right]_{s=1}. \tag{2.41}$$

(a) follows from the fact that $\mathbf{g}_{o,1}$ is Gamma distributed with shape m_D and rate m_D, see Definition A.1, and from the substitution $\psi_1 \triangleq (T - \text{SINR}_2)^+ m_D$. (b) follows from the substitution $Y \triangleq \psi_1(I_1 + \text{SNR}^{-1})$, and (c) is a result of the differentiation property for Laplace transforms [80, Sec. XIII.2].

The Laplace transform $\mathcal{L}_Y(s)$ is obtained as

$$\mathcal{L}_Y(s) = \mathbb{E}_{\{\mathbf{g}_{i,1}\}} \left[\exp\left(-s\psi_1 \left(\text{SNR}^{-1} + \sum_{x_i \in \Phi} \mathbf{g}_{i,1} \frac{y^\alpha}{\|x_i\|^\alpha} \right) \right) \right]$$

$$\stackrel{(a)}{=} \exp\left(-\frac{s\psi_1}{\text{SNR}} \right) \prod_{x_i \in \Phi} \mathbb{E}_{\mathbf{g}_{i,1}} \left[\exp\left(-s\psi_1 \mathbf{g}_{i,1} \frac{y^\alpha}{\|x_i\|^\alpha} \right) \right] \tag{2.42}$$

where (a) follows from the *i.i.d.* property of the $\{\mathbf{g}_{i,n}\}$. With (2.42), (2.41) can hence be rewritten as

$$\mathbb{P}\left(\mathbf{g}_{o,1} \geq (T - \text{SINR}_2)(I_1 + \text{SNR}^{-1}) \,\middle|\, \Phi, \text{SINR}_2 \right)$$
$$= \sum_{k=0}^{m_D-1} \frac{(-1)^k}{k!} \frac{d^k}{ds^k} \left[\exp\left(-\frac{s\psi_1}{\text{SNR}} \right) \prod_{x_i \in \Phi} \mathbb{E}_{\mathbf{g}_{i,1}} \left[\exp\left(-\frac{s\mathbf{g}_{i,1}\psi_1 y^\alpha}{\|x_i\|^\alpha} \right) \right] \right]_{s=1}. \tag{2.43}$$

In order to de-condition (2.43) on SINR_2 conditional on Φ, the PDF $f_{\text{SINR}_2|\Phi}(z)$ is first needed. It is obtained as

$$f_{\text{SINR}_2|\Phi}(z)$$
$$= \frac{d}{dz} \mathbb{P}\left(\text{SINR}_2 \leq z | \Phi \right)$$
$$= \frac{d}{dz} \mathbb{E}_{I_2} \left[\mathbb{P}\left(\mathbf{g}_{o,2} \leq z \left(I_2 + \text{SNR}^{-1} \right) \middle| \Phi \right) \right]$$
$$\stackrel{(a)}{=} \frac{d}{dz} \mathbb{E}_{I_2} \left[\frac{1}{\Gamma(m_D)} \gamma\left(m_D, zm_D \left(I_2 + \text{SNR}^{-1} \right) \right) \right]$$

$$\overset{\text{(b)}}{=} \mathbb{E}_{\mathsf{l}_2}\left[\frac{1}{\Gamma(m_{\mathrm{D}})}\frac{\mathrm{d}}{\mathrm{d}z}\gamma\left(m_{\mathrm{D}},\psi_2\left(\mathsf{l}_2+\mathtt{SNR}^{-1}\right)\right)\right]$$

$$\overset{\text{(c)}}{=} \frac{1}{z\,\Gamma(m_{\mathrm{D}})}\mathbb{E}_{\mathsf{l}_2}\left[\psi_2^{m_{\mathrm{D}}}(\mathsf{l}_2+\mathtt{SNR}^{-1})^{m_{\mathrm{D}}}\exp\left(-\psi_2(\mathsf{l}_2+\mathtt{SNR}^{-1})\right)\right]$$

$$\overset{\text{(d)}}{=} \frac{(-1)^{m_{\mathrm{D}}}}{z\,\Gamma(m_{\mathrm{D}})}\frac{\mathrm{d}^{m_{\mathrm{D}}}}{\mathrm{d}t^{m_{\mathrm{D}}}}\left[\exp\left(-\frac{t\psi_2}{\mathtt{SNR}}\right)\prod_{\mathsf{x}_i\in\Phi}\mathbb{E}_{\mathsf{g}_{i,2}}\left[\exp\left(-\frac{t\mathsf{g}_{i,2}\psi_2 y^\alpha}{\|\mathsf{x}_i\|^\alpha}\right)\right]\right]_{t=1},$$

$$(2.44)$$

where (a) follows from (A.2), (b) is allowed by the dominated convergence theorem [81], (c) follows from the relation $\mathrm{d}\gamma(a,x)/\mathrm{d}x = x^{a-1}e^{-x}$ [66] and from substituting $\psi_2 \triangleq zm_{\mathrm{D}}$, and (d) follows from applying the same technique for obtaining (2.42) and (2.43). Substituting (2.43) and (2.44) into (2.40), $\mathtt{P}_{\mathrm{c}}^{\mathrm{IA}}$ can be written as

$$\mathbb{E}_{\Phi,\mathtt{SINR}_2}\left[\sum_{k=0}^{m_{\mathrm{D}}-1}\frac{(-1)^k}{k!}\frac{\mathrm{d}^k}{\mathrm{d}s^k}\left[e^{-\frac{s\psi_1}{\mathtt{SNR}}}\prod_{\mathsf{x}_i\in\Phi}\mathbb{E}_{\mathsf{g}_{i,1}}\left[\exp\left(-\frac{s\mathsf{g}_{i,1}\psi_1 y^\alpha}{\|\mathsf{x}_i\|^\alpha}\right)\right]\right]_{s=1}\right]$$

$$= \sum_{k=0}^{m_{\mathrm{D}}-1}\frac{(-1)^k}{k!}\mathbb{E}_{\Phi,\mathtt{SINR}_2}\left[\frac{\mathrm{d}^k}{\mathrm{d}s^k}\left[\exp\left(-\frac{s\psi_1}{\mathtt{SNR}}\right)\right.\right.$$

$$\left.\left.\times\prod_{\mathsf{x}_i\in\Phi}\mathbb{E}_{\mathsf{g}_{i,1}}\left[\exp\left(-\frac{s\mathsf{g}_{i,1}\psi_1 y^\alpha}{\|\mathsf{x}_i\|^\alpha}\right)\right]\right]_{s=1}\right]$$

$$= \sum_{k=0}^{m_{\mathrm{D}}-1}\frac{(-1)^k}{k!}\int_0^\infty\frac{(-1)^{m_{\mathrm{D}}}}{z\,\Gamma(m_{\mathrm{D}})}\mathbb{E}_{\Phi}\left[\frac{\mathrm{d}^k}{\mathrm{d}s^k}\left[\exp\left(-\frac{s\psi_1}{\mathtt{SNR}}\right)\right.\right.$$

$$\left.\left.\times\prod_{\mathsf{x}_i\in\Phi}\mathbb{E}_{\mathsf{g}_{i,1}}\left[\exp\left(-\frac{s\mathsf{g}_{i,1}\psi_1 y^\alpha}{\|\mathsf{x}_i\|^\alpha}\right)\right]\right]_{s=1}f_{\mathtt{SINR}_2|\Phi}(z)\right]\mathrm{d}z$$

$$\overset{\text{(a)}}{=} \sum_{k=0}^{m_{\mathrm{D}}-1}\frac{(-1)^{k+m_{\mathrm{D}}}}{k!\,\Gamma(m_{\mathrm{D}})}\int_0^\infty z^{-1}\frac{\partial^{k+m_{\mathrm{D}}}}{\partial s^k\partial t^{m_{\mathrm{D}}}}\left[\exp\left(-\frac{s\psi_1}{\mathtt{SNR}}-\frac{t\psi_2}{\mathtt{SNR}}\right)\right.$$

$$\left.\times\mathbb{E}_{\Phi}\left[\prod_{\mathsf{x}_i\in\Phi}\mathbb{E}_{\mathsf{g}_{i,1}}\left[e^{-\mathsf{g}_{i,1}\frac{s\psi_1 y^\alpha}{\|\mathsf{x}_i\|^\alpha}}\right]\mathbb{E}_{\mathsf{g}_{i,2}}\left[e^{-\mathsf{g}_{i,2}\frac{t\psi_2 y^\alpha}{\|\mathsf{x}_i\|^\alpha}}\right]\right]\right]_{\substack{s=1\\t=1}}\mathrm{d}z$$

$$\overset{\text{(b)}}{=} \sum_{k=0}^{m_{\mathrm{D}}-1}\frac{(-1)^{k+m_{\mathrm{D}}}}{k!\,\Gamma(m_{\mathrm{D}})}\int_0^\infty z^{-1}$$

$$\times\frac{\partial^{k+m_{\mathrm{D}}}}{\partial s^k\partial t^{m_{\mathrm{D}}}}\left[\exp\left(-\frac{s\psi_1}{\mathtt{SNR}}-\frac{t\psi_2}{\mathtt{SNR}}-\pi\lambda\mathcal{A}(z,s,t)\right)\right]_{\substack{s=1\\t=1}}\mathrm{d}z,\ (2.45)$$

where (a) follows from the dominated convergence theorem [81] and (b) follows from the Probability Generating Functional (PGFL) for PPPs, see Theorem A.3, where

$$\mathcal{A}(z,s,t) = \int_0^\infty 2r \left(1 - \mathbb{E}_{\mathsf{g}_1}\left[\exp\left(-\frac{s\mathsf{g}_1\psi_1 y^\alpha}{\|\mathsf{x}_i\|^\alpha}\right)\right]\right.$$
$$\left.\times \mathbb{E}_{\mathsf{g}_2}\left[\exp\left(-\frac{t\mathsf{g}_2\psi_2 y^\alpha}{\|\mathsf{x}_i\|^\alpha}\right)\right]\right) \mathrm{d}r. \quad (2.46)$$

Using the same approach as in [49, Chap. 3.2], i.e., evaluating the integral over r first, (2.46) becomes

$$\mathcal{A}(z,s,t) = y^2 \, \Gamma(1 - 2/\alpha) \, \mathbb{E}_{\mathsf{g}_1,\mathsf{g}_2}\left[(s\psi_1\mathsf{g}_1 + t\psi_2\mathsf{g}_2)^{2/\alpha}\right]. \quad (2.47)$$

For $z \geq T$, one has $\psi_1 = 0$. Using Lemma A.1, (2.47) then reduces to

$$\mathcal{A}(z,s,t) = (m_{\mathrm{D}}zt)^{2/\alpha} \, y^2 \, \Gamma(1 - 2/\alpha) \, \frac{\Gamma(2/\alpha + m_{\mathrm{I}})}{m_{\mathrm{I}}^{2/\alpha}\Gamma(m_{\mathrm{I}})}. \quad (2.48)$$

For $0 \leq z \leq T$, the expectation in (2.47) can be obtained by invoking Lemma A.4 for computing fractional moments. For this, the Laplace transform of $\mathsf{G} \triangleq s\psi_1\mathsf{g}_1 + t\psi_2\mathsf{g}_2$ is first considered. Using Lemma A.2, this is obtained as

$$\mathcal{L}_{\mathsf{G}}(u) = \mathbb{E}\left[\exp\left(-u\mathsf{G}\right)\right]$$
$$\overset{(a)}{=} \mathbb{E}_{\mathsf{g}_1}\left[\exp\left(-us\psi_1\mathsf{g}_1\right)\right] \mathbb{E}_{\mathsf{g}_2}\left[\exp\left(-ut\psi_2\mathsf{g}_2\right)\right]$$
$$\overset{(b)}{=} \left(1 + \frac{us\psi_1}{m_{\mathrm{I}}}\right)^{-m_{\mathrm{I}}} \left(1 + \frac{ut\psi_2}{m_{\mathrm{I}}}\right)^{-m_{\mathrm{I}}}, \quad (2.49)$$

where (a) follows from the *i.i.d.* property of g_1 and g_2, and (b) follows from the Laplace transform for Gamma distributed random variables, see Lemma A.2. With (2.49) and Lemma A.4, the expectation in (2.47) can then be calculated as

$$\mathbb{E}_{\mathsf{g}_1,\mathsf{g}_2}\left[\mathsf{G}^{2/\alpha}\right] = \frac{2/\alpha}{\Gamma(1 - \frac{2}{\alpha})} \int_0^\infty \frac{1 - \mathcal{L}_{\mathsf{G}}(u)}{u^{1+2/\alpha}} \, \mathrm{d}u$$
$$= (s\kappa_{\mathrm{DI}}(T - z))^{2/\alpha} \, \Gamma(\tfrac{2}{\alpha} + 2m_{\mathrm{I}})$$
$$\times {}_2\mathbf{F}_1\left(-\tfrac{2}{\alpha}, m_{\mathrm{I}}, 2m_{\mathrm{I}}; 1 - \tfrac{zt}{(T-z)s}\right), \quad (2.50)$$

where $_2\mathbf{F}_1(a, b, c; z) \triangleq {}_2F_1(a, b, c; z) / \Gamma(c)$ is the *regularized* Gaussian hypergeometric function [66]. Hence, for $0 \le z \le T$,

$$
\mathcal{A}(z, s, t) = (s\kappa_{\mathrm{DI}}(T - z))^{2/\alpha} y^2 \Gamma(1 - \tfrac{2}{\alpha})\Gamma(\tfrac{2}{\alpha} + 2m_{\mathrm{I}})
$$
$$
\times {}_2\mathbf{F}_1\Big(-\tfrac{2}{\alpha}, m_{\mathrm{I}}, 2m_{\mathrm{I}}; 1 - \tfrac{zt}{(T-z)s}\Big). \tag{2.51}
$$

Combining (2.48), (2.51), and (2.45) finally yields the result.

2.7.2 Proof of Theorem 2.2

The dominant-interferer set $\mathcal{D}$ can be interpreted as another PPP on $\mathbb{R}^2$ obtained by independent thinning of the original PPP Φ, see Lemma A.5. Thus, $\mathrm{P}_{\mathrm{c,dom}}^{\mathrm{IA}}$ in (2.16) is simply the void probability for this new PPP, i.e., the probability of having no points in $\mathbb{R}^2$. Since the number of points in $\mathcal{D}$ is Poisson distributed, this probability becomes

$$
\mathrm{P}_{\mathrm{c,dom}}^{\mathrm{IA}} = \mathbb{P}\left(|\mathcal{D}| = 0\right) = e^{-\Lambda_{\mathrm{dom}}}. \tag{2.52}
$$

It remains to calculate the mean Λ_{dom}, which can be obtained as

$$
\Lambda_{\mathrm{dom}} = \mathbb{E}_{\Phi, \{\mathsf{g}_{o,n}\}, \{\mathsf{g}_{i,n}\}} \left[\sum_{\mathsf{x}_i \in \Phi} \mathbb{1}\left(\sum_{n=1}^{N} \frac{\mathsf{g}_{o,n}}{y^\alpha \mathsf{g}_{i,n} \|\mathsf{x}_i\|^{-\alpha}} < T\right)\right]
$$
$$
\overset{(a)}{=} \pi\lambda \int_0^\infty 2r\, \mathbb{E}_{\{\mathsf{v}_n\}}\left[\mathbb{1}\left(r < \frac{yT^{1/\alpha}}{\left(\sum_{n=1}^{N} \mathsf{v}_n\right)^{1/\alpha}}\right)\right] \mathrm{d}r
$$
$$
\overset{(b)}{=} \pi\lambda y^2 T^{2/\alpha}\, \mathbb{E}_{\{\mathsf{v}_n\}}\left[\left(\sum_{n=1}^{N} \mathsf{v}_n\right)^{-2/\alpha}\right], \tag{2.53}
$$

where (a) follows from the Campbell-Mecke theorem, see Theorem A.2, and from defining the random variable $\mathsf{v}_{i,n} \triangleq \mathsf{g}_{o,n}/\mathsf{g}_{i,n}$, and (b) follows from interchanging the order of integration and expectation and evaluating the integral. The random variables v_n are i.i.d. with PDF [82]

$$
f_{\mathsf{v}}(v) = \frac{\kappa_{\mathrm{DI}}^{m_{\mathrm{D}}}}{B(m_{\mathrm{D}}, m_{\mathrm{I}})} \left(1 + \kappa_{\mathrm{DI}}v\right)^{-m_{\mathrm{D}} - m_{\mathrm{I}}} v^{m_{\mathrm{D}} - 1}, \quad v > 0, \tag{2.54}
$$

where $B(x, y) \triangleq \frac{\Gamma(x)\Gamma(y)}{\Gamma(x+y)}$ is the Beta function [66]. Computing the fractional moment in (2.53) directly is too involved due to the sum to the

power of $-2/\alpha$ appearing inside the expectation. Instead, a detour via the Laplace transform is chosen, similarly as in the proof of Theorem 2.1. Invoking Lemma A.4, one then obtains

$$
\mathbb{E}_{\{v_n\}}\left[\left(\sum_{n=1}^{N} v_n\right)^{-2/\alpha}\right] = \frac{1}{\Gamma(2/\alpha)} \int_0^\infty u^{2/\alpha-1} \mathcal{L}_{\sum_n^N v_n}(u) \,\mathrm{d}u
$$

$$
\overset{(a)}{=} \frac{1}{\Gamma(2/\alpha)} \int_0^\infty u^{2/\alpha-1} \mathcal{L}_v(u)^N \,\mathrm{d}u
$$

$$
\overset{(b)}{=} \frac{\Gamma(m_\mathrm{D})^N}{B(m_\mathrm{D}, m_\mathrm{I})^N \Gamma(2/\alpha)}
$$

$$
\times \int_0^\infty u^{2/\alpha-1} U\left(m_\mathrm{D}, 1 - m_\mathrm{I}, u\tfrac{m_\mathrm{I}}{m_\mathrm{D}}\right)^N \mathrm{d}u, \quad (2.55)
$$

where (a) follows from the *i.i.d.* property of the $\{v_n\}$ and (b) follows from

$$
\mathbb{E}\left[e^{-sv}\right] = \int_0^\infty e^{-sv} f_v(v) \,\mathrm{d}v = \frac{\Gamma(m_\mathrm{D})}{B(m_\mathrm{D}, m_\mathrm{I})} U\left(m_\mathrm{D}, 1 - m_\mathrm{I}, s\tfrac{m_\mathrm{I}}{m_\mathrm{D}}\right), \quad (2.56)
$$

where $U(a_1, a_2, x) \triangleq \frac{1}{\Gamma(a_1)} \int_0^\infty t^{a_1-1}(1+t)^{a_2-a_1-1} e^{-xt} \,\mathrm{d}t$ with $a_1 > 0$ is the confluent hypergeometric function (Kummer's U-function) [66]. Combining (2.52), (2.53), and (2.55) yields the result.

2.7.3 Proof of Proposition 2.1

The proof is analogous to the proof of Theorem 2.7.1 until step (a) in (2.45). Due to distinct interferer sets for each antenna, the expectation with respect to Φ in (2.45) step (a) decomposes into the product

$$
\mathbb{E}_\Phi\left[\prod_{x_i \in \Phi} \mathbb{E}_{g_{i,1}}\left[\exp\left(-s\psi_1 \frac{y^\alpha g_{i,1}}{\|x_i\|^\alpha}\right)\right]\right] \times \mathbb{E}_\Phi\left[\prod_{x_i \in \Phi} \mathbb{E}_{g_{i,2}}\left[\exp\left(-t\psi_2 \frac{y^\alpha g_{i,2}}{\|x_i\|^\alpha}\right)\right]\right]
$$

$$
\overset{(a)}{=} \exp\left(-\lambda\pi \int_0^\infty 2r\left(2 - \mathbb{E}_{g_1}\left[e^{-s\psi_1 \frac{y^\alpha g_1}{r^\alpha}}\right] - \mathbb{E}_{g_2}\left[e^{-t\psi_2 \frac{y^\alpha g_2}{r^\alpha}}\right]\right) \mathrm{d}r\right),
$$

$$(2.57)$$

where (a) follows from the PGFL for PPPs, see Theorem A.3. Evaluating the integral with respect to r, using the fact that $\mathbb{E}[g_n^{2/\alpha}] = m_\mathrm{I}^{-2/\alpha}\Gamma(2/\alpha + m_\mathrm{I})/\Gamma(m_\mathrm{I})$, and substituting this result back into (2.45) step (a) concludes the proof.

2.7.4 Proof of Proposition 2.2

We first note that $\sum_{n=1}^{N} \mathsf{g}_{o,n}$ is Gamma distributed with shape Nm_{D} and rate m_{D}, see Appendix A. Define $\mathsf{I} \triangleq y^{\alpha} \sum_{\mathsf{x}_i \in \Phi} \mathsf{g}_i \|\mathsf{x}_i\|^{-\alpha}$. Applying the same technique as in the proof of Theorem 2.1, one obtains

$$
\begin{aligned}
\mathrm{P}_{\mathrm{c,FC}}^{\mathrm{IA}} &= \mathbb{E}_{\mathsf{I}} \left[\sum_{k=0}^{Nm_{\mathrm{D}}-1} \frac{\left(m_{\mathrm{D}}T(\mathsf{I}+\mathtt{SNR}^{-1}) \right)^k}{k!} \exp\left(-m_{\mathrm{D}}T(\mathsf{I}+\mathtt{SNR}^{-1}) \right) \right] \\
&= \sum_{k=0}^{Nm_{\mathrm{D}}-1} \frac{(-1)^k}{k!} \frac{\mathrm{d}^k}{\mathrm{d}s^k} \left[\mathcal{L}_{\mathsf{Y}}(s) \right]_{s=1},
\end{aligned}
\tag{2.58}
$$

where $\mathsf{Y} \triangleq m_{\mathrm{D}}T\left(\mathsf{I}+\mathtt{SNR}^{-1} \right)$. The Laplace transform $\mathcal{L}_{\mathsf{Y}}(s)$ is finally computed using the same approach as in the proof of Theorem 2.1.

2.7.5 Proof of Proposition 2.5

We first consider the Laplace transform of G in (2.49) of Appendix 2.7.1 as $m_{\mathrm{I}} \to \infty$. Since $\lim_{m_{\mathrm{I}} \to \infty} \mathcal{L}_{\mathsf{G}}(u) = \exp\left(-u\left(s\psi_1 + t\psi_2 \right) \right)$, this implies that G converges in distribution to a degenerate random variable with density $\delta(s\psi_1 + t\psi_2)$. Since G is uniformly integrable for $m_{\mathrm{I}} \geq 1/2$, it then follows from [81, Theorem 5.9] that

$$
\lim_{m_{\mathrm{I}} \to \infty} \mathbb{E}\left[\mathsf{G}^{2/\alpha} \right] = (s\psi_1 + t\psi_2)^{2/\alpha}.
\tag{2.59}
$$

On the other hand, using the same approach as in the proof of Theorem 2.1 until step (a) in (2.45), $\mathrm{P}_{\mathrm{c,FC}}^{\mathrm{IA}}$ can be written as

$$
\begin{aligned}
\sum_{k=0}^{m_{\mathrm{D}}-1} & \frac{(-1)^{k+m_{\mathrm{D}}}}{k!\,\Gamma(m_{\mathrm{D}})} \int_0^{\infty} z^{-1} \frac{\partial^{k+m_{\mathrm{D}}}}{\partial s^k \partial t^{m_{\mathrm{D}}}} \left[\exp\left(-\frac{s\psi_1}{\mathtt{SNR}} - \frac{t\psi_2}{\mathtt{SNR}} \right) \right. \\
& \left. \times \mathbb{E}_{\Phi} \left[\prod_{\mathsf{x}_i \in \Phi} \mathbb{E}_{\mathsf{g}_i} \left[\exp\left(-\mathsf{g}_i(s\psi_1 + t\psi_2) \frac{y^{\alpha}}{\|\mathsf{x}_i\|^{\alpha}} \right) \right] \right] \right]_{\substack{s=1\\t=1}} \mathrm{d}z,
\end{aligned}
\tag{2.60}
$$

where the fact that $\mathsf{g}_{i,m} \equiv \mathsf{g}_{i,n} \ \forall m,n \in \{1,\dots,N\}$ and $\mathsf{x}_i \in \Phi$ by Definition 2.3 is used. Using the PGFL for PPPs, see Theorem A.3, the

expectation with respect to Φ in (2.60) can be computed as

$$
\exp\left(-\lambda\pi\int_0^\infty 2r\left(1 - \mathbb{E}_{\mathbf{g}}\left[e^{-\mathbf{g}(s\psi_1 + t\psi_2)\frac{y^\alpha}{\|\mathsf{x}_i\|^\alpha}}\right]\right)\,\mathrm{d}r\right)
$$
$$
= \exp\left(-\pi\lambda y^2(s\psi_1 + t\psi_2)^{2/\alpha}\Gamma(1 - 2/\alpha)\frac{\Gamma(2/\alpha + m_\mathrm{I})}{m_\mathrm{I}^{2/\alpha}\Gamma(m_\mathrm{I})}\right) \quad (2.61)
$$

and shown to converge to $\exp(-\pi\lambda y^2(s\psi_1 + t\psi_2)^{2/\alpha}\Gamma(1 - 2/\alpha)$ as $m_\mathrm{I} \to \infty$. Finally comparing (2.61) for the FC model with the corresponding expression obtained after substituting (2.59) into (2.47) for the exact model, the asymptotic equivalence follows.

3

Diversity Combining in Multi-Antenna Heterogeneous Cellular Networks

---

Network densification and MIMO communications are two promising approaches to address the increasing rate and coverage demands in cellular systems [5]. Network densification is realized by deploying tiers of low-power BSs inside the existing network, e.g., to serve high-traffic areas within macro cells, thereby rendering the network increasingly *heterogeneous*. MIMO, on the other hand, can increase link reliability and/or capacity by leveraging the spatial degrees-of-freedom in fading channels. Due to the radical shift associated with HCNs, MIMO and HCNs cannot be analyzed separately; many characteristics unique to HCNs such as multi-tier deployment, limited site-planning, and heterogeneous parametrization clearly influence the channel "seen" by a multi-antenna receiver. Understanding this interplay, however, is challenging and makes a comprehensive analysis of MIMO in HCNs difficult. This chapter, which is based on [T3–T5], addresses the above challenge by developing a tractable stochastic model, which allows studying the performance of MIMO diversity in HCNs.

3.1 Related Work

MIMO techniques can be open-loop or closed-loop based and the latter have been the focus of many works on MIMO cellular networks, see for instance [83] and the references therein. These works show that closed-loop MIMO schemes can significantly improve performance when CSI-Tx is available. Reliable CSI-Tx, however, may not always be available in practice, e.g., in high mobility scenarios [84], and open-loop schemes requiring CSI only at the receiver (CSI-Rx) have to be used instead. For instance, 3GPP LTE supports different open-loop modes, e.g., transmission mode 2 uses a Space-Frequency Blockcode (SFBC) for Tx diversity over two or four Tx antennas [85]. On the mobile receiver side, space and complexity limitations typically preclude the use of many Rx antennas—often not exceeding two antennas—and allow only for simple linear combining schemes. One such combining scheme is MRC [12], which offers a good trade-off between performance and complexity, and is therefore ubiquitously found in multi-antenna consumer devices. Especially in the context of MIMO communications, MRC may sometimes be even more appealing than interference-canceling receivers, since the latter require accurate knowledge of the other-cell interference channels, which is harder to realize when multiple Tx antennas are active [20, Sec. 10.5.4].

Two types of MRC exist that differ in the way interference due to concurrent transmissions is treated, namely IB-MRC and IA-MRC. The former, and more popular, ignores the interference at all. The combiner coefficients then follow from the well-known channel matched-filter approach in this case [20, Sec. 3.3.1]. IA-MRC, in contrast, takes the interference power (*hereafter, simply* interference) into account. More specifically, the (possibly unequal) interference experienced at each Rx antenna in one block/frame is treated as additional Rx noise. Following the original MRC approach from [12], the combiner then give less weight to branches with poor reception quality, i.e., with strong interference and/or adverse fading states. Estimating the per-antenna interference can be done within the channel estimation phase, e.g., after decoding and removing the pilot symbols sent by the serving BS [86] or by using techniques from [87, 88]. Both types of MRC are well-understood for networks with fixed geometry, see for instance [12, 30–32], and recently also for wireless *ad hoc* networks with dynamic/varying geometry, see for instance [50–52], and in particular Chapter 2 in this thesis in the case of IA-MRC.

In the context of downlink HCNs, MIMO diversity with MRC is yet not well-understood, since prior works do not directly apply due to the specific nature of the interference governing HCNs. An interesting question, for instance, is whether the gain of IA-MRC over IB-MRC justifies the slightly higher complexity in a typical MIMO HCN setting, and how this trade-off varies with the number of Tx and Rx antennas.

Certainly, extensive system-level simulations can only partly help in addressing the above challenge as they usually offer only limited insights. As a viable alternative approach to simulations, spatial modeling using stochastic geometry [34] has gained much attention recently, see for instance [39, 89, 90] and in particular [91–95] for MIMO cellular networks. In [91], the Average Symbol Error Probability (ASEP) was analyzed for multi-antenna single-tier cellular networks with spatial-multiplexing, where it was found that Rx diversity can significantly improve performance. In [92], a unifying framework using the Equivalent-in-Distribution approach was presented, which studies the ASEP of MIMO diversity with IB-MRC in single-tier networks. The energy efficiency of small-cell MISO cellular system with maximal-ratio transmission in the downlink was analyzed in [93]. MIMO HCNs with different kinds of CSI-Tx based MIMO schemes were analyzed in [95] with load balancing and in [94] without load balancing. Complementing the above works, the main objective of this chapter is to derive a tractable model and to conduct a meaningful analysis in order to obtain a better understanding of MIMO diversity with IA-MRC/IB-MRC in HCNs.

3.2 Contributions and Outcomes

The main contributions and outcomes of this chapter are summarized below.

Analytical model: In Section 3.3, a tractable stochastic model for downlink MIMO diversity with OSTBCs and IB-MRC/IA-MRC is developed. To reflect the irregular and multi-tier deployment of BSs observed in practice, a PPP is used to model the BS locations of a K-tier HCN. The model captures relevant tier-specific parameters, such as BS density and Tx power, path loss exponent, and number of Tx antennas. Based on this model, the coverage probability for both types of MRC is then

derived in Section 3.5. For IA-MRC, focus is put on the case with two Rx antennas. The theoretical expressions can be evaluated fairly easily using standard numerical software, while in certain cases they can be further simplified analytically.

Second-order statistics of HCN interference: In Section 3.4, the interference dynamics experienced at a multi-antenna receiver in HCNs are analyzed, thereby complementing earlier work, which focused on Aloha-based *ad hoc* networks [55]. Interference dynamics affect the performance of IA diversity-combining schemes such as IA-MRC. The analysis shows that the interference variance measured at a typical user is tier-independent if the path loss exponent and the number of Tx antennas are constant across tiers. In direct comparison with the literature, the analysis indicates that the interference variance is smaller in HCNs than in Aloha-based *ad hoc* networks, where interferers can be much closer to a receiver. Moreover, the gains of IA diversity combining are expected to decrease when more Tx antennas are active (Tx diversity) as interference variance then becomes smaller. Interestingly, the interference correlation coefficient across Rx antennas is independent from the tier with which this user associates when the number of Tx antennas is equal in each tier. In this case, the correlation becomes entirely tier-independent and increases with the number of active Tx antennas. In line with the effect of decreasing interference variance explained above, the gains of IA diversity combining are expected to decrease when more Tx antennas are active due to the higher interference correlation across Rx antennas.

Design insights: In Section 3.6, the theoretical results are discussed using numerical examples. In a typical three-tier MIMO scenario with IB-MRC at the receivers, the gain of doubling the number of Rx antennas is roughly $2.5\,\mathrm{dB}$ at operating points of practical relevance. For IA-MRC, this gain is roughly $3.6\,\mathrm{dB}$. Adding more Tx antennas is beneficial only at large coverage probabilities. The gain of IA-MRC over IB-MRC decreases with the number of Tx antennas due to the higher interference correlation across Rx antennas resulting from the interference-smoothing effect of Tx diversity. The relative coverage probability gain of 1×2 SIMO over SISO transmission in the practical regime is between 12%–66% for IB-MRC, while an additional improvement of only 1%–3% is obtained by IA-MRC. Although interference estimation needed in IA-MRC can be realized with acceptable complexity, the outcome of this comparison hence suggests that IB-MRC is more favorable in MIMO HCNs with Tx diversity.

Spatial interference correlation across Rx antennas, caused by the common locations of interfering BSs, influences the performance of IA-MRC and should not be ignored in the analysis; ignoring this type of correlation significantly overestimates the true performance. In contrast, assuming full correlation underestimates the true performance only slightly. Moreover, it is shown that assuming full correlation in IA-MRC is equivalent to IB-MRC. Interestingly, it does not matter for the diversity order of IA-MRC if one assumes no correlation or full correlation of the interference as both simplifying assumptions result in the true diversity order.

The coverage probability for IA-SC is derived for SIMO HCNs and the resulting performance is compared with MRC. The results show that the gain of MRC over IA-SC is not overwhelming for small number of Rx antenna. The higher complexity of MRC may thus not be justified in this case. Moreover, the performance-complexity trade-off between both types of MRC and IA-SC in HCNs may differ significantly from the interference-free case.

3.3 System Model

3.3.1 Network Geometry and User Association

Consider a K-tier HCN in the downlink with BSs irregularly scattered in the plane, see Fig. 3.1. The irregular BS locations in tier $k \in \mathcal{K}$, where $\mathcal{K} = \{1, \ldots, K\}$, are modeled by an independent stationary PPP $\Phi_k \triangleq \{x_i\}$ on $\mathbb{R}^2$ with density λ_k, see Definition A.3. Denote by $\Phi \triangleq \cup_{k=1}^{K} \Phi_k$ the entire set of BSs, which is obtained by independent superposition of the K PPPs, see Lemma A.6. The spatial Poisson model is widely-accepted for analyzing (multi-tier) cellular networks [39, 89, 90], and recently also MIMO HCNs [94, 95]. All BSs in tier k transmit an OSTBC using M_k Tx antennas. Similarly, mobile receivers (users) are assumed to be equipped with N Rx antennas. The users are independently distributed on the plane according to some stationary point process. By Slivnyak's theorem, see Theorem A.1, and due to the stationarity of Φ, see Definition A.3, one can focus the analysis on a *typical* user located at the origin $o \in \mathbb{R}^2$.

BSs in tier k transmit with total power P_k, which is equally divided across all active Tx antennas. At the typical user, the long-term received
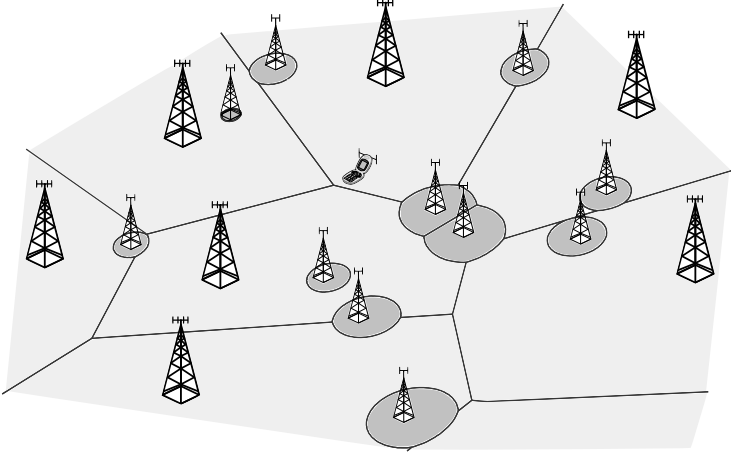
Figure 3.1: Example: Downlink HCN with $K = 2$. Tier-1 (macro) BSs have 4 Tx antennas; Tier-2 (small-cell) BSs have 2 Tx antennas. Typical user has 2 Rx antennas.

power from a tier k BS located at $\mathsf{x}_i \in \Phi_k$ is thus $P_k \|\mathsf{x}_i\|^{-\alpha_k}$, where $\|\cdot\|^{\alpha_k}$ is the distance-dependent path loss with path loss exponent $\alpha_k > 2$. Focusing on narrowband signaling, e.g., Orthogonal Frequency Division Multiplexing (OFDM) in 4th Generation (4G) LTE and proper antenna design in a rich scattering environment, it is reasonable to assume i.i.d. frequency-flat Rayleigh fading [86]. Table 3.1 summarizes frequently recurring notation used in this chapter.

Users are assumed to associate with the BS providing the strongest average measured received power, which is a common assumption in cellular systems. Note that this association rule is generally not coverage maximizing in MIMO HCNs with unequal M_k and requires a *biased* association rule, see [95] for more details. Including biasing in the model, i.e., using similar techniques as in [89, 95], is outside the scope of this chapter. For the typical user, the serving BS is hence the one maximizing $P_k \|\mathsf{x}_i\|^{-\alpha_k}$. Without loss of generality, the location of this BS is labeled as x_o to emphasize its association with the typical user located at o. Its distance to the typical user is denoted by $\mathsf{y} \triangleq \|\mathsf{x}_o\|$. For convenience, $\Phi^o \triangleq \Phi \setminus \{\mathsf{x}_o\}$ and $\Phi_k^o \triangleq \Phi_k \setminus \{\mathsf{x}_o\}$ are defined for short-hand notation, i.e., the set of interfering BSs.

Table 3.1: Notation used in this chapter

Notation	Description
$\Phi_k; \lambda_k$	PPP describing the BS locations in tier k; average density of BSs in tier k; $\Phi \triangleq \cup_{k=1}^{K} \Phi_k$
P_k	BS Tx power in tier k
α_k	Path loss exponent in tier k
$N; M_k$	Number Rx antennas at the typical user; number of Tx antennas at BS in tier k
$\mathbf{H}_i; \mathsf{h}_{i,nm}$	$N \times M_k$ channel matrix between typical user and i-th BS in tier k; entries of $\mathbf{H}_i$ from $\mathcal{CN}(0,1)$
σ^2	Rx noise power, AWGN variance
(M_k, L_k, r_k)	OSTBC with codeword length L_k, code rate r_k, and M_k Tx antennas
S_k	Number of symbols encoded in an (M_k, L_k, r_k)-OSTBC; number of active Tx antennas per slot
$\{\mathbf{A}_{nm}\}, \{\mathbf{B}_{nm}\}$	Dispersion matrices characterizing an OSTBC
$\mathsf{I}_n; \mathsf{I}_{i,\text{eqv}}$	Interference (power) at the n-th Rx antenna; interference (power) from i-th BS after diversity combining
$\mathtt{SNR}(\ell, y)$	Mean SNR from a serving ℓ-th tier BS at distance y
$\mathtt{SINR}_\Sigma(\ell, y)$	Post-combiner SINR from a serving ℓ-th tier BS at distance y
$\mathtt{SINR}_\Sigma$	Post-combiner SINR at the typical user
T	SINR threshold
P_c	Coverage probability $\mathbb{P}(\mathtt{SINR}_\Sigma > T)$

From the user association rule it follows that, given $\mathsf{y} = y$ and that the serving BS is from tier $\ell \in \mathcal{K}$, Φ_k^o is a homogeneous PPP on $\mathbb{R}^2 \setminus b(0, d_k)$, where $d_k = \hat{P}_k^{1/\alpha_k} y^{1/\hat{\alpha}_k}$ with $\hat{P}_k \triangleq P_k/P_\ell$ and $\hat{\alpha}_k \triangleq \alpha_k/\alpha_\ell$. It will be useful to know the probability that a user associates with a certain tier $\ell \in \mathcal{K}$ and the conditional PDF of the distance y to the serving BS.

Lemma 3.1 (Association probability and distance PDF [89]). *A user associates with the ℓ-th tier with probability*

$$A_\ell = 2\pi\lambda_\ell \int_0^\infty y \exp\left(-\pi \sum_{k=1}^{K} \lambda_k \hat{P}_k^{2/\alpha_k} y^{2/\hat{\alpha}_k}\right) \mathrm{d}y. \qquad (3.1)$$

The PDF of the distance $\mathsf{y} \triangleq \|\mathsf{x}_o\|$ to the serving BS, given that it belongs to tier $\ell \in \mathcal{K}$, is

$$f_{\mathsf{y},\ell}(y) = \frac{2\pi\lambda_\ell y}{A_\ell} \exp\left(-\pi \sum_{k=1}^{K} \lambda_k \hat{P}_k^{2/\alpha_k} y^{2/\hat{\alpha}_k}\right), \quad y \geq 0. \qquad (3.2)$$

3.3.2 OSTBC MIMO Signal Model

All BSs in tier k use an (M_k, L_k, r_k)-OSTBC, where $L_k \geq 1$ is the codeword length and $r_k \in (0, 1]$ is the code rate; L_k can be seen as the number of slots needed to convey $S_k = L_k r_k$ symbols using M_k Tx antennas. For analytical tractability, only *power-balanced* (M_k, L_k, r_k)-OSTBCs shall be considered, i.e., having the property that exactly S_k symbols are transmitted—or equivalently that S_k Tx antennas are active—in every slot. This allows assigning a constant power load of P_k/S_k to every symbol-antenna pair in every slot. Practical examples of balanced OSTBCs are for instance $(1, 1, 1)$ (single-antenna), $(2, 2, 1)$ (Alamouti), $(4, 4, 1/2)$, and $(4, 4, 3/4)$, see [96, 97]. The notation $\mathbf{v}_{i,\tau} \in \{0, 1\}^{M_k}$ is used to indicate the active Tx antennas of BS i in slot τ, i.e., the m-th entry of $\mathbf{v}_{i,\tau}$ is one if Tx antenna m is active and zero otherwise.

Assume for the moment that the typical user associates with the ℓ-th tier. It will then be served by an (M_ℓ, L_ℓ, r_ℓ)-OSTBC. The interference-plus-noise corrupted received signal at the typical user in slot $\tau \in \{1, \ldots, L_\ell\}$ can then be expressed by

$$\mathbf{r}_\tau = \mathbf{H}_o\, \mathbf{c}_{o,\tau} + \sum_{k=1}^{K} \sum_{\mathsf{x}_i \in \Phi_k^o} \mathbf{H}_i\, \mathbf{c}_{i,\tau} + \mathbf{n}_\tau, \qquad (3.3)$$

where

- $\mathbf{H}_i \in \mathbb{C}^{N \times M_k}$ is the channel matrix describing the fading from the i-th BS of the k-th tier to the typical user. The entries of $\mathbf{H}_i$, $\mathsf{h}_{i,nm}$, are $\mathcal{CN}(0, 1)$ distributed and typically assumed constant for the duration of one codeword.[2] From the *i.i.d.* fading property, it follows that $\mathbb{E}[\mathsf{h}_{i,nm}\mathsf{h}_{j,uv}^*] = 0$ unless $i = j$, $n = u$, and $m = v$.

---

[2] When $\mathbf{H}_i$ is time-varying and space-time coding is across multiple channel realizations, technique from [98] can be used to achieve also temporal diversity. Such extensions are outside the scope of this paper.

- $\mathbf{c}_{i,\tau} \in \mathbb{C}^{M_k}$ is a vector consisting of the space-time coded symbols of the i-th BS sent from the $S_k \leq M_k$ active Tx antennas in slot τ and received with average signal strength $\sqrt{\frac{P_k}{S_k}}\|\mathsf{x}_i\|^{-\alpha_k/2}$. It is assumed that $\mathbb{E}\left[\mathbf{c}_{i,\tau}\mathbf{c}_{j,\tau}^H\right] = \mathbf{0}_{M_k}$ for all $i \neq j$, where $\mathbf{0}_{M_k}$ is an $M_k \times M_k$ zero matrix. It is reasonable to assume also that $\mathbb{E}[\mathbf{c}_{i,\tau}] = [0,\ldots,0]^T$ and $\mathbb{E}[\mathbf{c}_{i,\tau}\mathbf{c}_{i,\tau}^H] = \frac{P_k}{S_k}\|\mathsf{x}_i\|^{-\alpha_k}\mathrm{diag}(\mathbf{v}_{i,\tau})$, where $\mathrm{diag}(\mathbf{v}_{i,\tau})$ is a diagonal matrix with entries $\mathbf{v}_{i,\tau}$. The latter assumption follows from the *balanced-power* property of the considered OSTBCs.

- $\mathbf{n}_\tau \in \mathbb{C}^N$ is a vector describing the Rx noise with independent $\mathcal{CN}(0,\sigma^2)$ entries.

Upon receiving all L_ℓ code symbols corresponding to one codeword, the typical user stacks the vectors $\mathbf{r}_1,\ldots,\mathbf{r}_{L_\ell}$ to form the new vector

$$\bar{\mathbf{r}} = \begin{bmatrix} \mathbf{H}_o\,\mathbf{c}_{o,1} \\ \vdots \\ \mathbf{H}_o\,\mathbf{c}_{o,L_\ell} \end{bmatrix} + \sum_{k=1}^{K}\sum_{\mathsf{x}_i \in \Phi_k^o} \bar{\mathbf{i}}_i + \begin{bmatrix} \mathbf{n}_1 \\ \vdots \\ \mathbf{n}_{L_\ell} \end{bmatrix}, \tag{3.4}$$

where

$$\bar{\mathbf{i}}_i = \begin{bmatrix} \mathbf{H}_i\,\mathbf{c}_{i,1} \\ \vdots \\ \mathbf{H}_i\,\mathbf{c}_{i,L_\ell} \end{bmatrix} \tag{3.5}$$

is the interference signal from the i-th BS received over the entire codeword period, i.e., $\bar{\mathbf{i}}_i \in \mathbb{C}^{NL_\ell}$. With CSI-Rx, $\bar{\mathbf{r}}$ is linearly combined to form a final decision variable. Two types of MRC are considered, which differ in the amount of required CSI-Rx. More specifically, IB-MRC requires knowledge of $\mathbf{H}_o$, while IA-MRC requires knowledge of $\mathbf{H}_o$ *and* of the interference-plus-noise power at all Rx antennas.

It is known that the performance of diversity-combining schemes is influenced by the second-order properties of the interference, as reported for instance in [52, 54, 55] for the *ad hoc* network model with slotted Aloha. In the following, these prior works are extended by analyzing the second-order statistics of the interference in MIMO HCNs.

3.4 Second-Order Statistics of HCN Interference

The performance of diversity combining is fundamentally limited by the nature of the channel observed by the receiver. More specifically, the variability of the reception quality on the one hand and the degree of its correlation across Rx antennas on the other hand, dictate how much can be gained by such techniques. Clearly, if the reception quality fluctuates considerably and independently across Rx antennas, large gains can be expected. If, in contrast, the channel quality remains constant or does not vary across Rx antennas, little to no gains can be expected.

From (3.3) it is evident that the resulting per-antenna reception quality is not only affected by the fading on the desired link but also by interference. Being a dynamic quantity, the latter contributes to the overall correlation structure and to the variability of the reception quality with its own statistical properties. Compared to the influence from the desired channel, this contribution is yet relatively unexplored, particularly within the context of HCNs. This motivates to take a closer look at the second-order characteristics of the interference experienced at the typical user.

Let $\mathbf{h}_{i,n} = [\mathsf{h}_{i,n1}, \dots, \mathsf{h}_{i,nM_k}]$ be the n-th row of $\mathbf{H}_i$. Then, the interference in slot τ (the time index τ is dropped in the following) measured at the n-th Rx antenna, averaged over the code symbols $\{\mathbf{c}_i\}$ in one frame, is

$$
\begin{aligned}
\mathsf{I}_n &= \mathbb{E}_{\{\mathbf{c}_i\}} \left[\left(\sum_{k=1}^{K} \sum_{\mathsf{x}_i \in \Phi_k^o} \mathbf{h}_{i,n} \mathbf{c}_i \right) \left(\sum_{k=1}^{K} \sum_{\mathsf{x}_i \in \Phi_k^o} \mathbf{h}_{i,n} \mathbf{c}_i \right)^H \right] \\
&\stackrel{(a)}{=} \sum_{k=1}^{K} \sum_{\mathsf{x}_i \in \Phi_k^o} \mathbf{h}_{i,n} \, \mathbb{E}\left[\mathbf{c}_i \mathbf{c}_i^H \right] \mathbf{h}_{i,n}^H \\
&\stackrel{(b)}{=} \sum_{k=1}^{K} \sum_{\mathsf{x}_i \in \Phi_k^o} \frac{P_k}{S_k \|\mathsf{x}_i\|^{\alpha_k}} \mathbf{h}_{i,n} \mathrm{diag}(\mathbf{v}_i) \mathbf{h}_{i,n}^H \\
&= \sum_{k=1}^{K} \sum_{\mathsf{x}_i \in \Phi_k^o} \frac{P_k}{S_k \|\mathsf{x}_i\|^{\alpha_k}} \|\mathbf{h}_{i,n}(S_k)\|_F^2 = \sum_{k=1}^{K} \mathsf{I}_{n,k}, \qquad (3.6)
\end{aligned}
$$

where (a) follows from the independence between the $\{\mathbf{c}_i\}$ across BSs and (b) follows from the correlation properties of the $\{\mathbf{c}_i\}$.

3.4.1 Interference Variance

Combining (3.6) and (3.3), one can see that the dynamic part not belonging to the fading on the desired channel is $\mathsf{I}_n + \sigma^2$. Since this term is essentially a function of the long-term received useful power $P_\ell y^{-\alpha_\ell}$ through the cell association rule, it is reasonable to consider the normalized version $(\mathsf{I}_n + \sigma^2)/(P_\ell y^{-\alpha_\ell}) \triangleq \mathsf{I}'_n$. The normalized interference I'_n can be intuitively understood as the interference-to-average-signal ratio at Rx antenna n. Given that the serving BS is at distance y and belongs to tier ℓ, the corresponding conditional variance seen by the typical user is

$$\mathrm{Var}_{\ell,y}\left[\mathsf{I}'_n\right] \overset{(a)}{=} \frac{y^{2\alpha_\ell}}{P_\ell^2} \sum_{k=1}^{K} \mathrm{Var}_{\ell,y}\left[\mathsf{I}_{n,k}\right]$$

$$\overset{(b)}{=} 2\pi y^{2\alpha_\ell} \sum_{k=1}^{K} \hat{P}_k^2 \lambda_k \frac{\mathbb{E}[\|\mathbf{h}_n(S_k)\|_F^4]}{S_k^2} \int_{d_k}^{\infty} r^{-2\alpha_k+1}\, \mathrm{d}r$$

$$\overset{(c)}{=} \pi \sum_{k=1}^{K} \frac{\lambda_k \hat{P}_k^{2/\alpha_k}}{\alpha_k - 1}\left(1 + \frac{1}{S_k}\right) y^{2/\hat{\alpha}_k}, \tag{3.7}$$

where (a) follows from the fact $\mathrm{Var}[\mathsf{z} + c] = \mathrm{Var}[\mathsf{z}]$ and from the independence of the $\{\mathsf{I}_{n,k}\}$ across tiers, (b) follows from the Campbell-Mecke theorem, see Theorem A.2, and from the radius d_k of the exclusion ball for the k-th tier due to the cell association rule, and (c) follows from Lemma A.3.

The expression in (3.7) reflects the variance of the normalized interference for a specific user location relative to the network. Thus, one still needs to de-condition on y and on the associated tier ℓ, which can be done using Lemma 3.1. To obtain a more tractable expression that reveals the underlying trend, equal path loss exponents and the same number of active Tx antennas across tiers are assumed next, i.e., $\alpha_k = \alpha$ and $S_k = S\ \forall k \in \mathcal{K}$. The normalized interference variance experienced at the typical user then becomes

$$\mathrm{Var}\left[\mathsf{I}'_n\right] = \sum_{\ell=1}^{K} 2\pi\lambda_\ell \int_0^{\infty} y\,\mathrm{Var}_{\ell,y}\left[\mathsf{I}'_n\right] \exp\left(-\pi y^2 \sum_{k=1}^{K} \lambda_k \hat{P}_k^{2/\alpha}\right) \mathrm{d}y$$

$$= \frac{1 + \frac{1}{S}}{\alpha - 1}. \tag{3.8}$$

The following observations can be made from (3.8):

- Interestingly, the variance of the normalized interference at the typical user neither depends on the number of tiers K, nor on their parameters $\{P_k\}$ and $\{\lambda_k\}$ when $\alpha_k = \alpha$ and $S_k = S \ \forall k \in \mathcal{K}$. This result is consistent with [89,90], where the invariance of the coverage probability with respect to the number/parameters of the tiers was shown for equal $\{\alpha_k\}$ and absence of Rx noise.

- In line with the intuition, the variance of the normalized interference increases when α becomes smaller as the interference contribution from far-off BSs then carries more weight. Conversely, for large α the interference is dominated by only a few close-by BSs, thereby reducing the variance. For typical α in HCNs around $\alpha = 3.7$ [99], the variance is 0.74 when $S = 1$.

- With the same path loss law $\| \cdot \|^{-\alpha}$, the interference variance in Aloha-based *ad hoc* networks diverges [38], as interfering transmitters can be arbitrarily close to the receiver in this case. Although this result is due to the singularity of the path loss law and has no physical relevance, it suggests that the interference variance in HCNs tends to be smaller than in Aloha-based *ad hoc* networks. This, in turn, means that IA diversity combining will generally perform lower in HCNs. This will be discussed further in Section 3.6.3.

- The interference variance decays with the number of active Tx antennas S. This is because adding more Tx antennas while reducing the per-antenna Tx power by S smoothes out the channel fluctuations. This effect is also referred to as *channel-hardening* [100]. Hence, for large S one expects IA diversity-combining schemes to perform similar to IB diversity-combining schemes due to a smaller interference variability. In the limit $S \to \infty$, the variance of the normalized interference becomes $\frac{1}{\alpha-1}$.

3.4.2 Interference Correlation across Rx Antennas

In order to study the interference correlation across Rx antennas, the covariance of the normalized interference, conditioned on the serving tier

ℓ and serving BS distance y, is first needed. It can be obtained as

$$
\begin{aligned}
\mathrm{Cov}_{\ell,y}\left[\mathsf{I}'_u, \mathsf{I}'_v\right] & \overset{(a)}{=} \frac{y^{2\alpha_\ell}}{P_\ell^2} \sum_{k=1}^K \mathrm{Cov}_{\ell,y}\left[\mathsf{I}_{u,k}, \mathsf{I}_{v,k}\right] \\
& \overset{(b)}{=} 2\pi y^{2\alpha_\ell} \sum_{k=1}^K \hat{P}_k^2 \lambda_k \frac{\mathbb{E}[\|\mathbf{h}_u(S_k)\|_F^2]^2}{S_k^2} \int_{d_k}^{\infty} r^{-2\alpha_k+1}\,\mathrm{d}r \\
& \overset{(c)}{=} \pi \sum_{k=1}^K \frac{\lambda_k \hat{P}_k^{2/\alpha_k}}{\alpha_k - 1} y^{2/\hat{\alpha}_k},
\end{aligned}
\tag{3.9}
$$

where (a) follows from $\mathrm{Cov}[\mathsf{z}_1 + c, \mathsf{z}_2 + c] = \mathrm{Cov}[\mathsf{z}_1, \mathsf{z}_2]$ and from the independence of the $\{\mathsf{I}_{n,k}\}$ across tiers, (b) follows from the Campbell-Mecke theorem, see Theorem A.2, and from $\mathbf{h}_n$ being independent across n, and (c) follows from Lemma A.3. With (3.7) and (3.9), the conditional correlation coefficient becomes

$$
\rho_{\ell,y} = \frac{\mathrm{Cov}_{\ell,y}\left[\mathsf{I}'_u, \mathsf{I}'_v\right]}{\mathrm{Var}_{\ell,y}\left[\mathsf{I}'_n\right]} = \frac{\mathrm{Cov}_{\ell,y}\left[\mathsf{I}_u, \mathsf{I}_v\right]}{\mathrm{Var}_{\ell,y}\left[\mathsf{I}_n\right]} \overset{S_k=S}{=} \frac{S}{1+S}.
\tag{3.10}
$$

The following observations can be made from (3.10):

- The correlation coefficient $\rho_{\ell,y}$ has the same form as the *temporal* correlation coefficient in Aloha-based *ad hoc* networks, which was derived in [38, Lem. 5.13]. Temporal correlation with fixed set of active interferers and spatial correlation across Rx antennas are mathematically the same, since in both cases fading varies while the interferer locations remain fixed.

- As expected, adding more Tx antennas increases the interference correlation across Rx antennas, since the channel fluctuations then undergo an *averaging* effect. For $S = 1$, one has $\rho_{\ell,y} = 1/2$. In the limit $S \to \infty$, the correlation of the normalized interference becomes maximal, i.e., $\rho_{\ell,y} = 1$. Similar to the above comment on normalized interference variance for large S, IA diversity-combining schemes are expected to have a similar performance as IB diversity-combining schemes in this regime.

- $\rho_{\ell,y}$ is independent of the tier with which the typical user associates and from the distance to the serving BS if the number of active Tx antennas is equal across tiers ($S_k = S \; \forall k \in \mathcal{K}$). In this case, $\rho_{\ell,y}$ is independent of K, $\{P_k\}$, $\{\lambda_k\}$, and, in contrast to the interference variance, also of the path loss exponents $\{\alpha_k\}$.

Remark 3.1 (Feasibility of interference estimation). *When the set of active Tx antennas of interfering BSs changes in every slot τ, I_n varies between every slot of the codeword. This is the case when $S_k < M_k$. Such rapid variations over τ are imperceptible to CSI estimation since the latter is usually designed to track channel-fading variations, which happen on a larger time scale. However, when full-rate OSTBCs are used ($r_k = 1$ for all $k \in \mathcal{K}$), I_n is identical across τ, since all $S_k = M_k$ Tx antennas are always active. In that case, the receiver can obtain knowledge of $\mathsf{I}_n + \sigma^2$ with acceptable complexity, e.g., after decoding and removing the pilot symbols sent by the serving BS [86] or by using techniques from [87, 88].*

3.5 Coverage Probability Analysis

This section analyzes the downlink performance at the typical user for both IB-MRC and IA-MRC. As explained in Remark 3.1, IA-MRC is practical only for full-rate OSTBCs ($r_k = 1 \ \forall k \in \mathcal{K}$). A common way for studying the performance of diversity-combining schemes is to analyze the distribution of the post-combiner SINR. The specific form of post-combiner SINR depends on the considered scheme and will be developed in Sections 3.5.1 and 3.5.2 for the two considered MRC types.

The performance analysis will focus on the *coverage probability* P_c as the performance metric, which was already introduced in Definition 2.1 in Chapter 2. The coverage probability P_c can be interpreted as the complementary CDF of the post-combiner SINR at the typical user or, alternatively, as the average fraction of users in the HCN covered by a post-combiner SINR no less than some threshold $T > 0$.

3.5.1 MIMO Diversity with IB-MRC

A useful feature of OSTBCs is that the MIMO channel (3.4) can be reduced to parallel SISO channels [21]. At the typical user, knowing $\mathbf{H}_o$, this is achieved by the linear combination

$$\sum_{n=1}^{N} \sum_{m=1}^{M_\ell} h_{o,nm}^* \mathbf{A}_{nm}^H \bar{\mathbf{r}} + h_{o,nm} \mathbf{B}_{nm}^T \bar{\mathbf{r}}^*, \tag{3.11}$$

where $\mathbf{A}_{nm}$ and $\mathbf{B}_{nm}$ are the $NL_\ell \times S_\ell$ dispersion matrices describing the OSTBC employed in the serving tier, see [17, 101] for further details. The resulting *equivalent channel model* allows treating the detection of each of the S_ℓ information symbols encoded in the current codeword separately. The post-combiner SINR at the decoder can then be expressed as

$$\mathtt{SINR}_\Sigma(\ell, y) = \frac{\frac{P_\ell}{S_\ell y^{\alpha_\ell}} \|\mathbf{H}_o\|_F^2}{\sum_{k=1}^{K} \sum_{\mathsf{x}_i \in \Phi_k^o} \mathsf{l}_{i,\mathrm{eqv}} + \sigma^2}, \tag{3.12}$$

where $\mathsf{l}_{i,\mathrm{eqv}}$ is the interference from the i-th BS in the equivalent channel model. $\mathsf{l}_{i,\mathrm{eqv}}$ is statistically the same for all S_ℓ symbols. Thus, focusing on an arbitrary symbol, i.e., considering a single arbitrary column of $\mathbf{A}_{nm}, \mathbf{B}_{nm}$, say $\mathbf{a}_{nm}, \mathbf{b}_{nm}$, the interference $\mathsf{l}_{i,\mathrm{eqv}}$ is

$$\mathsf{l}_{i,\mathrm{eqv}} = \mathrm{Var}_{\{\mathbf{c}_i\}} \left[\sum_{n=1}^{N} \sum_{m=1}^{M_\ell} \frac{\mathsf{h}_{o,nm}^*}{\|\mathbf{H}_o\|_F} \mathbf{a}_{nm}^H \bar{\mathbf{i}}_i + \frac{\mathsf{h}_{o,nm}}{\|\mathbf{H}_o\|_F} \mathbf{b}_{nm}^T \bar{\mathbf{i}}_i^* \right]. \tag{3.13}$$

The Rx noise statistics remain unaffected by the linear combination in (3.11) [21, 101]. However, the distribution of $\mathsf{l}_{i,\mathrm{eqv}}$ is more involved, particularly due to its dependence on $\mathbf{H}_o$. This was already observed in [50] for a similar MIMO network model, where it was shown that ignoring this dependence and assuming $\mathsf{l}_{i,\mathrm{eqv}}$ to be Gamma distributed yields a valid approximation. Following the same approach, one can thus assume $\mathsf{l}_{i,\mathrm{eqv}} \simeq \frac{P_k}{S_k \|\mathsf{x}_i\|^{\alpha_k}} \|\mathbf{H}_i(S_k)\|_F^2$ with $\mathsf{l}_{i,\mathrm{eqv}}$ being independent of $\mathbf{H}_o$, which can be viewed as effectively ignoring the effect of the receiver processing on the interference. The following two facts support this approximation:

- It can be shown that the above Gamma approximation is moment matching irrespective of the realization of $\mathbf{H}_o$, i.e., $\mathbb{E}_{\mathbf{H}_i}[\mathsf{l}_{i,\mathrm{eqv}}] = \frac{P_k}{S_k \|\mathsf{x}_i\|^{\alpha_k}} \mathbb{E}_{\mathbf{H}_i}[\|\mathbf{H}_i(S_k)\|_F^2] = \frac{P_k}{\|\mathsf{x}_i\|^{\alpha_k}}$ in (3.13).

- If $M_k = 1$, it follows from [96] that the above approximation is exact. In this case $\mathsf{l}_{i,\mathrm{eqv}}$ is also truly independent of $\mathbf{H}_o$.

Lemma 3.2 (Interference Laplace transform). *Consider the interference field* $\mathsf{l} = \sum_{k=1}^{K} \sum_{\mathsf{x}_i \in \Phi_k^o} \frac{P_k}{S_k \|\mathsf{x}_i\|^{\alpha_k}} \|\mathbf{H}_i(S_k)\|_F^2$. *Its Laplace transform is*

$$\mathcal{L}_\mathsf{l}(s) = \exp\left(-\pi \sum_{k=1}^{K} \lambda_k d_k^2 \left[{}_2F_1\left(-\tfrac{2}{\alpha_k}, S_k, 1 - \tfrac{2}{\alpha_k}; -\tfrac{s P_k}{S_k d_k^{\alpha_k}} \right) - 1 \right] \right). \tag{3.14}$$

Proof: See Section 3.8.1. ∎

Equipped with Lemma 3.2, one can now derive the coverage probability for IB-MRC.

Theorem 3.1 (Coverage probability for IB-MRC). *The coverage probability* $\mathrm{P_c^{IB}}$ *for IB-MRC in the described setting is given by*

$$
\mathrm{P_c^{IB}} = 2\pi \sum_{\ell=1}^{K} \sum_{m=0}^{NM_\ell-1} \frac{(-1)^m \lambda_\ell}{m!} \int_0^\infty y \frac{\mathrm{d}^m}{\mathrm{d}s^m} \left[\exp\left(-\frac{sS_\ell T}{\mathrm{SNR}(\ell,y)} \right. \right.
$$
$$
\left. \left. -\pi \sum_{k=1}^{K} \lambda_k \hat{P}_k^{2/\alpha_k} y^{2/\hat{\alpha}_k} {}_2F_1\!\left(-\tfrac{2}{\alpha_k}, S_k, 1-\tfrac{2}{\alpha_k}; -\tfrac{sT}{\hat{S}_k}\right) \right) \right]_{s=1} \mathrm{d}y, \quad (3.15)
$$

where $\mathrm{SNR}(\ell,y) \triangleq P_\ell\, y^{-\alpha_\ell}/\sigma^2$ *and* $\hat{S}_k \triangleq S_k/S_\ell$.

Proof: See Section 3.8.2. ∎

The Gaussian hypergeometric function ${}_2F_1(\cdot,\cdot,\cdot;\cdot)$ can be given in terms of elementary functions for certain α_k [66]. For instance, ${}_2F_1\!\left(1,-\tfrac{1}{2},\tfrac{1}{2};-u\right) = 1 + \sqrt{u}\arctan\sqrt{u}$ if $\alpha_k = 4$. For general $\alpha_k > 2$, (3.15) can be easily evaluated using standard numerical software programs.

The derivative $\mathrm{d}^m/\mathrm{d}s^m$ in (3.15) can be calculated using Faà di Bruno's formula for higher-order derivatives of composite functions [66], i.e., with an inner and outer function. While the outer function of the integrand is simple due to the exp-term, the inner function, more specifically ${}_2F_1(-2/\alpha_k, S_k, 1-2/\alpha_k; -sT/\hat{S}_k)$, is more involved. With [66], its derivative is obtained as

$$
\frac{\mathrm{d}^m}{\mathrm{d}s^m} \left[{}_2F_1\!\left(-\tfrac{2}{\alpha_k}, S_k, 1-\tfrac{2}{\alpha_k}; -\tfrac{sT}{\hat{S}_k}\right) \right]_{s=1}
$$
$$
= \left(-\frac{T}{\hat{S}_k}\right)^m \frac{-2\,\Gamma(S_k+m)}{\alpha_k(m-\tfrac{2}{\alpha_k})\,\Gamma(S_k)}
$$
$$
\times {}_2F_1\!\left(-\tfrac{2}{\alpha_k}+m, S_k+m, 1-\tfrac{2}{\alpha_k}+m; -\tfrac{T}{\hat{S}_k}\right). \quad (3.16)
$$

In dense deployments, the performance is typically limited by interference rather than by Rx noise [19], which yields $\sigma^2 = 0 \Leftrightarrow 1/\mathrm{SNR}(\ell,y) = 0$ for all ℓ, y. In addition, the path loss exponent usually does not vary significantly across tiers in practice with typical values around $\alpha_k \approx 3.7$ [99]. When in addition the number of Tx antennas is also equal across tiers, the following corollary applies.

Corollary 3.1 (Special case). *In the absence of Rx noise ($\sigma^2 = 0$) and with equal path loss exponents ($\alpha_k = \alpha \; \forall k \in \mathcal{K}$) and number of Tx antennas ($M_k = M$, $S_k = S \; \forall k \in \mathcal{K}$), $\mathtt{P}_c^{\mathrm{IB}}$ simplifies to*

$$\mathtt{P}_c^{\mathrm{IB}} = \sum_{m=0}^{NM-1} \frac{(-1)^m}{m!} \frac{\mathrm{d}^m}{\mathrm{d}s^m} \left[\frac{1}{{}_2F_1\left(-\frac{2}{\alpha}, S, 1 - \frac{2}{\alpha}; -sT\right)} \right]_{s=1} . \qquad (3.17)$$

The coverage probability in (3.17) neither depends on the BS densities $\{\lambda_k\}$ and powers $\{P_k\}$, nor on the number of tiers K, which is consistent with the literature, see for instance [90]. Note that the first term $m = 0$ in (3.17) corresponds to the coverage probability for the SISO case [89].

3.5.2 MIMO Diversity with IA-MRC

It is now assumed that $M_k \leq 2 \; \forall k \in \mathcal{K}$, meaning that BSs now use full-rate OSTBCs (either no space-time coding or Alamouti scheme). This ensures that the receiver can estimate the interference-plus-noise power at each Rx antenna with acceptable complexity once within the current block/frame, see Remark 3.1. Note that, in theory, $M_k > 2$ is also possible though not practical as the estimation would then have to be performed in each slot τ in the presence of the desired code symbols $\mathbf{c}_{o,\tau}$ to be decoded. When $M_k \leq 2$, one has $S_k = M_k \; \forall k \in \mathcal{K}$, meaning that either Alamouti space-time coding ($M_k = 2$) or no space-time coding ($M_k = 1$) is used in tier k. In both cases, the interference at each Rx antenna, given by (3.6), then remains constant for the entire duration of the desired codeword. In the following, the current per-antenna interference-plus-noise power $\mathsf{I}_n + \sigma^2$ at each Rx antenna is assumed to be known to the receiver in addition to $\mathbf{H}_o$. Interference is still treated as white noise.

In IA-MRC, the phase-corrected and channel-weighted received signals are normalized by the interference-plus-noise power experienced at each Rx antenna, thereby following the original MRC approach from [12]. The receiver hence performs the linear combination

$$\sum_{n=1}^{N} \sum_{m=1}^{M_\ell} \frac{\mathsf{h}_{o,nm}^*}{\mathsf{I}_n + \sigma^2} \mathbf{A}_{nm}^H \bar{\mathbf{r}} + \frac{\mathsf{h}_{o,nm}}{\mathsf{I}_n + \sigma^2} \mathbf{B}_{nm}^T \bar{\mathbf{r}}^*, \qquad (3.18)$$

yielding the equivalent channel model for IA-MRC. Similarly as in Section 3.5.1, one can focus again on an arbitrary symbol and therefore consider an arbitrary column $\mathbf{a}_{nm}$, $\mathbf{b}_{nm}$ of $\mathbf{A}_{nm}$, $\mathbf{B}_{nm}$. The post-combiner SINR for IA-MRC can then be expressed as

$$\mathtt{SINR}_\Sigma(\ell, y) = \frac{\frac{P_\ell}{M_\ell\, y^{\alpha_\ell}} \left(\sum_{n=1}^{N} \frac{\|\mathbf{h}_{o,n}\|_F^2}{\mathsf{I}_n + \sigma^2}\right)^2}{\sum_{k=1}^{K} \sum_{\mathsf{x}_i \in \Phi_k^o} \mathsf{I}_{i,\text{eqv}} + \sum_{n=1}^{N} \frac{\|\mathbf{h}_{o,n}\|_F^2 \sigma^2}{(\mathsf{I}_n + \sigma^2)^2}}, \tag{3.19}$$

where now $\mathsf{I}_{i,\text{eqv}}$ is

$$\mathsf{I}_{i,\text{eqv}} = \text{Var}_{\{\mathbf{c}_i\}} \left[\sum_{n=1}^{N} \sum_{m=1}^{M_\ell} \frac{\mathsf{h}_{o,nm}^*}{\mathsf{I}_n + \sigma^2} \mathbf{a}_{nm}^H \bar{\mathbf{i}}_i + \frac{\mathsf{h}_{o,nm}}{\mathsf{I}_n + \sigma^2} \mathbf{b}_{nm}^T \bar{\mathbf{i}}_i^* \right]. \tag{3.20}$$

By (3.4), one has $\mathbb{E}_{\mathbf{c}_i}[\bar{\mathbf{i}}_i \bar{\mathbf{i}}_i^H] = \frac{P_k}{M_k \|\mathsf{x}_i\|^{\alpha_k}} \left(\|\mathbf{h}_{i,n}\|_F^2 \mathbf{I}_{NL_\ell} + \mathbf{R}_i \right)$, where $\mathbf{R}_i = \text{diag}(\tilde{\mathbf{H}}_i, \ldots, \tilde{\mathbf{H}}_i)$ is a block diagonal matrix with the $N \times N$ square matrix $\tilde{\mathbf{H}}_i$ on the diagonal. The entries of $\tilde{\mathbf{H}}_i$ are

$$(\tilde{\mathbf{H}}_i)_{pq} = \begin{cases} \mathbf{h}_{i,p} \mathbf{h}_{i,q}^H, & p \neq q \tag{3.21a} \\ 0, & p = q. \tag{3.21b} \end{cases}$$

Note that, in contrast to $\mathbf{I}_{NL_\ell}$, $\mathbf{R}_i$ has non-zero off-diagonal matrix entries. Invoking the orthogonality properties of the $\{\mathbf{A}_{nm}\}$, $\{\mathbf{B}_{nm}\}$, i.e., $\mathbf{A}_{nm}^H \mathbf{A}_{uv} + \mathbf{B}_{uv}^T \mathbf{B}_{nm}^* = \delta_{nu} \delta_{mv} \mathbf{I}_{NL_\ell}$ and $\mathbf{A}_{nm}^H \mathbf{B}_{uv} + \mathbf{B}_{uv}^T \mathbf{A}_{nm}^* = \mathbf{0}_{L_\ell}$, $1 \leq n, u \leq N$ and $1 \leq m, v \leq M_\ell$, where $\delta_{ij} = 1$ if $i = j$ and zero otherwise, and exploiting the mathematical structure of $\mathbb{E}_{\mathbf{c}_i}[\bar{\mathbf{i}}_i \bar{\mathbf{i}}_i^H]$, (3.20) can be computed following the same approach as in [101, Sec. 2.2.3] as

$$\mathsf{I}_{i,\text{eqv}} = \frac{P_k}{M_k \|\mathsf{x}_i\|^{\alpha_k}} \sum_{n=1}^{N} \|\mathbf{h}_{o,n}\|_F^2 \frac{\|\mathbf{h}_{i,n}\|_F^2}{(\mathsf{I}_n + \sigma^2)^2} + \frac{\mathsf{Z}_{i,n}}{(\mathsf{I}_n + \sigma^2)^2}. \tag{3.22}$$

In (3.22), $\mathsf{Z}_{i,n}$ describes the part resulting from $\mathbf{R}_i$ having non-zero off-diagonal matrix entries. From (3.21), it can be inferred that $\mathsf{Z}_{i,n}$ depends on the channel phases of $\mathbf{H}_i$. Since $\mathsf{h}_{i,nm} \sim \mathcal{CN}(0,1)$, it can be shown that $\mathbb{E}_{\angle \mathbf{H}_i}[\mathbf{R}_i] = 0$, which implies $\mathbb{E}_{\angle \mathbf{H}_i}[\mathsf{Z}_{i,n}] = 0$ irrespective of $\mathbf{H}_o$, indicating that the effect of $\mathsf{Z}_{i,n}$ vanishes "in the long run". To obtain a more tractable expression, the $\{\mathsf{Z}_{i,n}\}$ in (3.22) are hence ignored. With this simplification and after some algebraic manipulations, (3.19) then becomes

$$\mathtt{SINR}_\Sigma(\ell, y) = \frac{P_\ell}{M_\ell\, y^{\alpha_\ell}} \sum_{n=1}^{N} \frac{\|\mathbf{h}_{o,n}\|_F^2}{\mathsf{I}_n + \sigma^2}. \tag{3.23}$$

Remark 3.2 (SINR$_\Sigma$ approximation). *It follows by Jensen's inequality [81] that*

$$\mathbb{E}_{\angle\mathbf{H}_1,\angle\mathbf{H}_2,\ldots}\left[\mathtt{SINR}_\Sigma(\ell,y)\right] \geq \frac{P_\ell}{M_\ell\,y^{\alpha_\ell}} \sum_{n=1}^{N} \frac{\|\mathbf{h}_{o,n}\|_F^2}{\mathsf{I}_n + \sigma^2}, \tag{3.24}$$

where $\mathtt{SINR}_\Sigma(\ell,y)$ *on the left-hand side corresponds to the exact post-combiner SINR from (3.19). Hence, (3.23) provides a lower bound to the phase-averaged exact post-combiner SINR. The resulting error when (3.23) is used to approximate the exact post-combiner SINR is negligibly small, as confirmed by simulations in Section 3.6 and discussed in Appendix B.*

Although the $\{\mathbf{h}_{i,n}\}$ in (3.23) are mutually independent, the $\{\mathsf{I}_n\}$ are correlated across Rx antennas due to the common locations of interfering BSs. More specifically, the expression in (3.23) is a sum of correlated random variables exhibiting a complicated correlation structure. This renders the computation of the coverage probability for IA-MRC for general N challenging. In practical systems, however, the number of antennas in mobile devices is limited due to space/complexity limitations, thereby often not exceeding $N = 2$. This special case is addressed next.

Theorem 3.2 (Coverage probability for dual-antenna IA-MRC). *The coverage probability* $\mathrm{P}_c^{\mathrm{IA}}$ *for dual-antenna IA-MRC in the described setting is*

$$\mathrm{P}_c^{\mathrm{IA}} = 2\pi \sum_{\ell=1}^{K} \sum_{m=0}^{M_\ell-1} \frac{(-1)^{m+M_\ell}\lambda_\ell}{m!\,\Gamma(M_\ell)} \int_0^\infty \int_0^\infty yz^{-1}$$

$$\times \frac{\partial^{m+M_\ell}}{\partial s^m\,\partial t^{M_\ell}}\left[\exp\left(-\frac{M_\ell}{\mathtt{SNR}_\ell(y)}\left(s\,(T-z)^+ + tz\right)\right)\right.$$

$$\times \exp\left(-\pi\sum_{k=1}^{K}\lambda_k\hat{P}_k^{2/\alpha_k}y^{2/\hat{\alpha}_k}\right.$$

$$\left.\left.\times\left[1 + \Psi\left(\frac{s\,(T-z)^+}{\hat{M}_k}, \frac{tz}{\hat{M}_k}, M_k, \alpha_k\right)\right]\right)\right]_{\substack{s=1\\t=1}} \mathrm{d}y\,\mathrm{d}z, \tag{3.25}$$

for $1 \leq M_k \leq 2$ *and* $N = 2$, *where* $\hat{M}_k \triangleq M_k/M_\ell$ *and* $\Psi(\cdot,\cdot,\cdot,\cdot)$ *is given by (3.45) in Section 3.8.3.*

Proof: See Section 3.8.3 ∎

The function $\Psi(\cdot,\cdot,\cdot,\cdot)$ in (3.25) can be given in terms of Gaussian hypergeometric functions ${}_2F_1(\cdot,\cdot,\cdot;\cdot)$, which can be further simplified in some cases, refer to the comment after Theorem 3.1 in Section 3.5.1. This fact will be used in Section 3.6.3.

Compared to P_c^{IB} in (3.15), P_c^{IA} is more involved due to the mathematical form of (3.23), which translates into the convolution-type integral over z. Nevertheless, the expression in (3.25) can be evaluated with acceptable complexity using semi-analytical tools, see Chapter 2 for an example. Besides, (3.25) covers the general case and the expression can be further simplified in certain specific cases as discussed next. The counterpart to Corollary 3.1 is given next.

Corollary 3.2 (Special case)**.** *In the absence of Rx noise ($\sigma^2 = 0$), and with equal path loss exponents ($\alpha_k = \alpha \; \forall k \in \mathcal{K}$) and number of Tx antennas ($M_k = M \leq 2 \; \forall k \in \mathcal{K}$), P_c^{IA} reduces to*

$$P_c^{IA} = \sum_{m=0}^{M-1} \frac{(-1)^{m+M}}{m!\,\Gamma(M)} \int_0^\infty z^{-1}$$
$$\times \frac{\partial^{m+M}}{\partial s^m\,\partial t^M} \left[\frac{1}{1 + \Psi\left(s\,(T-z)^+, tz, M, \alpha\right)} \right]_{\substack{s=1 \\ t=1}} \mathrm{d}z. \quad (3.26)$$

The expression in (3.26) is less complicated than (3.25). When the threshold T is not large, the $\Psi\left(s\,(T-z)^+, tz, M, \alpha\right)$ term can be further simplified as shown next.

Corollary 3.3 (Small-T approximation)**.** *For small T, the approximation*

$$1 + \Psi\left(\frac{s\,(T-z)^+}{\hat{M}_k}, \frac{tz}{\hat{M}_k}, M_k, \alpha_k\right) \simeq {}_2F_1\left(-\frac{2}{\alpha_k}, M_k, 1 - \frac{2}{\alpha_k}; -\frac{s\,(T-z)^+ + tz}{\hat{M}_k}\right). \quad (3.27)$$

becomes tight.

The right-hand side of (3.27) may be easier to evaluate than the original expression in certain cases since the Gaussian hypergeometric function is available in most numerical software programs. Moreover, its higher-order derivatives with respect to both s and t appearing in (3.25) can be evaluated fairly easily following the same procedure as in (3.16) for differentiating composite functions.

Table 3.2: System Parameters used for Numerical Examples

Parameter	Tier 1	Tier 2	Tier 3
BS density λ_k	$4\,\mathrm{BS/km}^2$	$16\,\mathrm{BS/km}^2$	$40\,\mathrm{BS/km}^2$
BS power P_k	$46\,\mathrm{dBm}$	$30\,\mathrm{dBm}$	$24\,\mathrm{dBm}$
BS Tx antennas M_k	4	2 (Alamouti)	1 (no OSTBC)
Path loss exponent α_k	3.76	3.67	3.5

3.6 Discussion

In this section, the theoretical results developed in the prior sections are leveraged to study the performance of MIMO diversity in HCNs through numerical examples. Besides, the approximations introduced in Section 3.5.1 and Section 3.5.2 are verified by numerical simulations. Unless stated otherwise, a three-tier ($K = 3$) HCN with the typical tier-specific system parameters given in Table 3.2 is assumed, see [99]. The dispersion matrices $\{\mathbf{A}_{nm}\}$, $\{\mathbf{B}_{nm}\}$ are chosen from [96, Sec. 2.2.3].

3.6.1 Multi-Tier & MIMO: IB-MRC vs. IA-MRC

First, the performance of IB-MRC in a typical HCN scenario with the parameters shown in Table 3.2 is considered. The $(4, 4, 3/4)$-OSTBC from [97, 7.4.10] is chosen for tier one. Fig. 3.2 shows the coverage probability $\mathrm{P}_c^{\mathrm{IB}}$ versus the SINR threshold T for IB-MRC and different number of Rx antennas N. It can be seen that the theoretical expressions perfectly match the simulation results, thereby validating the Gamma approximation explained in Section 3.5.1. As expected, increasing N improves $\mathrm{P}_c^{\mathrm{IB}}$ since the typical user enjoys a larger array/diversity gain. For practical target coverage probabilities, i.e. around 80% of covered users, the horizontal gap between the $\mathrm{P}_c^{\mathrm{IB}}$ curves is roughly 2.5 dB. Fig. 3.3 shows the coverage probability $\mathrm{P}_c^{\mathrm{IA}}$ for IA-MRC. Here, the interference-limited case ($\sigma^2 = 0$) is considered with equal path loss exponents ($\alpha_k = 3.7$ $\forall k \in \mathcal{K}$) and the same number of Tx antennas $M_k = 2$ $\forall k \in \mathcal{K}$. Again, simulation results and theoretical expressions are fairly close over the entire range of T, thus justifying the approximation made in Section 3.5.2, see Remark 3.2. It can be further observed that, for IA-MRC, doubling N yields a gain of around 3.6 dB for the same target coverage probability.
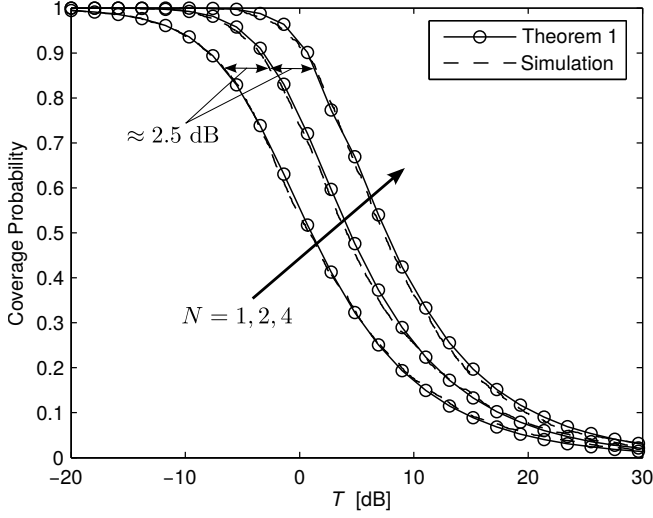
Figure 3.2: Coverage probability $\mathtt{P}_{\mathrm{c}}^{\mathrm{IB}}$ for different N and Rx noise power $\sigma^2 = -104\,\mathrm{dBm}$.
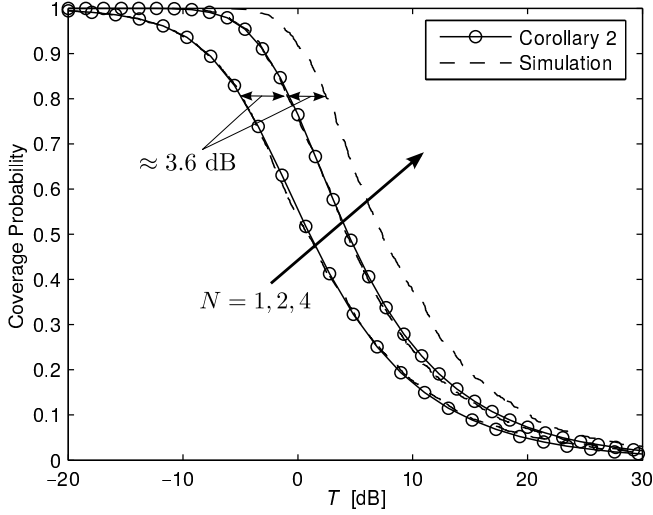
Figure 3.3: Coverage probability $\mathtt{P}_{\mathrm{c}}^{\mathrm{IA}}$ for different N. Parameters: $\sigma^2 = 0$, $\alpha_k = 3.7$ and $M_k = 2 \ \forall k \in \mathcal{K}$.

Next, the performance of IB-MRC and IA-MRC is compared for the same scenario, i.e., $\sigma^2 = 0$, $\alpha_k = 3.7$ and $M_k = M \; \forall k \in \mathcal{K}$. In Fig. 3.4, the relative coverage probability gain of IA-MRC over IB-MRC, which is defined as $\Delta_{P_c}^{IA\text{-}IB} \triangleq P_c^{IA}/P_c^{IB} - 1$, is shown for $M = 1, 2$ Tx antennas. This relative gain is somewhat disappointingly small ($< 2\%$ in this example). In fact, IA-MRC becomes even less favorable when adding more Tx antennas. This is due to the fact that adding more Tx antennas effectively smoothes out the fading on the interfering channels, which renders the interference increasingly similar across Rx antennas. This trend was already predicted in Section 3.4, where the second-order statistics of the interference were analyzed. Thus, with almost equal interference levels across Rx antennas, the performance of IB-MRC and IA-MRC becomes similar due to less interference diversity. In conclusion, the additional, though not overwhelming, complexity of IA-MRC must hence be traded-off against an insignificant improvement relative to IB-MRC; with Tx diversity, IB-MRC may then be the better choice in MIMO HCNs.

3.6.2 Multi-Tier & MISO: Effect of OSTBC

As can be inferred from (3.15) in Theorem 3.1, Tx diversity increases the number of diversity paths on the one hand, while it affects the interference statistics on the other. Next, this trade-off is studied by focusing on OSTBC Tx diversity in a MISO setting ($N = 1$) with different Tx antenna configurations. To capture the *net gain* of OSTBC one has to account for the rate loss resulting from code rates $r_\ell < 1$ when being associated with the ℓ-th tier. This can be done by introducing a tier-specific SINR threshold $T \Rightarrow T_\ell$ in (3.25) with $T_\ell \triangleq (1 + T)^{1/r_\ell} - 1$, assuming the Shannon capacity formula $r_\ell \log_2(1 + T_\ell)$ [102]. The latter adaptation makes sure that the same amount of information is transmitted in every OSTBC word of length L_ℓ. Fig. 3.5 shows that the MISO coverage probability increases only slightly with the number of Tx antennas in the low SINR regime. For target SINRs larger than a few dB, Tx diversity is not beneficial. In fact, for OSTBCs with rates $r_k < 1$, e.g., $M_k = 4$ $\forall k \in \mathcal{K}$, Tx diversity even reduces the coverage probability in this regime due to the aforementioned rate loss. This is in line with prior findings for the single-user case [16] and single-tier cellular networks [92], where little to no gains of OSTBC-based Tx diversity with more than two Tx antennas were reported at reasonable operating points.

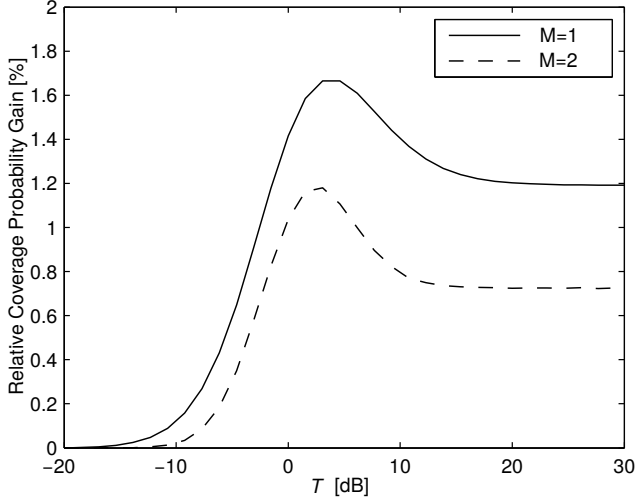**Figure 3.4:** Relative coverage probability gain $\Delta_{\mathrm{P_c}}^{\mathrm{IA\text{-}IB}}$. Parameters: $\sigma^2 = 0$, $\alpha_k = 3.7$ and $M_k = M \; \forall k \in \mathcal{K}$.
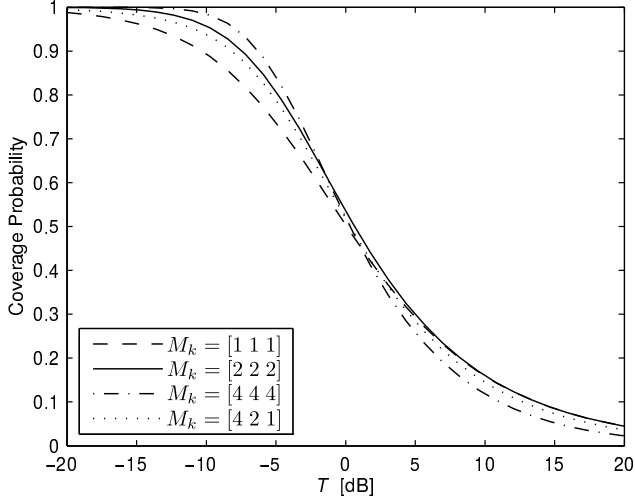
Figure 3.5: Coverage probability for MISO case with different Tx-antenna configurations.

3.6.3 Multi-Tier & SIMO: Gain of MRC over SISO

From an information-theoretic viewpoint, Rx diversity with MRC is more appealing than Tx diversity with space-time coding as the latter incurs a power penalty [19]. The potential gains of Rx diversity with MRC in HCNs, however, are yet not well-understood due to their dependence on many system parameters. While in Section 3.6.1 the relative performance of IB-MRC and IA-MRC was studied, the gains provided solely by MRC Rx diversity ($M_k = 1 \; \forall k \in \mathcal{K}$) over SISO transmission are analyzed next. Focus is again on the interference-limited regime ($\sigma^2 = 0$) with equal path loss exponents across tiers ($\alpha_k = \alpha \; \forall k \in \mathcal{K}$) and $N = 2$. In this case, one obtains the expressions

$$
\mathrm{P_c^{IB}} = \frac{1}{{}_2F_1\big(-\frac{2}{\alpha}, 1, 1 - \frac{2}{\alpha}; -T\big)} + \underbrace{\frac{\frac{\mathrm{d}}{\mathrm{d}s}\big[{}_2F_1\big(-\frac{2}{\alpha}, 1, 1 - \frac{2}{\alpha}; -sT\big)\big]_{s=1}}{{}_2F_1\big(-\frac{2}{\alpha}, 1, 1 - \frac{2}{\alpha}; -T\big)^2}}_{\triangleq \; G^{\mathrm{IB}}(\alpha, T)} \quad (3.28)
$$

for IB-MRC and

$$
\mathrm{P_c^{IA}} = \frac{1}{{}_2F_1\big(-\frac{2}{\alpha}, 1, 1 - \frac{2}{\alpha}; -T\big)} + \underbrace{\int_0^T \frac{\frac{\mathrm{d}}{\mathrm{d}t}\big[\mathcal{A}(T - z, tz, \alpha)\big]_{t=1}}{z\,\mathcal{A}(T - z, z, \alpha)^2}\,\mathrm{d}z}_{\triangleq \; G^{\mathrm{IA}}(\alpha, T)}. \quad (3.29)
$$

for IA-MRC, where $\mathcal{A}(\cdot, \cdot, \cdot) \triangleq 1 + \Psi(\cdot, \cdot, 1, \cdot)$ is

$$
\mathcal{A}(a_1, a_2, q) = \frac{a_1}{a_1 - a_1}\, {}_2F_1\Big(-\frac{2}{q}, 1, 1 - \frac{2}{q}; -a_1\Big) \\
- \frac{a_2}{a_1 - a_2}\, {}_2F_1\Big(-\frac{2}{q}, 1, 1 - \frac{2}{q}; -a_2\Big). \quad (3.30)
$$

Remark 3.3. *The first terms in* (3.28) *and* (3.29) *correspond to the SISO coverage probability [89]*

$$
\mathrm{P_c^{SISO}} = \frac{1}{{}_2F_1\big(-\frac{2}{\alpha}, 1, 1 - \frac{2}{\alpha}; -T\big)}. \quad (3.31)
$$

This, in turn, means that $G^{IB}(\alpha, T)$ *in* (3.28) *and* $G^{IA}(\alpha, T)$ *in* (3.29) *quantify the absolute coverage probability increase of dual-antenna IB-MRC and IA-MRC, respectively, over SISO transmission in HCNs.*

The derivative inside $G^{\mathrm{IB}}(\alpha, T)$ and $G^{\mathrm{IA}}(\alpha, T)$ can be computed using (3.16). As a result of Remark 3.3, $G^{\mathrm{IB}}(\alpha, T)$ and $G^{\mathrm{IA}}(\alpha, T)$ are identified

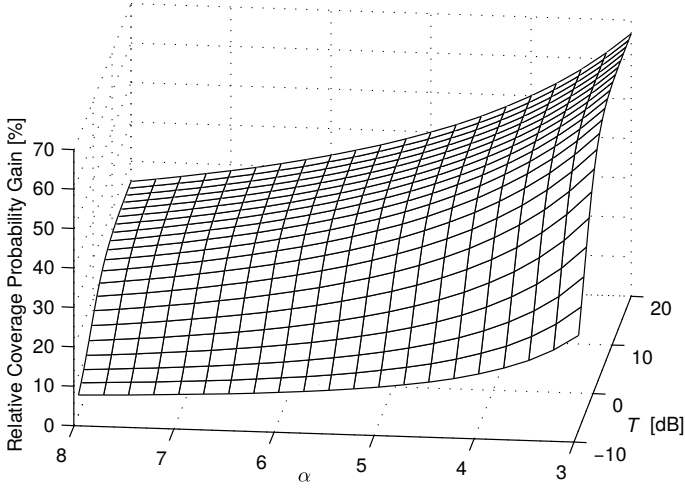**Figure 3.6:** Relative coverage probability gain $\Delta_{P_c}^{\text{IB-MRC-SISO}}$. Parameters: $N = 2$, $\sigma^2 = 0$, and $M_k = 1$ and $\alpha_k = \alpha \; \forall k \in \mathcal{K}$.
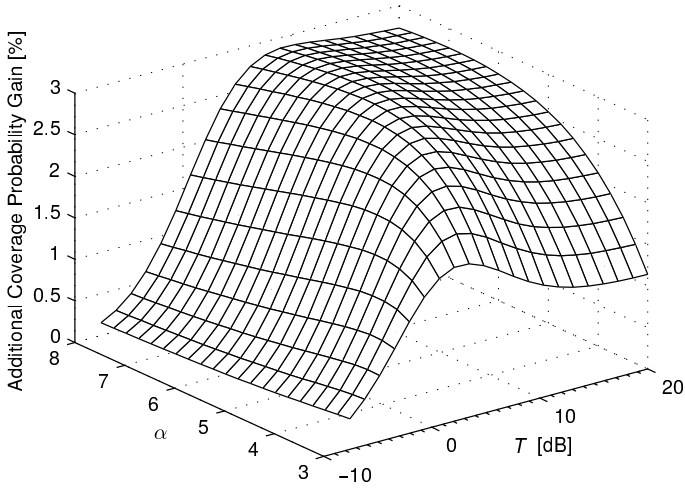
Figure 3.7: Additional relative gain $\Delta_{P_c}^{\text{IA-MRC-SISO}} - \Delta_{P_c}^{\text{IB-MRC-SISO}}$ due to IA-MRC. Parameters: $N = 2$, $\sigma^2 = 0$, and $M_k = 1$ and $\alpha_k = \alpha \; \forall k \in \mathcal{K}$.

as the characteristic terms for analyzing the performance of dual-antenna MRC relative to SISO transmission. This relative gain can be defined as $\Delta_{P_c}^{\text{IB-MRC-SISO}} \triangleq P_c^{\text{IB}}/P_c^{\text{SISO}} - 1 = G^{\text{IB}}(\alpha, T)\, _2F_1(-2/\alpha, 1, 1 - 2/\alpha; -T)$ and $\Delta_{P_c}^{\text{IA-MRC-SISO}} \triangleq P_c^{\text{IA}}/P_c^{\text{SISO}} - 1 = G^{\text{IA}}(\alpha, T)\, _2F_1(-2/\alpha, 1, 1 - 2/\alpha; -T)$ for IB-MRC and IA-MRC, respectively.

Figure 3.6 shows the relative coverage probability gain $\Delta_{P_c}^{\text{IB-MRC-SISO}}$ versus α and T. The relative gain monotonically decreases with α and monotonically increases with T. Interestingly, $\Delta_{P_c}^{\text{IB-MRC-SISO}}$ saturates at large T, although in the corresponding interference-free case the relative gain of MRC over SISO grows unboundedly in T [19, 7.2.4]. For typical values $3 < \alpha < 5$ and $T > -6$ dB, the relative gain of IB-MRC is between 12%–66%. Fig. 3.7 illustrates the *additional* relative gain $\Delta_{P_c}^{\text{IA-MRC-SISO}} - \Delta_{P_c}^{\text{IB-MRC-SISO}}$ when switching from IB-MRC to IA-MRC. In line with Fig. 3.4, IB-MRC already harvests most of the gains over SISO transmission as the additional improvement of IA-MRC does not exceed 3% in this example. Nevertheless, the largest additional improvement for realistic path loss exponents around $\alpha = 4$ lies entirely in the practical regime $-5 < T < 10$ dB.

3.6.4 Effect of Spatial Interference Correlation

As explained in the beginning of this chapter and in Section 3.4, interference correlation across Rx antennas influences the performance of IA-MRC. Mathematically, this can be seen by noting that the post-combiner SINR in (3.23) is a sum of correlated random variables. The difficulty of characterizing the coverage probability for general N is due to the complicated correlation structure inherent to this sum, see Section 3.5.2. To increase mathematical tractability, two simpler correlation models are thus typically used in the literature: 1) NC model, and 2) FC model. Using the results from Section 3.5.2, the validity of these models for IA-MRC will be discussed next.

No-Correlation Model

A commonly made assumption to maintain analytical tractability is to assume that the $\{I_n\}$ in (3.23) are uncorrelated, i.e., the locations of interfering BSs in I_n originate from separate independent point processes

for each Rx antenna n. Under this assumption, the following coverage probability $\mathtt{P}^{\mathrm{IA}}_{\mathrm{c,NC}}$ for the NC model can be obtained.

Proposition 3.1 (Coverage Probability $\mathtt{P}^{\mathrm{IA}}_{\mathrm{c,NC}}$). *The coverage probability* $\mathtt{P}^{\mathrm{IA}}_{\mathrm{c,NC}}$ *for dual-antenna IA-MRC in the NC model is given by* (3.25) *with* $1 + \Psi(\cdot, \cdot, \cdot, \cdot)$ *replaced by*

$$
\begin{aligned}
{}_2F_1\Big(-\tfrac{2}{\alpha_k}, M_k, 1 - \tfrac{2}{\alpha_k}; -\tfrac{s}{M_k}\,(T-z)^+\Big) \\
+ {}_2F_1\Big(-\tfrac{2}{\alpha_k}, M_k, 1 - \tfrac{2}{\alpha_k}; -\tfrac{t}{M_k}z\Big) - 1.
\end{aligned}
\tag{3.32}
$$

Proof: See Section 3.8.4. ∎

By comparing the mathematical form of the expression in (3.32) with $1 + \Psi(\cdot, \cdot, \cdot, \cdot)$ in (3.25), the influence of spatial interference correlation becomes apparent: in (3.32) the first two terms result in a product of PDFs of the form $f_{\mathtt{SINR}_1}(T-z)f_{\mathtt{SINR}_2}(z)$ inside the integral over z, which corresponds to the well-known convolution-type integral for sums of independent random variables [80, Sec. V.4]. Note that by looking at $1 + \Psi(\cdot, \cdot, \cdot, \cdot)$, it becomes clear that no such product form can be obtained for the joint PDF of $\mathtt{SINR}_1$ and $\mathtt{SINR}_2$ due to the interference correlation across Rx antennas.

Full-Correlation Model

Another frequently used approach in the literature to simplify the analysis is to assume that the $\{\mathsf{I}_n\}$ are fully correlated, i.e., the fading gains $\mathbf{h}_{i,n}$ yield the same realization across n for all $\mathsf{x}_i \in \Phi^o$. Under this assumption, the corresponding coverage probability $\mathtt{P}^{\mathrm{IA}}_{\mathrm{c,FC}}$ for the FC model can be derived for arbitrary N as shown next.

Proposition 3.2 (Coverage probability $\mathtt{P}^{\mathrm{IA}}_{\mathrm{c,FC}}$). *The coverage probability* $\mathtt{P}^{\mathrm{IA}}_{\mathrm{c,FC}}$ *for N-antenna IA-MRC in the FC model is the same as for IB-MRC, see* (3.15) *in Theorem 3.1.*

Proof: See Section 3.8.5. ∎

Figure 3.8 shows the relative coverage probability deviation for the two simpler correlation models for $M_k = 1, 2\ \forall k \in \mathcal{K}$. The relative deviation is defined as $\delta^{\mathrm{NC}}_{\mathtt{P_c}} \triangleq \mathtt{P}^{\mathrm{IA}}_{\mathrm{c,NC}}/\mathtt{P}^{\mathrm{IA}}_{\mathrm{c}} - 1$ ($\delta^{\mathrm{FC}}_{\mathtt{P_c}} \triangleq \mathtt{P}^{\mathrm{IA}}_{\mathrm{c,FC}}/\mathtt{P}^{\mathrm{IA}}_{\mathrm{c}} - 1$) for the respective

Figure 3.8: Relative coverage probability deviation $\delta_{P_c}^{NC}$ and $\delta_{P_c}^{FC}$. Parameters: $\sigma^2 = 0$, $M_k = M$ and $\alpha_k = 3.7 \ \forall k \in \mathcal{K}$.

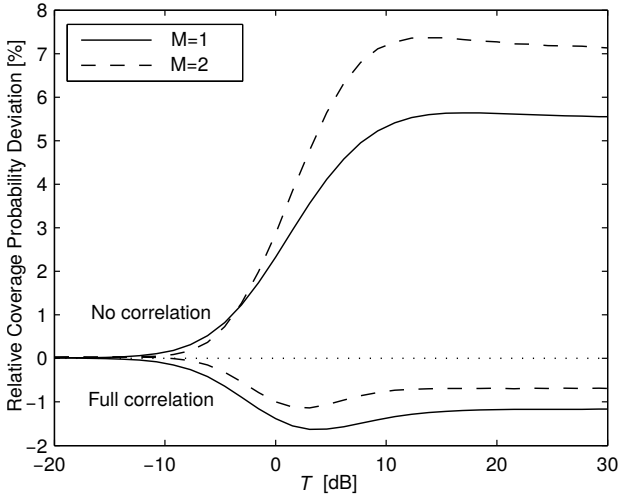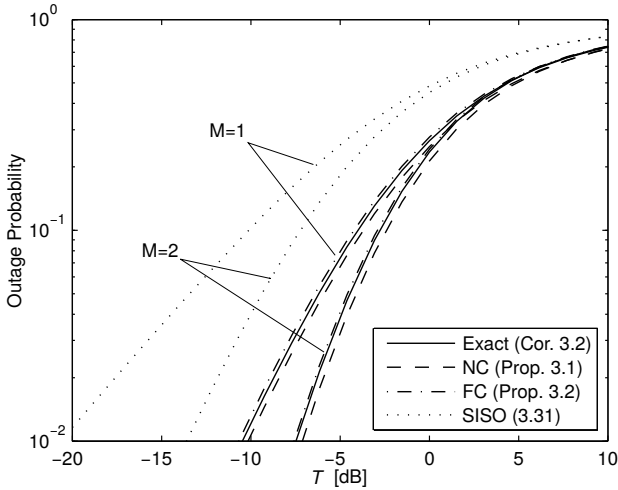**Figure 3.9:** Outage probability comparison between exact correlation, NC, and FC model. SISO is also shown for reference. Parameters: $\sigma^2 = 0$, $M_k = M$ and $\alpha_k = 3.7 \ \forall k \in \mathcal{K}$.

correlation models. First, it can be seen that both models reflect the true performance at small T. For $T > 0$ dB, the NC model yields a significantly optimistic performance prediction ($3\% < \delta_{\text{P}_\text{c}}^{\text{NC}} < 8\%$), depending on the number of Tx antennas. In contrast, the FC model slightly underestimates the true performance ($\delta_{\text{P}_\text{c}}^{\text{FC}} < 2\%$). In line with the intuition, adding a second Tx antenna increases $\delta_{\text{P}_\text{c}}^{\text{NC}}$ due to the smaller interference variance and larger interference correlation across Rx antennas, see Section 3.4. Consequently, $\delta_{\text{P}_\text{c}}^{\text{FC}}$ decreases in this case. The smaller deviation for the FC model was already reported in Chapter 2 for Aloha-based *ad hoc* networks and is reconfirmed in this chapter for HCNs. Fig. 3.9 illustrates the outage probability $(1 - \text{P}_\text{c})$ for the exact, NC, and FC model for $M_k = 1, 2 \; \forall k \in \mathcal{K}$. It can be seen that the simpler correlation models preserve the true diversity order for dual-antenna IA-MRC. Interestingly, the diversity order due to IA-MRC (equal to N) remains unaffected by the interference correlation across Rx antennas. This is in sharp contrast to the *ad hoc* network model considered in Chapter 2, where the NC model fails to recover the true diversity behavior, see Section 2.5.2. This difference results from the fact that, unlike in HCNs, interfering transmitters may be significantly closer to the receiver than the desired transmitter in *ad hoc* networks, thereby imprinting a different law to the interference statistics compared to in HCNs. As expected, the diversity order of IA-MRC for $M = 2$ and $N = 2$ is $NM = 4$.

In conclusion, the FC model offers a tight approximation to the performance of IA-MRC in HCNs, particularly when BSs employ multiple Tx antennas. This result is congruent with the prior observation that the performance gap between IA-MRC and IB-MRC is not significant and further decreases with the number of Tx antennas.

3.6.5 Comparison with IA Selection Combining

Complexity constraints may sometimes prohibit the use of MRC and allow only for simpler combining schemes. Importantly, while hardware requirements of combining schemes are independent of the communication environment, their performance obviously is not. To properly balance performance-complexity trade-offs, it is hence important to compare the performance of MRC to other combining schemes using a realistic model. In the following, such a comparison is conducted for the example of

IA-SC, which is a widespread scheme with lower complexity compared to MRC. A similar comparison can be found in Chapter 2 for wireless *ad hoc* networks. Focus will be on the case $M_k = 1 \; \forall k \in \mathcal{K}$, while an extension to $M_k > 1$ is deferred to possible future work. The following result is a generalization of [55] and gives the coverage probability for IA-SC with Rx noise in HCNs.

Theorem 3.3 (Coverage probability $\mathrm{P}_\mathrm{c}^\mathrm{SC}$). *The coverage probability $\mathrm{P}_\mathrm{c}^\mathrm{SC}$ for N-antenna IA-SC in the described setting with $M_k = 1 \; \forall k \in \mathcal{K}$ is given by*

$$
\mathrm{P}_\mathrm{c}^\mathrm{SC} = 2\pi \sum_{\ell=1}^{K} \sum_{n=1}^{N} \binom{N}{n} (-1)^{n+1} \lambda_\ell \int_0^\infty y \exp\left(-\frac{nT}{\mathsf{SNR}(\ell, y)} \right.
$$
$$
\left. -\pi \sum_{k=1}^{K} \lambda_k \hat{P}_k^{2/\alpha_k} y^{2/\hat{\alpha}_k} {}_2F_1\left(-\tfrac{2}{\alpha_k}, n, 1 - \tfrac{2}{\alpha_k}; -T\right) \right) \mathrm{d}y. \quad (3.33)
$$

Proof: See Section 3.8.6. ∎

Without Rx noise and with equal path loss exponents across tiers, (3.33) can be further simplified as shown next.

Corollary 3.4 (Special case). *In the absence of Rx noise ($\sigma^2 = 0$) and with equal path loss exponents ($\alpha_k = \alpha \; \forall k \in \mathcal{K}$), (3.33) simplifies to*

$$
\mathrm{P}_\mathrm{c}^\mathrm{SC} = \sum_{n=1}^{N} \frac{(-1)^{n+1}\binom{N}{n}}{{}_2F_1\left(-\tfrac{2}{\alpha}, n, 1 - \tfrac{2}{\alpha}; -T\right)}. \quad (3.34)
$$

Remark 3.4 (Comment on Corollary 3.4). *Corollary 3.4 coincides with the result in [103, Corollary 2] for IA-SC over multiple resource blocks without Rx noise in single-tier ($K = 1$) cellular networks. Thus, Corollary 3.4, and especially Theorem 3.3, represent a generalization of the results from [103] for HCNs.*

Figure 3.10 shows the relative coverage probability gain of MRC over IA-SC for $N = 2, 4$. The relative gain is defined as $\Delta_{\mathrm{P}_\mathrm{c}}^{\mathrm{IB\text{-}MRC\text{-}SC}} \triangleq \mathrm{P}_\mathrm{c}^\mathrm{IB}/\mathrm{P}_\mathrm{c}^\mathrm{SC} - 1$ for IB-MRC and $\Delta_{\mathrm{P}_\mathrm{c}}^{\mathrm{IA\text{-}MRC\text{-}SC}} \triangleq \mathrm{P}_\mathrm{c}^\mathrm{IA}/\mathrm{P}_\mathrm{c}^\mathrm{SC} - 1$ for IA-MRC. The result for IA-MRC with $N = 4$ was obtained by numerical simulations as Theorem 3.2 and Corollary 3.2 treat only the case $N = 2$. As expected, MRC outperforms IA-SC, particularly at large T. However, for practical T
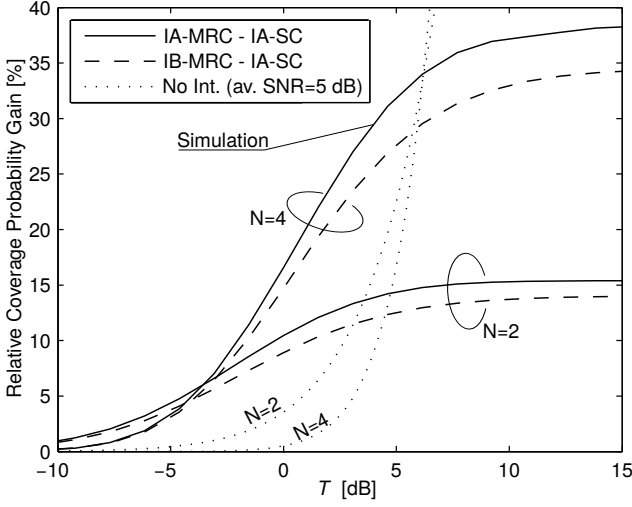
Figure 3.10: Relative coverage probability gain $\Delta_{\mathsf{P_c}}^{\text{IA-MRC-SC}}$ and $\Delta_{\mathsf{P_c}}^{\text{IB-MRC-SC}}$ for different N. Parameters: $\sigma^2 = 0$, $\alpha_k = 3.7$ and $M_k = 1 \; \forall k \in \mathcal{K}$. Dotted line refers to interference-free case from [19, Sec. 7.2] with average SNR 5 dB.

around a few dB (which corresponds to between 70-80% covered users), the gap is less than 10% for $N = 2$. Here, the additional complexity associated with MRC may not be justified as IA-SC achieves similar performance. Nevertheless, adding more Rx antennas increases the relative performance (about 25% for $N = 4$ at practical T). Note that, in sharp contrast to the interference-free case (dotted line in Fig. 3.10), the relative gain of MRC over IA-SC saturates at large T due to the effect of correlated interference.

3.7 Summary

A stochastic model for analyzing the performance of downlink MIMO diversity with OSTBC and MRC in HCNs was developed using tools from stochastic geometry. It was shown that adding more Tx antennas at the BSs increases the coverage probability on the one hand, while it impacts the relative performance of IB-MRC and IA-MRC on the other

hand. One important design insight that arises from the analysis is that IA-MRC is less favorable than IB-MRC when multiple Tx antennas are used. Another key insight is that the FC model provides a reasonably tight approximation for IA-MRC; this could enable the analysis of more sophisticated MIMO techniques, which may be hopeless when considering the exact correlation structure.

3.8 Proofs

3.8.1 Proof of Lemma 3.2

The result is obtained by noting that

$$
\mathbb{E}\left[\exp\left(-s\sum_{k=1}^{K}\sum_{x_i\in\Phi_k^o}\frac{P_k}{S_k\|x_i\|^{\alpha_k}}\|\mathbf{H}_i(S_k)\|_F^2\right)\right]
$$

$$
\overset{(a)}{=}\prod_{k=1}^{K}\mathbb{E}\left[\prod_{x_i\in\Phi_k^o}\mathcal{L}_{\|\mathbf{H}_i(S_k)\|_F^2}\left(\frac{sP_k}{S_k\|x_i\|^{\alpha_k}}\right)\right]
$$

$$
\overset{(b)}{=}\prod_{k=1}^{K}\mathbb{E}\left[\prod_{x_i\in\Phi_k^o}\left(1+\frac{sP_k}{S_k\|x_i\|^{\alpha_k}}\right)^{-S_k}\right]
$$

$$
\overset{(c)}{=}\exp\left\{-\pi\sum_{k=1}^{K}\lambda_k\int_{d_k}^{\infty}2r\left(1-\left(1+\frac{sP_k}{S_k r^{\alpha_k}}\right)^{-S_k}\right)\mathrm{d}r\right\}, \quad (3.35)
$$

where (a) follows from the independence of the $\{\Phi_k^o\}$ across k and from the independence of the $\{\|\mathbf{H}_i(S_k)\|_F^2\}$ across i, (b) follows from the Laplace transform of the Erlang distributed $\|\mathbf{H}_i(S_k)\|_F^2$, see Lemma A.2, and (c) follows from the PGFL for PPPs, see Theorem A.3.

3.8.2 Proof of Theorem 3.1

Applying the law of total probability and making use of Lemma 3.1, the coverage probability $\mathtt{P}_c^{\mathrm{IB}}$ of IB-MRC can be written as

$$
\mathtt{P}_c^{\mathrm{IB}}=\sum_{\ell=1}^{K}A_\ell\int_0^{\infty}f_{\mathsf{y},\ell}(y)\,\mathbb{P}\left(\mathtt{SINR}_\Sigma(\ell,y)\geq T\right)\mathrm{d}y, \quad (3.36)
$$

where $\mathbb{P}\left(\text{SINR}_\Sigma(\ell, y) \geq T\right)$ can be seen as the *conditional* $\text{P}_\text{c}^\text{IB}$ given ℓ, y. With Lemma A.3, the conditional $\text{P}_\text{c}^\text{IB}$ can be rewritten as

$$\mathbb{P}\left(\text{SINR}_\Sigma(\ell, y) \geq T\right) = \mathbb{P}\left(\|\mathbf{H}_o\|_F^2 \geq \frac{S_\ell T}{P_\ell y^{-\alpha_\ell}}\left(\sum_{k=1}^K \sum_{x_i \in \Phi_k^o} \mathsf{I}_{i,\text{eqv}} + \sigma^2\right)\right)$$

$$\overset{(a)}{=} \sum_{m=0}^{NM_\ell-1} \frac{(-1)^m}{m!} \mathbb{E}_\mathsf{Y}\left[(-1)^m \mathsf{Y}^m e^{-\mathsf{Y}}\right]$$

$$\overset{(b)}{=} \sum_{m=0}^{NM_\ell-1} \frac{(-1)^m}{m!} \frac{\text{d}^m}{\text{d}s^m}\left[\mathcal{L}_\mathsf{Y}(s)\right]_{s=1}, \tag{3.37}$$

where in (a) $\mathsf{Y} \triangleq \frac{S_\ell T}{P_\ell y^{-\alpha_\ell}}\left(\sum_{k=1}^K \sum_{x_i \in \Phi_k^o} \mathsf{I}_{i,\text{eqv}} + \sigma^2\right)$ has been defined and (b) follows from the differentiation rule for Laplace transforms [80, Sec. XIII.2]. With Lemma 3.2, $\mathcal{L}_\mathsf{Y}(s)$ can be obtained as

$$\mathcal{L}_\mathsf{Y}(s) = \exp\left(-\frac{s S_\ell T}{\text{SNR}(\ell, y)} - \pi \sum_{k=1}^K \lambda_k \hat{P}_k^{2/\alpha_k} y^{2/\hat{\alpha}_k}\right.$$

$$\left.\times \left[{}_2F_1\left(-\tfrac{2}{\alpha_k}, S_k, 1 - \tfrac{2}{\alpha_k}; -\tfrac{sT}{\hat{S}_k}\right) - 1\right]\right), \tag{3.38}$$

where $\text{SNR}(\ell, y) \triangleq P_\ell y^{-\alpha_\ell}/\sigma^2$ is the average SNR and $\hat{S}_k \triangleq S_k/S_\ell$. Substituting (3.38) back into (3.37) and de-conditioning on y and ℓ yields the result.

3.8.3 Proof of Theorem 3.2

Following the same approach as in the proof of Theorem 3.1, the coverage probability $\text{P}_\text{c}^\text{IA}$ of IA-MRC can be written as

$$\text{P}_\text{c}^\text{IA} = \sum_{\ell=1}^K A_\ell \int_0^\infty f_{\mathsf{y},\ell}(y) \mathbb{P}\left(\text{SINR}_\Sigma(\ell, y) \geq T\right) \text{d}y. \tag{3.39}$$

After conditioning on Φ^o, $\mathbb{P}\left(\text{SINR}(\ell, y) \geq T\right)$ can be expressed as

$$\mathbb{E}_{\Phi^o}\left[\mathbb{P}(\text{SINR}_1 \geq T - \text{SINR}_2|\Phi^o)\right]$$

$$= \mathbb{E}_{\Phi^o}\left[\int_0^\infty \mathbb{P}(\text{SINR}_1 \geq T - z|\Phi^o) f_{\text{SINR}_2|\Phi^o}(z)\,\text{d}z\right], \tag{3.40}$$

where

$$\text{SINR}_n \triangleq \frac{P_\ell}{M_\ell y^{\alpha_\ell}} \frac{\|\mathbf{h}_{o,n}\|_F^2}{I_n + \sigma^2}. \tag{3.41}$$

was defined as the per-antenna conditional SINR_n for short-hand notation. Applying the same steps as in (3.37), $\mathbb{P}(\text{SINR}_1 \geq T - z|\Phi^o)$ inside the integral in (3.40) can be obtained as

$$\sum_{m=0}^{M_\ell - 1} \frac{(-1)^m}{m!} \frac{\mathrm{d}^m}{\mathrm{d}s^m} \left[\exp\left(-\frac{sM_\ell(T-z)^+}{\text{SNR}(\ell,y)} \right) \right.$$
$$\left. \times \prod_{k=1}^{K} \prod_{x_i \in \Phi_k^o} \left(1 + \frac{s(T-z)^+ \hat{P}_k y^{\alpha_\ell}}{\hat{M}_k \|x_i\|^{\alpha_k}} \right)^{-M_k} \right]_{s=1}, \tag{3.42}$$

where the fact that the $\{\|\mathbf{h}_{i,1}\|_F^2\}$ are Erlang distributed with Laplace transform given by Lemma A.2 was used. Similarly, one has

$$f_{\text{SINR}_2|\Phi^o}(z) = \frac{\mathrm{d}}{\mathrm{d}w} \left[\mathbb{P}\left(\text{SINR}_2 \leq w|\Phi^o \right) \right]_{w=z}$$
$$= \frac{(-1)^{M_\ell}}{z\,\Gamma(M_\ell)} \frac{\mathrm{d}^{M_\ell}}{\mathrm{d}t^{M_\ell}} \left[\exp\left(-\frac{tM_\ell z}{\text{SNR}(\ell,y)} \right) \right.$$
$$\left. \times \prod_{k=1}^{K} \prod_{x_i \in \Phi_k^o} \left(1 + \frac{tz\hat{P}_k y^{\alpha_\ell}}{\hat{M}_k \|x_i\|^{\alpha_k}} \right)^{-M_k} \right]_{t=1}. \tag{3.43}$$

By Fubini's theorem [81], the expectation $\mathbb{E}_{\Phi^o}$ can be moved inside the integral over z in (3.40). By Leibniz integration rule for infinite integrals [66], the differentiations $\mathrm{d}^m/\mathrm{d}s^m$ in (3.42) and $\mathrm{d}^{M_\ell}/\mathrm{d}t^{M_\ell}$ in (3.43) can be moved outside $\mathbb{E}_{\Phi^o}$. Since the $\{\Phi_k^o\}$ are independent, one then has

$$\mathbb{E}\left[\prod_{k=1}^{K} \prod_{x_i \in \Phi_k^o} \left(1 + \frac{s(T-z)^+ \hat{P}_k y^{\alpha_\ell}}{\hat{M}_k \|x_i\|^{\alpha_k}} \right)^{-M_k} \left(1 + \frac{tz\hat{P}_k y^{\alpha_\ell}}{\hat{M}_k \|x_i\|^{\alpha_k}} \right)^{-M_k} \right]$$
$$= \exp\left\{ -\pi \sum_{k=1}^{K} \lambda_k \hat{P}_k^{2/\alpha_k} y^{2/\hat{\alpha}_k} \Psi\left(\frac{s}{\hat{M}_k}(T-z)^+, \frac{tz}{\hat{M}_k}, M_k, \alpha_k \right) \right\}, \tag{3.44}$$

where $\hat{M}_k \triangleq M_k/M_\ell$ and

$$\Psi(a_1, a_2, p, q) = \int_1^\infty 1 - \left[\left(1 + \frac{a_1}{u^{q/2}} \right) \left(1 + \frac{a_2}{u^{q/2}} \right) \right]^{-p} \mathrm{d}u. \tag{3.45}$$

Combining (3.39) – (3.44) yields the result.

3.8.4 Proof of Proposition 3.1

Recall that in the NC model the interferer locations originate from different point processes, say Φ^o and $\Phi^{o\prime}$, for each of the two Rx antennas. Then, (3.44) decomposes to

$$
\mathbb{E}_{\Phi^o}\left[\prod_{k=1}^{K}\prod_{\mathsf{x}_i\in\Phi_k^o}\left(1+\frac{s\,(T-z)^+\hat{P}_k y^{\alpha_\ell}}{\hat{M}_k\|\mathsf{x}_i\|^{\alpha_k}}\right)^{-M_k}\right]
$$

$$
\times\mathbb{E}_{\Phi^{o\prime}}\left[\prod_{k=1}^{K}\prod_{\mathsf{x}_i\in\Phi_k^o}\left(1+\frac{tz\hat{P}_k y^{\alpha_\ell}}{\hat{M}_k\|\mathsf{x}_i\|^{\alpha_k}}\right)^{-M_k}\right]
$$

$$
\overset{(a)}{=}\exp\Bigg(-\pi\sum_{k=1}^{K}\lambda_k\hat{P}_k^{2/\alpha_k}y^{2/\hat{\alpha}_k}
$$

$$
\times\left[{}_2F_1\!\left(-\tfrac{2}{\alpha_k},M_k,1-\tfrac{2}{\alpha_k};-\tfrac{s}{\hat{M}_k}(T-z)^+\right)-1\right.
$$

$$
\left.+\,{}_2F_1\!\left(-\tfrac{2}{\alpha_k},M_k,1-\tfrac{2}{\alpha_k};-\tfrac{tz}{\hat{M}_k}\right)-1\right]\Bigg), \quad (3.46)
$$

where (a) follows from Lemma 3.2.

3.8.5 Proof of Proposition 3.2

Since $\mathbf{h}_{i,u}\equiv\mathbf{h}_{i,v}$ for all $u,v\in\{1,\dots,N\}$ and $\mathsf{x}_i\in\Phi^o$, it follows that $\mathsf{I}_u\equiv\mathsf{I}_v$ for all $u,v\in\{1,\dots,N\}$. Then, the post-combiner SINR expression for IA-MRC in (3.23) collapses to the corresponding expression in (3.12) for IB-MRC.

3.8.6 Proof of Theorem 3.3

By [55, Eq. (8)], $\mathsf{P}_\mathrm{c}^{\mathrm{SC}}$ can be expressed as

$$
\mathsf{P}_\mathrm{c}^{\mathrm{SC}}=\sum_{n=1}^{N}(-1)^{n+1}\binom{N}{n}\mathsf{P}_n, \quad (3.47)
$$

where $\mathsf{P}_n\triangleq\mathbb{P}(\mathtt{SINR}_1>T,\dots,\mathtt{SINR}_n>T)$ is the *joint success probability*, i.e., the probability of the per-antenna SINR being greater than T at

n Rx antennas simultaneously. Invoking Lemma 3.1 and following the same line of thoughts as in [54, Appendix A], the conditional $\mathsf{P}_n(\ell, y)$ (conditioned on tier ℓ and serving BS distance y) can be written as

$$\mathsf{P}_n(\ell, y) \stackrel{(a)}{=} \mathbb{E}_{\Phi^o} \left[\prod_{q=1}^{n} \mathbb{P}\left(|\mathsf{h}_{o,q}|^2 > \tfrac{Ty^\alpha}{P_\ell}(\mathsf{I}_q + \sigma^2)|\Phi^o\right) \right]$$

$$\stackrel{(b)}{=} \exp\left(-\frac{nT}{\mathsf{SNR}(\ell, y)}\right) \prod_{k=1}^{K} \mathbb{E}\left[\prod_{\mathsf{x}_i \in \Phi_k^o} \left(1 + T\frac{y^{\alpha_\ell} \hat{P}_k}{\|\mathsf{x}_i\|^{\alpha_k}}\right)^{-n} \right], \quad (3.48)$$

where (a) follows from the independence of the $\{\mathsf{h}_{o,q}\}$ across Rx antennas and (b) follows from the independence of the interfering channel gains $\{\mathsf{h}_{i,q}\}$ and from the independence of the $\{\Phi_k^o\}$ across tiers. Applying Lemma 3.2 to (3.48) and de-conditioning on ℓ and y yields the result.

4

Diversity Combining Beyond Multi-Antenna Receivers

Chapter 2 and Chapter 3 focused on diversity combining in multi-antenna systems, which use the additional spatial degrees-of-freedom to provide diversity. In general, diversity can be obtained in various ways, see [20, Chap. 5] for an overview, and is not limited to multi-antenna systems. In this chapter, two popular approaches for providing diversity in single-antenna systems are considered and their performance under interference correlation is studied. In Section 4.1, cooperative diversity using relay communication is examined, while frequency-diversity reception in HCNs is treated in Section 4.2. This chapter is based on [T6–T8].

4.1 Cooperative Diversity in Wireless Networks

In spite of steadily increasing data rate demands, cooperative diversity—and most saliently, cooperative relaying—has become a viable solution to increase reliability and/or throughput. The concept of relaying is found for instance in 3GPP Rel-10 for LTE 4G networks [104]. Its performance

in the absence of interference has been a research topic of great interest since the seminal work by [105] in 1979 and is now fairly well-understood. This, however, is not true for the interference-limited case, where outage can be due to adverse fading states *and* strong interference. Analyzing cooperative relaying under the additional influence of interference is difficult. This is because interference depends on the geometry of interfering transmitters, which can be highly dynamic due to heterogeneous deployments, limited site-planning, and mobility, thereby letting interference appear effectively *random* to a given receiver. Furthermore, interference can be spatially correlated across the cooperating nodes, which may affect the diversity behavior of cooperative relaying. A better understanding of cooperative relaying in the presence of random interference is hence mandatory. Compared to the interference-free case, there exist only a few works that take into account the effect of random interference, see for instance [56, 106, 107]. This section complements earlier work by focusing on the diversity order of cooperative relaying under interference.

The diversity order metric [108] is a commonly used tool to quantify the performance of diversity schemes. As explained in Section 2.5.2 in Chapter 2 and in [54], applying the diversity order metric to a multi-user scenario with interference is not straightforward and different formulations exist. Yet another possible formulation will be introduced and discussed here. This formulation may be more suitable for wireless *ad hoc* networks as it takes the spatial resource—being considered as the critical resource in interference-limited networks—into account. Equipped with this new metric, the diversity behavior of cooperative relaying in the presence of random interference is then studied and the effect of spatial interference correlation and fading on the system performance is analyzed.

Contributions and Outcomes:

- The outage probability for a fixed source-relay-destination configuration employing SDF in the presence of a Poisson field of interferers is derived.

- The Spatial Diversity Order (SDO) metric is introduced, which quantifies the diversity behavior in interference-limited networks taking into account the spatial resource by controlling the density of simultaneously active transmitters.

- In the considered relay scenario, the SDO is equal to one (no diversity order gain) irrespective of the type of fading distribution, which is mainly due to the inability of the relay to counteract the interference experienced by the destination in the Multiple Access Channel (MAC) phase (Tx diversity).

- In the Broadcast (BC) phase (Rx diversity), the SDO depends on the amount of both fading and spatial interference correlation. In the absence of fading, there is a hard transition between an SDO of either one or two (maximal for one relay), depending on the system parametrization. This suggests that SIMO systems with spatially-distributed Rx antennas are, in principle, able to recover the diversity order gains known for the interference-free case.

4.1.1 System Model

A three-node configuration consisting of a source located at x_S, a destination located at x_D and a half-duplex relay located at x_R on $\mathbb{R}^2$ is considered. The locations x_S, x_D and x_R are arbitrary but fixed. Hence, the destination can be placed at the origin without loss of generality ($x_D = o \in \mathbb{R}^2$). The total available transmission time for conveying a packet from the source to the destination is divided into two consecutive time slots over which the cooperative transmission takes place. Selection decode-and-forward (SDF) [108] is used as the relay protocol. In SDF, the source broadcasts a packet in the first time slot, while the destination buffers the received packet and the relay tries to decode the packet. Depending on whether the relay was able to correctly decode the packet, either the relay or the source then re-transmits the packet to the destination in the second time slot. Finally, the destination appropriately combines the two copies prior to decoding the packet. The term *selection* indicates that either the relay or the source is selected to transmit to the destination in the second time slot, which recovers the dimension loss of conventional decode-and-forward whenever the relay fails to decode the packet. This, however, requires a reliable 1-bit feedback from the relay to the source node.

As the three-node configuration is part of a multi-user environment, it will suffer from interference created by other transmitters. In one snapshot, the locations of these interfering transmitters are assumed to

Figure 4.1: Illustration of the considered cooperative scenario with randomly located interfering transmitters distributed according to a PPP.

follow a stationary planar PPP Φ with density λ, see Definition A.3. As already discussed in the preceding chapters, the PPP model is commonly accepted for capturing dynamic interference in various kinds wireless networks, see for instance [42, 109]. All transmitted signals are subject to distance-dependent path loss. The power path loss between two locations $x_1, x_2 \in \mathbb{R}^2$ is given by the path loss function $\|x_1 - x_2\|^\alpha$, where $\alpha > 2$ denotes the path loss exponent.

In addition to path loss, the signals undergo channel fading, meaning that the interference power (*hereafter, simply* interference) from interferer i to the destination and relay are subject to the fading gains $\mathbf{g}_{i,\mathrm{D}}$ and $\mathbf{g}_{i,\mathrm{R}}$, respectively. Similarly, for the channels between the source, relay, and destination, the fading gains $\mathbf{g}_{\mathrm{S,R}}$, $\mathbf{g}_{\mathrm{S,D}}$, and $\mathbf{g}_{\mathrm{R,D}}$ are introduced. Independent frequency-flat Rayleigh fading is assumed, which yields a valid model for rich scattering None-Line-of-Sight (NLoS) environments. Thus, $\mathbf{g}_{i,j}$ follows a unit-mean exponential distribution for all $i \in \mathbb{N} \cup \{\mathrm{S, R}\}$ and $j \in \{\mathrm{R, D}\}$. In Section 4.1.3, the Rayleigh fading assumption will be dropped and the pure path loss model will be considered instead. The fading gains $\mathbf{g}_{i,j}$ are assumed constant for the duration of the cooperative transmission, i.e., over the two time slots used by SDF. Furthermore, relay and destination are assumed to have perfect CSI-Rx. The considered scenario is illustrated in Fig. 4.1 and the notation used in Section 4.1 is shown in Table 4.1.

Table 4.1: Notation used in Section 4.1

Notation	Description
$\Phi; \lambda$	Set of (random) interferer locations modeled as PPP; spatial density of interferers
$x_{\mathrm{S}}; x_{\mathrm{R}}; x_{\mathrm{D}}$	Location of source; relay; destination on $\mathbb{R}^2$; $x_{\mathrm{D}} = o$
α	Path loss exponent
$\mathsf{g}_{i,j}$	Power fading gain from transmitter $i \in \mathbb{N} \cup \{\mathrm{S}, \mathrm{R}\}$ to receiver $j \in \{\mathrm{R}, \mathrm{D}\}$
$\mathsf{I}_{\mathrm{R}}; \mathsf{I}_{\mathrm{D}}$	Current interference (power) at relay; at destination
$\mathsf{SIR}_{\mathrm{SRD}}; \mathsf{SIR}_{\mathrm{SD}}$	Post-combiner SIR at destination with relay; without
$\mathsf{SIR}_{\mathrm{R}}$	SIR at relay
T	SIR threshold
P_c	Success probability
λ_d	Spatial diversity order

The effect of Rx noise is ignored and focus is put on the interference-limited regime. All nodes are assumed to transmit with the same fixed Tx power, which can be set equal to one without loss of generality. The sum interference experienced at the relay and destination within the two time slots can then be expressed as

$$\mathsf{I}_{\mathrm{R}} \triangleq \sum_{\mathsf{x}_i \in \Phi} \mathsf{g}_{i,\mathrm{R}} \|\mathsf{x}_i - x_{\mathrm{R}}\|^{-\alpha} \tag{4.1}$$

$$\mathsf{I}_{\mathrm{D}} \triangleq \sum_{\mathsf{x}_i \in \Phi} \mathsf{g}_{i,\mathrm{D}} \|\mathsf{x}_i\|^{-\alpha}. \tag{4.2}$$

It the first time slot, both the relay and destination overhear the source's transmission, while the relay then tries to decode the packet. The Signal-to-Interference Ratio (SIR) at the relay is given by

$$\mathsf{SIR}_{\mathrm{SR}} = \frac{\mathsf{g}_{\mathrm{S},\mathrm{R}} \|x_{\mathrm{S}} - x_{\mathrm{R}}\|^{-\alpha}}{\mathsf{I}_{\mathrm{R}}}. \tag{4.3}$$

Given that the relay was able to decode the packet sent by the source, it then forwards the re-encoded version to the destination in the second time slot. At the destination, the two copies of the packet are combined using MRC, which yields the post-combiner SIR

$$\mathsf{SIR}_{\mathrm{SRD}} = \frac{\mathsf{g}_{\mathrm{S},\mathrm{D}} \|x_{\mathrm{S}}\|^{-\alpha} + \mathsf{g}_{\mathrm{R},\mathrm{D}} \|x_{\mathrm{R}}\|^{-\alpha}}{\mathsf{I}_{\mathrm{D}}}. \tag{4.4}$$

In case the relay fails to decode the packet sent by the source, the source re-transmits it in the second time slot, resulting in the post-combiner SIR

$$\texttt{SIR}_{\text{SD}} = \frac{2\texttt{g}_{\text{S,D}}\|x_{\text{S}}\|^{-\alpha}}{\texttt{I}_{\text{D}}}. \tag{4.5}$$

4.1.2 Outage Analysis

Since strong interference and/or adverse fading states may lead to an outage of the cooperative transmission, a reasonable performance metric is the success probability $\texttt{P}_{\text{c}}$, which was already introduced in Definition 2.1. Recall that the outage probability is defined as $1 - \texttt{P}_{\text{c}}$.

Following the same approach as in [108], the success probability for SDF can be decomposed as

$$\texttt{P}_{\text{c}} = 1 - \underbrace{\mathbb{P}\left(\texttt{SIR}_{\text{SD}} < T, \texttt{SIR}_{\text{SR}} < T\right)}_{\triangleq\ q_{\text{BC}}} - \underbrace{\mathbb{P}\left(\texttt{SIR}_{\text{SRD}} < T, \texttt{SIR}_{\text{SR}} \geq T\right)}_{\triangleq\ q_{\text{MAC}}}, \tag{4.6}$$

where q_{BC} and q_{MAC} are the outage probability in the BC phase and MAC phase, respectively. Analyzing these two expressions separately will turn out to be advantageous in the subsequent analysis.

Proposition 4.1 (Outage probability with Rayleigh fading). *Let $\|x_{\text{S}}\| \neq \|x_{\text{R}}\|$. The BC and MAC outage probabilities are given by*

$$\begin{aligned}
q_{\text{BC}} = 1 &- \exp\left(-\lambda\Omega\left[0, \frac{T\|x_{\text{S}}\|^{\alpha}}{2r^{\alpha}}\right]\right) \\
&- \exp\left(-\lambda\Omega\left[\frac{T\|x_{\text{S}} - x_{\text{R}}\|^{\alpha}}{(r^2 + x_{\text{R}}^2 - 2rx_{\text{R}}\cos\phi)^{\frac{\alpha}{2}}}, 0\right]\right) \\
&+ \exp\left(-\lambda\Omega\left[\frac{T\|x_{\text{S}} - x_{\text{R}}\|^{\alpha}}{(r^2 + x_{\text{R}}^2 - 2rx_{\text{R}}\cos\phi)^{\frac{\alpha}{2}}}, \frac{T\|x_{\text{S}}\|^{\alpha}}{2r^{\alpha}}\right]\right) \tag{4.7}
\end{aligned}$$

and

$$\begin{aligned}
q_{\text{MAC}} = \ &\exp\left(-\lambda\Omega\left[\frac{T\|x_{\text{S}} - x_{\text{R}}\|^{\alpha}}{(r^2 + x_{\text{R}}^2 - 2rx_{\text{R}}\cos\phi)^{\alpha/2}}, 0\right]\right) \\
&- \frac{\|x_{\text{R}}\|^{\alpha}}{\|x_{\text{R}}\|^{\alpha} - \|x_{\text{S}}\|^{\alpha}}\exp\left(-\lambda\Omega\left[\frac{T\|x_{\text{S}} - x_{\text{R}}\|^{\alpha}}{(r^2 + x_{\text{R}}^2 - 2rx_{\text{R}}\cos\phi)^{\frac{\alpha}{2}}}, \frac{T\|x_{\text{S}}\|^{\alpha}}{r^{\alpha}}\right]\right) \\
&+ \frac{\|x_{\text{S}}\|^{\alpha}}{\|x_{\text{R}}\|^{\alpha} - \|x_{\text{S}}\|^{\alpha}}\exp\left(-\lambda\Omega\left[\frac{T\|x_{\text{S}} - x_{\text{R}}\|^{\alpha}}{(r^2 + x_{\text{R}}^2 - 2rx_{\text{R}}\cos\phi)^{\frac{\alpha}{2}}}, \frac{T\|x_{\text{R}}\|^{\alpha}}{r^{\alpha}}\right]\right),
\end{aligned} \tag{4.8}$$

where

$$\Omega[f, g] \triangleq \int_0^\infty \int_0^\pi 2r \left(1 - \frac{1}{(1 + f(r, \phi))(1 + g(r))} \right) \mathrm{d}\phi \, \mathrm{d}r. \quad (4.9)$$

Proof: See Section 4.3.1. ∎

Remark 4.1. *The outage probability for the special case* $\|x_\mathrm{S}\| = \|x_\mathrm{R}\|$ *can be obtained using a similar approach, e.g., as in Chapter 2 and [107], however, with no additional insights. Note that in this case,* $\mathsf{g}_{\mathrm{S,D}}\|x_\mathrm{S}\|^{-\alpha} + \mathsf{g}_{\mathrm{R,D}}\|x_\mathrm{R}\|^{-\alpha}$ *is Erlang distributed with shape equal to two and rate* $\|x_\mathrm{S}\|^\alpha = \|x_\mathrm{R}\|^\alpha.$

Diversity Order Analysis

As discussed in the beginning of Section 4.1, characterizing the diversity order in the multi-user scenario is not straightforward. A novel formulation for the diversity order that is based on controlling the spatial density of simultaneously transmitting nodes is therefore proposed next.

Definition 4.1 (Spatial diversity order). *The SDO is defined as*

$$d_\lambda \triangleq \lim_{\lambda \to 0} \frac{\log 1 - \mathsf{P_c}}{\log \lambda}. \quad (4.10)$$

The subscript "λ" in d_λ emphasizes that the spatial density of concurrent transmissions is used as the scaling parameter. The SDO is a suitable metric for characterizing the diversity order in interference-limited wireless networks if one wants to take into account the spatial resource—which is considered the critical resource wireless networks with spatial reuse. Besides, the SDO has some practical relevance: medium access protocols such as Aloha (spatial reuse with predefined medium access probability) and Carrier Sense Multiple Access (CSMA) (spatial inhibition of active transmitters) control the density of simultaneous transmissions as well. As an application example, consider the baseline scenario, where the source communicates with the destination without help of the relay. The corresponding success probability is given by (2.33) with $y = \|x_\mathrm{S}\|$. In this case the SDO can be shown to yield $d_\lambda = 1$, which is intuitive since direct transmission cannot provide any diversity order gain.

The following Lemma will be helpful in the later diversity analysis.

Lemma 4.1. *Let* $w(t) = \sum_{k=0}^{\xi} a_k \left(1 - e^{-tz_k}\right)$, *where* $t \geq 0$ *and* $a_k, z_k \in \mathbb{R}$ *for all* $k = 0, \ldots, \xi < \infty$. *Then,* $w(t) \propto t$ *as* $t \to 0$ *if and only if* $\sum_{k=0}^{\xi} a_k z_k \neq 0$.

Proof: See Section 4.3.2. ■

With Lemma 4.1, the SDO of SDF can now be computed.

Theorem 4.1 (SDO of SDF with Rayleigh fading)**.** *The SDO of SDF for exponentially distributed fading gains (Rayleigh fading) is* $d_\lambda = 1$.

Proof: See Section 4.3.3. ■

Theorem 4.1 states that there is no gain in terms of SDO by relaying the packet sent by the source. This somewhat disappointing result is in contrast to the interference-free case, where SDF is known to provide a diversity order gain [108]. The reason for this result is that, although the relay can lead to an array gain at the destination in the MAC phase, it cannot reduce the interference level at the destination just by forwarding the packet. Hence, outages due to strong interference may still occur, leading to the diversity bottleneck $q_{\mathrm{MAC}} \propto \lambda$ as $\lambda \to 0$.

On the other hand, spatial correlation of the interference renders the BC phase not as effective as in the interference-free case, yielding $q_{\mathrm{BC}} \propto \lambda$ as $\lambda \to 0$; more specifically, if the destination is in outage in the first time slot, then it is (more or less) likely that the relay is in outage as well, since the interference is correlated over space. This observation suggests that increasing the relay-destination distance reduces the spatial interference correlation across these two nodes, however, it turns out that the asymptotic slope of q_{BC} does not change, i.e., $q_{\mathrm{BC}} \propto \lambda$ as $\lambda \to 0$. It is important to note, though, that the fading distribution co-determines the spatial interference correlation properties, and that abandoning the Rayleigh fading assumption may indeed change the SDO at least in the BC phase.[3] This will be verified in Section 4.1.3, where the Rayleigh fading assumption is dropped and the SDO in the BC phase is revisited.

---

[3]Obviously, assuming a different fading distribution does not change the SDO in the MAC phase due to the inability of the relay to reduce interference at the destination node as explained before.
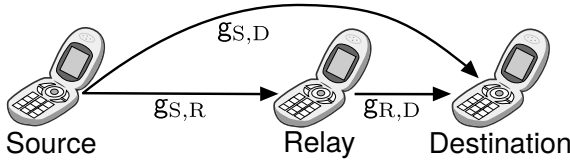
Figure 4.2: Line configuration of the cooperative three-node network

Optimal Relay Position

Theorem 4.1 and the ensuing discussion give rise to the question about the optimal relay location. Using Proposition 4.1, the optimal relay location optimizing P_c can be found by maximizing (4.6) over x_R given x_S. For this purpose, the relay is assumed to be located on a line connecting the source and the destination, see Fig. 4.2.

Figure 4.3 shows the optimal relay position relative to the position of the destination for different path loss exponents α. The relative position is obtained as $\|x_S - x_R\|/\|x_S\|$, since $x_D = o$. It can be seen that it is strictly better to place the relay closer to the destination for reasonable path loss exponents around $\alpha = 4$, in particular for small outage probabilities on the order of 10^{-3} to 10^{-2}, which corresponds to $\lambda = 10^{-6}$ (solid line). For practically non-relevant large outage probabilities on the order of 10^{-1}, which corresponds to $\lambda = 10^{-3}$ (dashed line), this observation is weaker as the optimal relay position is now closer to the half-line. In conclusion, these observations suggest that there is a slight trend for outage-optimal SDF in the sense that Rx diversity is more beneficial than Tx diversity. The intuition behind this result is that the ability to boost the received power through the relay-destination link outweighs the reliability loss of the source-relay link.

4.1.3 Diversity Analysis in BC Phase without Fading

The main conclusion of Section 4.1.2 was that SDF under interference cannot provide a diversity order gain, mainly because of the relay not being capable to counteract the interference problem at the destination in the MAC phase. Obviously, this fact does not change when assuming a different fading distribution. In contrast, the SDO associated with the BC
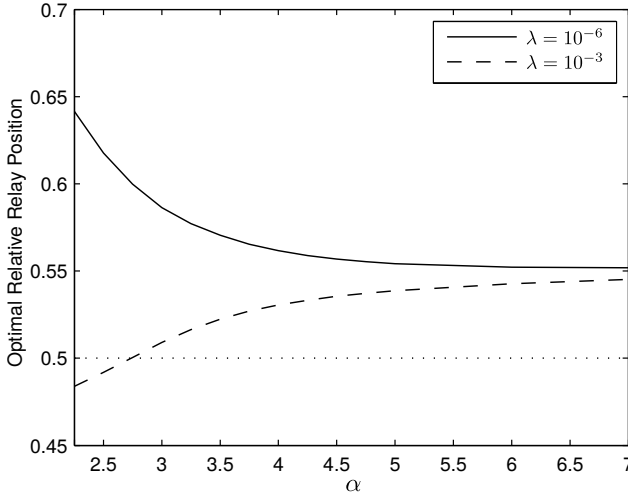
Figure 4.3: Optimal relay position relative to source-destination distance, i.e., $\|x_S - x_R\|/\|x_S\|$, versus α. Line configuration assumed. Parameters: $\|x_S\| = 10$ and $T = 4$.

phase may depend on the amount of fading, since fading co-determines the spatial interference correlation. Recall that the Rayleigh fading model applies to rich scattering NLoS environments. On the other extreme, the pure path loss model applies to scenarios with negligible scattering and a dominant Line-of-Sight (LoS) path. Since the SDO analysis in Section 4.1.2 focused on the Rayleigh fading model, it is reasonable to redo the analysis now assuming the other extreme, namely the pure path loss model. In the pure path loss model, the fading gains are no longer random and now become $g_{i,j} \equiv 1$ for all $i \in \mathbb{N} \cup \{S, R\}$ and $j \in \{R, D\}$. Clearly, with unit fading gains, the spatial interference correlation now depends exclusively on the spatial distribution of nodes in the network.

The BC phase can be viewed as a distributed SIMO system, where the destination has two spatially separated Rx antennas connected through some high-capacity link. The distributed-SIMO concept is found for instance in cellular networks with Radio Remote Heads (RRHs) or Coordinated Multi-Point (CoMP) with joint-processing in the uplink [110, 111].

As already discussed in Section 2.4.2, the dominant-interferer bounding technique from [42] yields a remarkably tight approximation for the outage probability in the asymptotic regime $\lambda \to 0$. The following result exploits this fact and gives the SDO under the pure path loss model.

Theorem 4.2 (Outage probability and SDO in BC phase without fading)**.** *Define the two (dominant-interferer) regions* $A_{\mathrm{R}} \triangleq b(x_{\mathrm{R}}, T^{1/\alpha}\|x_{\mathrm{S}} - x_{\mathrm{R}}\|)$, $A_{\mathrm{D}} \triangleq b(o, (\frac{T}{2})^{1/\alpha}\|x_{\mathrm{S}}\|)$, *and their intersection* $A_{\mathrm{RD}} \triangleq A_{\mathrm{R}} \cap A_{\mathrm{D}}$. *Then,* q_{BC} *for SDF under the pure path loss model becomes*

$$q_{\mathrm{BC}} \sim \begin{cases} \lambda|A_{\mathrm{RD}}|, & |A_{\mathrm{RD}}| \neq 0 & \text{(4.11a)} \\ \lambda^2|A_{\mathrm{R}}|\,|A_{\mathrm{D}}|, & |A_{\mathrm{RD}}| = 0, & \text{(4.11b)} \end{cases}$$

as $\lambda \to 0$. *The SDO in the BC phase is*

$$d_\lambda = \begin{cases} 1, & \|x_{\mathrm{R}} - o\| \leq T^{1/\alpha}\|x_{\mathrm{S}} - x_{\mathrm{R}}\| + (\frac{T}{2})^{1/\alpha}\|x_{\mathrm{S}}\| & \text{(4.12a)} \\ 2, & \textit{otherwise.} & \text{(4.12b)} \end{cases}$$

Proof: See Section 4.3.4. ∎

As can be seen by (4.11) and (4.12), the intersection A_{RD} of the two regions A_{R} and A_{D} plays a crucial role for the SDO: if $|A_{\mathrm{RD}}| = 0$, i.e., there is no overlapping of the individual dominant-interferer regions A_{R} and A_{D}, the interference across the relay and the destination becomes uncorrelated as $\lambda \to 0$, thus yielding $d_\lambda = 2$. Note that q_{BC} in (4.11b) scales with $T^{4/\alpha}$, which is consistent with the diversity order results obtained in Section 2.5.2. It is interesting to note that, by looking at (4.12), there exists a hard transition from $d_\lambda = 1$ to $d_\lambda = 2$ in the pure path loss model, which depends only on the geometrical distance between the relay and destination node. Under a more general fading model, e.g., Nakagami-m, which captures the continuum between Rayleigh and no fading, one may thus conjecture that the smoothness of the transition will further depend on the amount of fading.

The theoretical result from Theorem 4.2 is shown in Fig. 4.4, along with simulation results validating the analysis. In particular, it can be seen that the dominant-interferer bounding technique yields a tight approximation to the true q_{BC} in the small outage probability regime. As expected, the slope of q_{BC} does not change ($d_\lambda = 1$) until the relay-destination distance becomes sufficiently large such that the respective dominant-interferer regions do not overlap ($|A_{\mathrm{RD}}| = 0 \Rightarrow d_\lambda = 2$). In this example, the

Figure 4.4: Outage probability q_{BC} versus λ for relay locations $x_{\mathrm{R}} = (5,0)$, $(10,0)$, $(15,0)$. Parameters: $x_{\mathrm{S}} = (18,0)$, $\alpha = 4$, $T = 0.25$.

relay-destination distance has to be at least $\|x_{\mathrm{R}} - o\| = 13.72$ for the dominant-interferer regions A_{R} and A_{D} to be disjoint, which can be verified by the inequality in (4.12a). Note that the radii of these regions and hence, of their intersection A_{RD} are proportional to $T^{1/\alpha}$. This suggests that small target SIRs, e.g., as in direct-sequence Code Division Multiple Access (CDMA) *ad hoc* networks [112, 113], are desirable from the viewpoint of the SDO in distributed Rx diversity systems.

4.1.4 Summary

The analysis showed that, although spatially separated, nodes may experience correlated interference due to common locations of interfering transmitters. In this sense, interference correlation is not limited to a few centimeters across Rx antennas, but it propagates through the space surmounting meters. This obviously affects the performance of cooperative diversity schemes; the diversity order in a simple one-relay SDF scenario with Rayleigh fading cannot exceed that of a conventional transmission between two single-antenna nodes. However, the picture changes when

considering an Rx diversity system with an error-free relay-destination link. In this case, a diversity order increase is achievable in the absence of channel fading. This is because in the asymptotic regime, outage events are dominated by interfering transmitters within the so-called dominant-interferer regions around the relay and the destination; if these regions are disjoint, the diversity order is two (maximal for single-relay case). For small SIR thresholds T, the interferer regions become disjoint already for small separations between the relay and destination. This suggests that signaling schemes that operate at low effective SIR thresholds T, e.g., direct-sequence CDMA, are more desirable when optimizing the diversity order of cooperative Rx diversity systems.

4.2 Frequency Diversity in Heterogeneous Cellular Networks

Flexible segmentation and resource allocation of potentially large transmission bandwidths is a prominent feature of 4G cellular networks, and is considered no less important for 5th Generation (5G) cellular networks [5]. In LTE, for instance, it is possible to assign non-contiguous spectrum to certain users using Distributed Virtual Resource Blocks (DVRBs) [86]. Carrier aggregation [114], on the other side, allows users to operate on much larger bandwidths. Such techniques offer *frequency diversity* as the different parts of the allocated spectrum usually undergo independent fading. Besides, analyzing cellular networks has become increasingly complex, particularly due to their heterogeneity caused by the massive deployment of small cells within macro coverage areas. Existing works that analyze the performance of such HCNs, e.g., [115], mostly assume that users are served on *purely coherent* resources. Consequently, these works do not capture non-contiguous spectrum allocation nor allocations larger than the coherence bandwidth, and hence they cannot capture the effect of frequency diversity. But analyzing this effect is challenging since the experienced interference is usually correlated across different parts of the allocated spectrum due to the common locations of interfering BSs. This type of correlation was considered in [116], where the *ergodic* rate with carrier aggregation was studied. To obtain a better understanding of frequency diversity in HCNs, one has to look at the probability distribution of the rate, which is the main focus of this section.

Contributions and Outcomes:

- A tractable while realistic model for a generic K-tier HCN with frequency diversity is developed and the rate distribution for a typical user in the downlink under frequency diversity and spatial interference correlation is studied. The BS locations are modeled by a PPP and a two-block independent-fading model is assumed for capturing the basic effect of frequency diversity.

- The results indicate that, depending on the degree of spectrum diversification, rate gains of 40–90% are obtained in a typical three-tier HCN scenario.
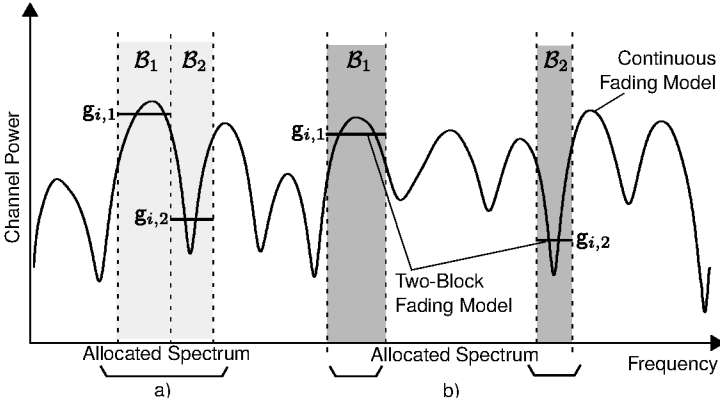
Figure 4.5: Two-block independent-fading model: a) allocated contiguous spectrum exceeds coherence bandwidth (light gray); b) non-contiguous spectrum allocation (dark gray).

- When spatial interference correlation is ignored, the offered rate is overestimated by about 3 6%.

4.2.1 System Model

A generic K-tier HCN with single-antenna BSs is considered in the downlink. Similarly as in Chapter 3, the BS locations of tier k, where $\mathcal{K} = \{1, \ldots, K\}$, are modeled by a stationary PPP Φ_k on $\mathbb{R}^2$ with density λ_k, see Definition A.3. It is further assumed that single-antenna users are scattered in the plane according to some stationary PPP. By Slivnyak's theorem, see Theorem A.1, one can focus the analysis on a typical user located at the origin $o \in \mathbb{R}^2$. At the typical user, the long-term signal power received from a k-th tier BS located at $x_i \in \Phi_k$ is $P_k\|x_i\|^{-\alpha_k}$, where P_k is the tier-specific BS transmit power and $\|\cdot\|^{\alpha_k}$ is the distance-dependent path loss with exponent $\alpha_k > 2 \ \forall k \in \mathcal{K}$. Users associate with the BS providing the highest long-term received power. The location of the BS serving the typical user is hence given by the point from $\Phi \triangleq \cup_{k=1}^K \Phi_k$ associated with the cell covering the origin o, see Chapter 3. Assuming that the serving BS is from tier $\ell \in \mathcal{K}$, its location is denoted by $x_o \in \Phi_\ell$ without loss of generality. For convenience, the notation $\Phi^o \triangleq \Phi \setminus \{x_o\}$ and $\Phi_k^o \triangleq \Phi_k \setminus \{x_o\}$, i.e., the set of interfering BSs, is introduced. Table 4.2 summarizes the notation used in Section 4.2.

Table 4.2: Notation used in Section 4.2

Notation	Description
$\Phi_k; \lambda_k$	PPP describing the BS locations in tier k; average density of BSs in tier k; $\Phi \triangleq \cup_{k=1}^{K} \Phi_k$
P_k	BS transmit power in tier k
α_k	Path loss exponent in tier k
$\mathsf{g}_{i,m}$	Power fading gain from BS i to typical user in band m
σ^2	Rx noise power, AWGN variance
$\mathcal{B}_m; B_m$	Resource subset m; $B_m = |\mathcal{B}_m|$
$\mathsf{I}_{m,k}$	Interference (power) from tier k in band m
$\mathtt{SNR}(\ell, y)$	Mean SNR from a serving ℓ-th tier BS at distance y
$\mathtt{SINR}_m(\ell, y)$	SINR in band m from a serving ℓ-th tier BS at distance y
$\mathtt{SINR}_m$	SINR in band m
$\mathtt{R}; \mathtt{R}_m$	Data rate at typical user; in band m
R	Data rate threshold
$\mathsf{P}_{\mathtt{c,R}}$	Rate coverage probability $\mathbb{P}(\mathtt{R} > R)$

BS x_o uses a total of B_{tot} (frequency) resources for serving the typical user.[4] It is reasonable to assume that channel fading on each resource is frequency-flat. Yet some resources may experience a different fading realization than others, e.g., if B_{tot} exceeds the coherence bandwidth or if the allocation is non-contiguous, see Fig. 4.5. To capture this effect while maintaining analytical tractability, the following two-block fading model is assumed.

Two-block independent-fading model: The set of resources allocated to the typical user is partitioned into two subsets $\mathcal{B}_1$ and $\mathcal{B}_2$ such that (i) all resources falling into one subset experience the *same* fading realization, (ii) while the fading is considered *independent* across the two subsets. For a given BS located at x_i operating on any resource from $\mathcal{B}_1$ ($\mathcal{B}_2$), the corresponding signal is thus received at the typical user under a common fading gain $\mathsf{g}_{i,1}$ ($\mathsf{g}_{i,2}$). By assumption (ii) $\mathsf{g}_{i,1}$ and $\mathsf{g}_{i,2}$ are statistically independent. For instance, in time domain only, this corresponds to the well-known block-fading model [19], and information would be aggregated

---

[4]The analysis does not change when considering time-frequency resources.

over two time slots, each with an independent channel realization. See Fig. 4.5 for an illustration.

The fading gains $\{g_{i,m}\}$ are assumed to be i.i.d. following a unit-mean exponential distribution (Rayleigh fading). Let B_1 and B_2 be the cardinality of $\mathcal{B}_1$ and $\mathcal{B}_2$, respectively. Hence, $B_{\text{tot}} = B_1 + B_2$ is the total number of resources assigned to the typical user. Note that the frequently used case of fully coherent resources can be recovered by setting either B_1 or B_2 equal to zero.

It will be useful in the later analysis to know the probability that a user associates with the ℓ-th tier as well as the conditional PDF of the distance to the serving BS. Both are given by Lemma 3.1 in Chapter 3.

4.2.2 Rate Coverage Probability Analysis

The (instantaneous) rate offered to the typical user depends on B_1, B_2 one the one hand, and on the SINRs experienced on the corresponding resources on the other hand. Given that the typical user associates with an ℓ-th-tier BS at distance y, the resulting $\texttt{SINR}_m$ on any resource from set $\mathcal{B}_m$ is

$$\texttt{SINR}_m(\ell, y) \triangleq \frac{g_{o,m} P_\ell \, y^{-\alpha_\ell}}{\sum_{k=1}^{K} I_{k,m} + \sigma^2}, \tag{4.13}$$

where $I_{k,m} \triangleq \sum_{x_i \in \Phi_k^o} g_{i,m} P_k \|x_i\|^{-\alpha_k}$ is the other-cell interference treated as white noise and σ^2 is the Rx noise power, i.e., AWGN variance. Assuming communication close to the Shannon capacity [102], the total rate conveyed to the typical user can then be expressed as

$$R \triangleq R_1 + R_2 = \sum_{m=1}^{2} B_m \log_2 \left(1 + \texttt{SINR}_m\right), \tag{4.14}$$

where R_m denotes the product of link spectral efficiency corresponding to a channel realization from the subset $\mathcal{B}_m$ and the number of resources corresponding to the subset $\mathcal{B}_m$. The expression in (4.14) is a reasonable measure of rate if strong channel coding is employed [76,77]; alternatively, a coding/modulation-specific gap to Shannon capacity can be included in the analysis, see [117] for further details.

Although the individual $\mathtt{R}_m$ in (4.14) comprise only statistically independent quantities, they exhibit a complicated correlation structure across the different bands: while the interfering channels $\{\mathbf{g}_{i,m}\}$ have a decorrelation effect on the interference signals, the common locations of interfering BSs result in correlated interference across the different bands. Hence, $\mathtt{R}$ is a sum of correlated random variables. As a counterpart to the success/coverage probability for SINR, see Definition 2.1, the rate coverage probability is introduced next.

Definition 4.2 (Rate coverage probability). *The rate coverage probability is defined as*

$$\mathtt{P}_{\mathtt{c,R}} \triangleq \mathbb{P}\left(\mathtt{R} \geq R\right) \tag{4.15}$$

for a target rate $R > 0$.

The superscript "$\mathtt{R}$" in $\mathtt{P}_{\mathtt{c,R}}$ is used to avoid confusion with the SINR-based coverage probability $\mathtt{P}_{\mathtt{c}}$ introduced in Definition 2.1. Again, $\mathtt{P}_{\mathtt{c,R}}$ can be interpreted as the complementary distribution of $\mathtt{R}$ at the typical user or as the average fraction of users inside the HCN covered by a rate no less than R, given the stationarity of the $\{\Phi_k\}$. The following result characterizes $\mathtt{P}_{\mathtt{c,R}}$ under frequency diversity in HCNs.

Theorem 4.3 (Rate coverage probability). *The rate coverage probability for the typical user in the described setting is given by*

$$\mathtt{P}_{\mathtt{c,R}} = -2\pi \sum_{\ell=1}^{K} \lambda_\ell \int_0^\infty \int_0^\infty y \exp\left(-\frac{\beta(z)}{\mathtt{SNR}(\ell,y)}\right) \frac{\mathrm{d}}{\mathrm{d}w}\left[\exp\left(-\frac{\gamma(w)}{\mathtt{SNR}(\ell,y)}\right.\right.$$
$$\left.\left.-\pi\sum_{k=1}^{K}\lambda_k \hat{P}_k^{2/\alpha_k} y^{2/\hat{\alpha}_k}\left(1+\mathcal{F}\left[\beta(z),\gamma(w),\alpha_k\right]\right)\right)\right]_{w=z} \mathrm{d}y\,\mathrm{d}z, \tag{4.16}$$

where $\mathtt{SNR}(\ell,y) \triangleq P_\ell y^{-\alpha_\ell}/\sigma^2$, $\beta(z) \triangleq 2^{(R-z)^+/B_1}-1$, $\gamma(w) \triangleq 2^{w/B_2}-1$, and $\mathcal{F}[a,b,c]$ is given in (4.36).

Proof: See Section 4.3.5. ∎

As can be seen in (4.16), Theorem 4.3 is given as a double integral, which can be solved fairly easily using standard numerical software. The rate coverage probability result for purely coherent resources from [115] can

be recovered by setting B_1 or B_2 equal to zero. The computational complexity can be further reduced as discussed next.

Due to the exponential form of the integrand, the expression inside the exponent in (4.16) is the relevant part regarding the $\mathrm{d}/\mathrm{d}w$ operation.

Remark 4.2. *The differentiation* $\mathrm{d}\mathcal{F}[\beta(z), \gamma(w), \alpha_k]/\mathrm{d}w$ *at* $w = z$ *can be calculated as*

$$
\left[\frac{\mathrm{d}}{\mathrm{d}w} \mathcal{F}[\beta(z), \gamma(w), \alpha_k] \right]_{w=z}
$$

$$
= \frac{\beta(z)\, 2^{z/B_2} \log 2}{B_2 (\beta(z) - \gamma(z))^2} \left[\Psi(\beta(z), \alpha_k) - \left(1 - \frac{\gamma(z)}{\beta(z)} \right) \frac{2/\alpha_k}{1 + \gamma(z)^{-1}} \right.
$$

$$
\left. - \left(1 + \frac{2}{\alpha_k} \left(1 - \frac{\gamma(z)}{\beta(z)} \right) \right) \Psi(\gamma(z), \alpha_k) \right], (4.17)
$$

where $\Psi(p, q)$ *is given by (4.37).*

It is possible to express $\Psi(p, q)$ in terms of the Gaussian hypergeometric function, i.e., $\Psi(p, q) = 2\pi p^{2/q} \csc(2\pi/q)/q - {}_2F_1(1, 2/q, 1 + 2/q; -1/p)$. With [66,68] ${}_2F_1(\cdot, \cdot, \cdot; \cdot)$ can in some cases be expressed through elementary functions, for instance when $\alpha_k = 4$,

$$
\mathcal{F}[\beta(z), \gamma(w), 4] = \frac{\beta(z)^{3/2} \arctan \sqrt{\beta(z)}}{\beta(z) - \gamma(w)} - \frac{\gamma(w)^{3/2} \arctan \sqrt{\gamma(w)}}{\beta(z) - \gamma(w)}. (4.18)
$$

Furthermore, HCNs are typically interference-limited due to dense deployments in crowded areas. In this case interference dominates Rx noise and one can set $\sigma^2 = 0$. If, in addition, the path loss law does not differ significantly across tiers, then the coverage probability result from Theorem 4.3 reduces to the following single-integral form.

Corollary 4.1 (No Rx noise, equal path loss exponent). *In the absence of Rx noise ($\sigma^2 = 0$) and with equal path loss exponents ($\alpha_k = \alpha \; \forall k \in \mathcal{K}$), (4.16) simplifies to*

$$
\mathrm{P}_{\mathrm{c,R}} = - \int_0^\infty \frac{\mathrm{d}}{\mathrm{d}w} \left[\frac{1}{\mathcal{F}[\beta(z), \gamma(w), \alpha]} \right]_{w=z} \mathrm{d}z. \tag{4.19}
$$

Table 4.3: Tier-Specific Parameters used for Numerical Examples

Parameter	Tier 1	Tier 2	Tier 3
BS density λ_k	$4\,\mathrm{BS/km^2}$	$16\,\mathrm{BS/km^2}$	$40\,\mathrm{BS/km^2}$
BS power P_k	$46\,\mathrm{dBm}$	$30\,\mathrm{dBm}$	$24\,\mathrm{dBm}$
Path loss α_k	3.76	3.67	3.5

4.2.3 Discussion

In this section, the theoretical results are used to discuss the effect of frequency diversity under spatial interference correlation. A typical three-tier scenario ($K = 3$) with macro, pico, and femto BSs is assumed similarly as in Section 3.6, see Table 4.3. The number of total resources assigned to the typical user is set to $B_{\mathrm{tot}} = 49 \times 180$ kHz, which is comparable to 7 resource blocks assuming the LTE standard [86]. Rx noise is set to $\sigma^2 = -104$ dBm.

Effect of spectrum diversification: Fig. 4.6 shows the rate coverage probability $\mathsf{P}_{\mathrm{c,R}}$ for $\eta = [0; 0.1; 0.2; 0.5]$, where $\eta \triangleq B_1/B_{\mathrm{tot}}$ is the fraction of total resources spanned by $\mathcal{B}_1$. First, it can be seen that the theoretical results perfectly match the simulation results, which were obtained by averaging over 10^5 network realizations. Furthermore, the coverage probability increases as more diverse spectrum is occupied, with the maximum increase attained at $\eta = 0.5$ (equal split between $\mathcal{B}_1$ and $\mathcal{B}_2$). This so-called frequency-diversity gain is exploited in non-contiguous resource allocation, e.g., DVRB allocation in LTE [86]. Fig. 4.7 shows the rate gain relative to $\eta = 0 \triangleq \eta_0$ for different $\mathsf{P}_{\mathrm{c,R}}$ and $\eta > 0$. The relative gain is defined as $\Delta_{\mathrm{R}}^{\eta\text{-}\eta_0} \triangleq R(\mathsf{P}_{\mathrm{c,R}}, \eta)/R(\mathsf{P}_{\mathrm{c,R}}, \eta_0) - 1$. For typical values of $\mathsf{P}_{\mathrm{c,R}}$, e.g., around 90% of covered users, the rate gain ranges from roughly 40% for $\eta = 0.1$ to 90% for $\eta = 0.5$. For very low $\mathsf{P}_{\mathrm{c,R}}$, frequency diversity becomes less favorable.

Effect of spatial interference correlation: Recall that assuming purely coherent resources yields a pessimistic performance prediction for systems with non-contiguous resource allocation or large transmission bandwidths, see Fig. 4.7. In contrast, assuming that the $\{\mathtt{SINR}_m\}$ in (4.14) are independent across m, e.g., for analytical tractability, yields an optimistic prediction as the correlation of the $\{\mathsf{I}_{k,m}\}$ across bands due to common locations of interfering BSs is ignored. For this case, a
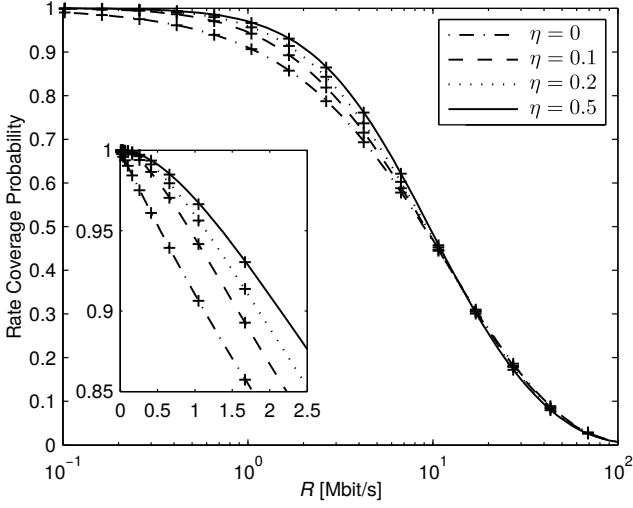
Figure 4.6: Rate coverage probability $P_{c,R}$ for different η. Marks represent simulation results.
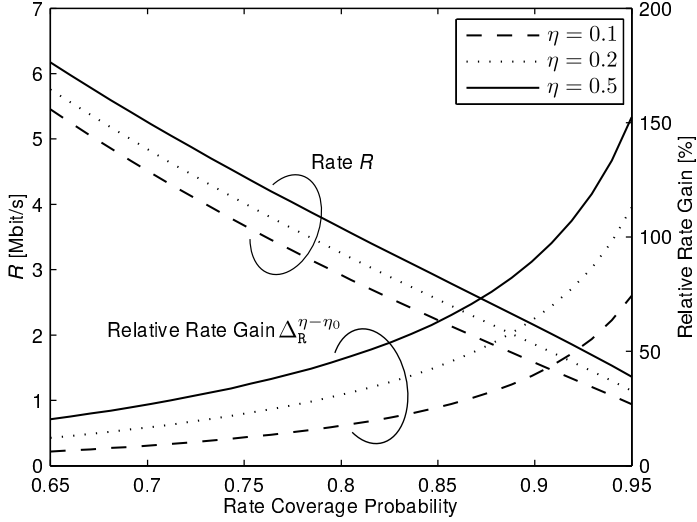

Figure 4.7: Rate R and relative rate gain $\Delta_R^{\eta-\eta_0}$ for different target $P_{c,R}$ and $\eta > 0$.
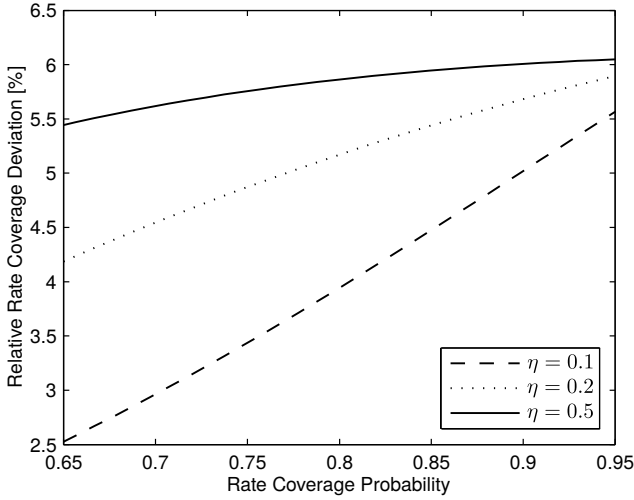
Figure 4.8: Relative rate deviation $\delta_{\mathrm{R}}^{\mathrm{NC}}$ when interference correlation is ignored for different $\mathrm{P_{c,R}}$ and $\eta > 0$.

corresponding expression for $\mathrm{P_{c,R}}$ can be obtained using the same approach as in the proof of Proposition 3.1, see Section 3.8.4, i.e., decomposing the expectation in (4.34) into the product of two expectations over independent point sets Φ_k^o and $\Phi_k^{o\prime}$ for every tier k. In this case, one obtains the modified expression $\mathcal{F}[a, b, c] = \Psi(a, c) + \Psi(b, c)$.

Equipped with Theorem 4.3, the impact of interference correlation across bands on the system performance can now be studied by comparing the exact $\mathrm{P_{c,R}}$ to the case when interference correlation is ignored. Fig. 4.8 shows the relative rate deviation, defined as $\delta_{\mathrm{R}}^{\mathrm{NC}} \triangleq R^{\mathrm{NC}}(\mathrm{P_{c,R}})/R(\mathrm{P_{c,R}}) - 1$, when ignoring correlation. It can be seen that, depending on the degree of diversification, the rate is overestimated by 3–6%. For $\eta = 0.5$ and $\mathrm{P_{c,R}} = 0.9$ for instance, the absolute rate difference is 129 kbit/s.

4.2.4 Summary

A tractable while realistic stochastic model for analyzing frequency diversity, e.g., using non-contingeous or large spectrum allocations, in downlink HCNs was developed. Assuming a two-block independent-fading model,

the rate coverage probability was derived, taking into account the interference correlation across the different parts of the allocated spectrum due to common locations of interfering BSs. Several practical insights followed from the theoretical results, which show that system design should factor in the interference correlation in order to not overestimate or underestimate the gains of frequency diversity.

4.3 Proofs

4.3.1 Proof of Proposition 4.1

The expression in (4.6) is first conditioned on Φ, yielding

$$
\begin{aligned}
&1 - \mathsf{P_c} \\
&\stackrel{(a)}{=} \mathbb{E}_\Phi \left[\mathbb{P}\left(\mathsf{g_{S,D}} < \frac{T\,\mathsf{I_D}}{\|x_S\|^{-\alpha}} \,\bigg|\, \Phi \right) \mathbb{P}\left(\mathsf{g_{S,R}} < \frac{T\,\mathsf{I_R}}{\|x_S - x_R\|^{-\alpha}} \,\bigg|\, \Phi \right) \right] \\
&\quad + \mathbb{E}_\Phi \left[\mathbb{P}\left(\frac{\mathsf{g_{S,D}}}{\|x_S\|^\alpha} + \frac{\mathsf{g_{R,D}}}{\|x_R\|^\alpha} < T\,\mathsf{I_D} \,\bigg|\, \Phi \right) \mathbb{P}\left(\mathsf{g_{S,R}} \geq \frac{T\,\mathsf{I_R}}{\|x_S - x_R\|^{-\alpha}} \,\bigg|\, \Phi \right) \right] \\
&\stackrel{(b)}{=} \mathbb{E}_\Phi \left[\left(1 - \prod_{\mathsf{x}_i \in \Phi} \frac{1}{1 + T\frac{\|x_S\|^\alpha}{\|\mathsf{x}_i\|^\alpha}} \right) \left(1 - \prod_{\mathsf{x}_i \in \Phi} \frac{1}{1 + T\frac{\|x_S - x_R\|^\alpha}{\|\mathsf{x}_i - x_R\|^\alpha}} \right) \right] \\
&\quad + \frac{\|x_S\|^\alpha}{\|x_R\|^\alpha - \|x_S\|^\alpha} \mathbb{E}_\Phi \left[\prod_{\mathsf{x}_i \in \Phi} \frac{1}{1 + T\frac{\|x_R\|^\alpha}{\|\mathsf{x}_i\|^\alpha}} \frac{1}{1 + T\frac{\|x_S - x_R\|^\alpha}{\|\mathsf{x}_i - x_R\|^\alpha}} \right] \\
&\quad - \frac{\|x_R\|^\alpha}{\|x_R\|^\alpha - \|x_S\|^\alpha} \mathbb{E}_\Phi \left[\prod_{\mathsf{x}_i \in \Phi} \frac{1}{1 + T\frac{\|x_S\|^\alpha}{\|\mathsf{x}_i\|^\alpha}} \frac{1}{1 + T\frac{\|x_S - x_R\|^\alpha}{\|\mathsf{x}_i - x_R\|^\alpha}} \right],
\end{aligned} \tag{4.20}
$$

where (a) follows from the independence of the fading gains $\mathsf{g_{S,D}}, \mathsf{g_{S,R}}, \mathsf{g_{R,D}}$ and from the *linearity* property of the expectation, and (b) follows from the *i.i.d. exponential fading* assumption, see Definition A.1 and Lemma A.2, and from the complementary CDF of $\mathsf{z} \triangleq \mathsf{g_{S,D}}\|x_S\|^{-\alpha} + \mathsf{g_{R,D}}\|x_R\|^{-\alpha}$, which can be obtained using [80, Sec. V.4] as

$$
\mathbb{P}\left(\mathsf{z} > z \right) = \frac{\|x_S\|^\alpha \exp\left(-z\|x_R\|^\alpha \right)}{\|x_R\|^\alpha - \|x_S\|^\alpha} - \frac{\|x_R\|^\alpha \exp\left(-z\|x_S\|^\alpha \right)}{\|x_R\|^\alpha - \|x_S\|^\alpha}. \tag{4.21}
$$

Invoking the PGFL for PPPs in (4.20), see Theorem A.3, and switching to polar coordinates yields the result.

4.3.2 Proof of Lemma 4.1

Using the power series $e^{-tz} = \sum_{\ell=0}^{\infty} \frac{(-tz)^\ell}{\ell!}$, $w(t)$ can be rewritten as

$$w(t) = t \sum_{k=0}^{\xi} a_k z_k - \frac{t^2}{2} \sum_{k=0}^{\xi} a_k z_k^2 + \dots . \tag{4.22}$$

To obtain linear scaling in t, $\sum_{k=0}^{\xi} a_k z_k$ must be non-zero.

4.3.3 Proof of Theorem 4.1

Expressing the exp-terms in (4.7) and (4.8) as a power series yields

$$
\begin{aligned}
1 - \mathrm{P_c} = \lambda &\left(-\Omega \left[\frac{T\|x_\mathrm{S} - x_\mathrm{R}\|^\alpha}{(r^2 + x_\mathrm{R}^2 - 2rx_\mathrm{R}\cos\phi)^{\alpha/2}}, \frac{T\|x_\mathrm{S}\|^\alpha}{2r^\alpha} \right] \right. \\
&\left. \Omega \left[0, \frac{T\|x_\mathrm{S}\|^\alpha}{2r^\alpha} \right] + \Omega \left[\frac{T\|x_\mathrm{S} - x_\mathrm{R}\|^\alpha}{(r^2 + x_\mathrm{R}^2 - 2rx_\mathrm{R}\cos\phi)^{\alpha/2}}, 0 \right] \right) \\
+ \lambda &\left(-\Omega \left[\frac{T\|x_\mathrm{S} - x_\mathrm{R}\|^\alpha}{(r^2 + x_\mathrm{R}^2 - 2rx_\mathrm{R}\cos\phi)^{\alpha/2}}, 0 \right] \right. \\
&+ \frac{\|x_\mathrm{R}\|^\alpha}{\|x_\mathrm{R}\|^\alpha - \|x_\mathrm{S}\|^\alpha} \Omega \left[\frac{T\|x_\mathrm{S} - x_\mathrm{R}\|^\alpha}{(r^2 + x_\mathrm{R}^2 - 2rx_\mathrm{R}\cos\phi)^{\frac{\alpha}{2}}}, \frac{T\|x_\mathrm{S}\|^\alpha}{r^\alpha} \right] \\
&\left. - \frac{\|x_\mathrm{S}\|^\alpha}{\|x_\mathrm{R}\|^\alpha - \|x_\mathrm{S}\|^\alpha} \Omega \left[\frac{T\|x_\mathrm{S} - x_\mathrm{R}\|^\alpha}{(r^2 + x_\mathrm{R}^2 - 2rx_\mathrm{R}\cos\phi)^{\frac{\alpha}{2}}}, \frac{T\|x_\mathrm{R}\|^\alpha}{r^\alpha} \right] \right) \\
+ \mathcal{R}(\lambda) &,
\end{aligned}
\tag{4.23}
$$

where $\mathcal{R}(\lambda)$ contains all higher-order terms in λ and $\Omega[\cdot, \cdot]$ is given in (4.9). By Lemma 4.1, the linear term of $1 - \mathrm{P_c}$ must be non-vanishing for Theorem 4.1 to hold. Thus, one needs to prove that the linear term is non-zero, for which strictly positiveness of the expressions inside the two parentheses in (4.23) is a sufficient condition. Focusing on the sufficient condition, (4.23) is rewritten by combining all three integrals represented by $\Omega[\cdot, \cdot]$ into a single one for each of the two parentheses. This is allowed by the *linearity* property of integrals. Then, the resulting two integrals are strictly positive if their integrands are strictly positive. Thus, after some algebraic manipulations, it has to be checked if

$$
\begin{aligned}
&1 + \left(1 + \frac{T\|x_\mathrm{S} - x_\mathrm{R}\|^\alpha}{(r^2 + x_\mathrm{R}^2 - 2rx_\mathrm{R}\cos\phi)^{\alpha/2}} \right)^{-1} \left(1 + \frac{T\|x_\mathrm{S}\|^\alpha}{2r^\alpha} \right)^{-1} \\
&- \left(1 + \frac{T\|x_\mathrm{S}\|^\alpha}{2r^\alpha} \right)^{-1} - \left(1 + \frac{T\|x_\mathrm{S} - x_\mathrm{R}\|^\alpha}{(r^2 + x_\mathrm{R}^2 - 2rx_\mathrm{R}\cos\phi)^{\alpha/2}} \right)^{-1} > 0 \quad (4.24)
\end{aligned}
$$

for the q_{BC}-part and

$$\frac{\|x_{\mathrm{S}}\|^\alpha}{\|x_{\mathrm{R}}\|^\alpha - \|x_{\mathrm{S}}\|^\alpha}\left(1 + \frac{T\|x_{\mathrm{S}}\|^\alpha}{r^\alpha}\right) - \frac{\|x_{\mathrm{R}}\|^\alpha}{\|x_{\mathrm{R}}\|^\alpha - \|x_{\mathrm{S}}\|^\alpha}\left(1 + \frac{T\|x_{\mathrm{R}}\|^\alpha}{r^\alpha}\right)$$
$$+ \left(1 + \frac{T\|x_{\mathrm{S}}\|^\alpha}{r^\alpha}\right)\left(1 + \frac{T\|x_{\mathrm{R}}\|^\alpha}{r^\alpha}\right) > 0 \quad (4.25)$$

for the q_{MAC}-part. It can be readily shown that the left-hand side of (4.24) is strictly positive for all $r \in \mathbb{R}_+$ and $\phi \in [0, 2\pi)$ and bounded distances. Similarly, the left-hand side of (4.25) is strictly positive for all $r \in \mathbb{R}^2$ and bounded distances. Thus, this implies that the linear term of $1 - \mathsf{P}_{\mathrm{c}}$ in (4.23) is strictly positive as well. The same holds also for the case $\|x_{\mathrm{R}}\| = \|x_{\mathrm{S}}\|$ by letting $\|x_{\mathrm{R}}\| \to \|x_{\mathrm{S}}\|$ in (4.25), which is allowed by the dominated convergence theorem [66].

4.3.4 Proof of Theorem 4.2

The dominant-interferer sets for the relay and destination are

$$\Phi_{\mathrm{dom,R}} \triangleq \left\{ \mathsf{x}_i \in \Phi : \frac{\|x_{\mathrm{S}} - x_{\mathrm{R}}\|^{-\alpha}}{\|\mathsf{x}_i - x_{\mathrm{R}}\|^{-\alpha}} < T \right\} \quad (4.26)$$

$$\Phi_{\mathrm{dom,D}} \triangleq \left\{ \mathsf{x}_i \in \Phi : \frac{\|x_{\mathrm{S}}\|^{-\alpha}}{\|\mathsf{x}_i\|^{-\alpha}} < \frac{T}{2} \right\} \quad (4.27)$$

and

$$\Phi_{\mathrm{dom,RD}} \triangleq \left\{ \mathsf{x}_i \in \Phi_{\mathrm{dom,R}} \cap \Phi_{\mathrm{dom,D}} \right\}. \quad (4.28)$$

The sets $\Phi_{\mathrm{dom,R}}$ and $\Phi_{\mathrm{dom,D}}$ correspond to the regions A_{R} and A_{D} around the relay and the destination, respectively, where the joint occurrence of interfering transmitters in both regions already leads to an outage, irrespective of the interference contribution from far-off transmitters. From (4.26) and (4.27), it follows that $A_{\mathrm{R}} = b\left(x_{\mathrm{R}}, T^{1/\alpha}\|x_{\mathrm{S}} - x_{\mathrm{R}}\|\right)$ and $A_{\mathrm{D}} = b\left(o, (\frac{1}{2}T)^{1/\alpha}\|x_{\mathrm{S}}\|\right)$. Then, as $\lambda \to 0$, the outage probability q_{BC} can be tightly lower bounded as

$$q_{\mathrm{BC}} \gtrsim \mathbb{P}\left(\Phi(A_{\mathrm{R}}) \cap \Phi(A_{\mathrm{D}}) \neq \emptyset\right)$$
$$\overset{(a)}{=} \mathbb{P}\left(\Phi(A_{\mathrm{RD}}) \neq \emptyset\right) + \mathbb{P}\left(\Phi(A_{\mathrm{R}} \setminus A_{\mathrm{D}}) \neq \emptyset\right)\mathbb{P}\left(\Phi(A_{\mathrm{D}} \setminus A_{\mathrm{R}}) \neq \emptyset\right)$$
$$= 1 - \exp\left(-\lambda|A_{\mathrm{RD}}|\right) + \left(1 - \exp\left(-\lambda|A_{\mathrm{R}} \setminus A_{\mathrm{D}}|\right)\right)$$
$$\times \left(1 - \exp\left(-\lambda|A_{\mathrm{D}} \setminus A_{\mathrm{R}}|\right)\right)$$
$$\overset{(b)}{\sim} \lambda|A_{\mathrm{RD}}| + \lambda^2|A_{\mathrm{R}} \setminus A_{\mathrm{D}}||A_{\mathrm{D}} \setminus A_{\mathrm{R}}|, \quad (4.29)$$

where (a) follows from the *independence* property of the PPP, see Definition A.2 (ii), and (b) follows from $1 - e^{-z} \sim z$ for small z.

4.3.5 Proof of Theorem 4.3

Using the law of total probability and Lemma 3.1, (4.15) can be written as

$$\mathtt{P_c} = \sum_{\ell=1}^{K} A_\ell \int_0^\infty f_{\mathsf{y},\ell}(y)\, \mathbb{P}(\mathtt{R}(\ell, y) \geq R)\, \mathrm{d}y, \tag{4.30}$$

where $\mathtt{R}(\ell, y) = \mathtt{R_1}(\ell, y) + \mathtt{R_2}(\ell, y)$ is the rate offered to the typical user, conditioned on being served by a BS of tier k at distance y. After conditioning $\mathbb{P}(\mathtt{R}(\ell, y) \geq R)$ on Φ^o to remove the dependency between $\mathtt{R_1}(\ell, y)$ and $\mathtt{R_2}(\ell, y)$, this term can be written as

$$\begin{aligned}
\mathbb{P}(\mathtt{R}(\ell, y) \geq R) &= \mathbb{E}_{\Phi^o}\left[\mathbb{P}(\mathtt{R_1}(\ell, y) \geq R - \mathtt{R_2}(\ell, y)\,|\,\Phi^o)\right] \\
&= \mathbb{E}_{\Phi^o}\left[\int_0^\infty \mathbb{P}(\mathtt{R_1}(\ell, y) \geq R - z\,|\,\Phi^o)\, f_{\mathtt{R_2}(\ell,y)\,|\,\Phi^o}(z)\, \mathrm{d}z\right].
\end{aligned} \tag{4.31}$$

The first term inside the integral in (4.31) can be written as

$$\begin{aligned}
&\mathbb{P}(\mathtt{R_1}(\ell, y) \geq R - z|\Phi^o) \\
&\overset{(a)}{=} \mathbb{P}\left(\mathtt{SINR_1}(\ell, y) \geq \beta(z)\,|\,\Phi^o\right) \\
&= \mathbb{P}\left(\mathsf{g}_{o,1} \geq \frac{\beta(z)}{P_\ell y^{-\alpha_\ell}}\left(\sum_{k=1}^{K}\mathsf{I}_{k,1} + \sigma^2\right)\Bigg|\Phi^o\right) \\
&\overset{(b)}{=} \exp\left(-\frac{\beta(z)}{\mathtt{SNR}(\ell, y)}\right)\prod_{k=1}^{K}\prod_{\mathsf{x}_i\in\Phi_k^o}\mathbb{E}_{\mathsf{g}_{i,1}}\left[\exp\left(-\beta(z)\frac{\hat{P}_k y^{\alpha_\ell}\mathsf{g}_{i,1}}{\|\mathsf{x}_i\|^{\alpha_k}}\right)\right] \\
&\overset{(c)}{=} \exp\left(-\frac{\beta(z)}{\mathtt{SNR}(\ell, y)}\right)\prod_{k=1}^{K}\prod_{\mathsf{x}_i\in\Phi_k^o}\frac{1}{1 + \beta(z)\frac{\hat{P}_k y^{\alpha_\ell}}{\|\mathsf{x}_i\|^{\alpha_k}}},
\end{aligned} \tag{4.32}$$

where (a) follows from the substitutions $\beta(z) \triangleq 2^{(R-z)^+/B_1} - 1$ and $\mathtt{SNR}(\ell, y) \triangleq P_\ell y^{-\alpha_\ell}/\sigma^2$, (b) follows from evaluating the probability with respect to $\mathsf{g}_{o,1}$ and noting that all remaining fading gains are i.i.d. across all BSs, and (c) is obtained using Lemma A.2. Using the same approach,

the conditional PDF $f_{\mathtt{R}_2(\ell,y)|\Phi^o}(z)$ inside the integral in (4.31) can be obtained as

$$
\begin{aligned}
&f_{\mathtt{R}_2(\ell,y)|\Phi^o}(z)\\
&= \frac{\mathrm{d}}{\mathrm{d}w}\left[\mathbb{P}\left(\mathtt{R}_2(\ell,y)\leq w\right)\right]_{w=z}\\
&= -\frac{\mathrm{d}}{\mathrm{d}w}\left[\exp\left(-\frac{\gamma(w)}{\mathtt{SNR}(\ell,y)}\right)\prod_{k=1}^{K}\prod_{\mathsf{x}_i\in\Phi_k^o}\frac{1}{1+\gamma(w)\frac{\hat{P}_k y^{\alpha_\ell}}{\|\mathsf{x}_i\|^{\alpha_k}}}\right]_{w=z}, \quad (4.33)
\end{aligned}
$$

where $\gamma(w)\triangleq 2^{w/B_2}-1$. Now observe that the expectation $\mathbb{E}_{\Phi^o}$ can be moved inside the integral over z in (4.31) by Fubini's theorem [81]. By Leibniz integration rule for infinite integrals [66], the derivative $\mathrm{d}/\mathrm{d}w$ in (4.33) can be moved outside the expectation $\mathbb{E}_{\Phi^o}$. Exploiting the fact that the $\{\Phi_k\}$ are mutually independent, (4.31) can hence be rewritten as

$$
\begin{aligned}
\mathbb{P}(\mathtt{R}(\ell,y)\geq R) = -\int_0^\infty &\exp\left(-\frac{\beta(z)}{\mathtt{SNR}(\ell,y)}\right)\frac{\mathrm{d}}{\mathrm{d}w}\left[\exp\left(-\frac{\gamma(w)}{\mathtt{SNR}(\ell,y)}\right)\right.\\
&\left.\times\prod_{k=1}^{K}\mathbb{E}_{\Phi_k^o}\left[\prod_{\mathsf{x}_i\in\Phi_k^o}\frac{1}{1+\beta(z)\frac{\hat{P}_k y^{\alpha_\ell}}{\|\mathsf{x}_i\|^{\alpha_k}}}\frac{1}{1+\gamma(w)\frac{\hat{P}_k y^{\alpha_\ell}}{\|\mathsf{x}_i\|^{\alpha_k}}}\right]\right]_{w=z}\mathrm{d}z. \quad (4.34)
\end{aligned}
$$

After invoking the PGFL for PPPs, see Theorem A.3, expanding $\frac{1}{1+\beta(z)\dots}$ $\frac{1}{1+\gamma(w)\dots}$ using partial-fraction decomposition, and further algebraic manipulations, the second line in (4.34) becomes

$$
\exp\left(-\pi\sum_{k=1}^{K}\lambda_k\hat{P}_k^{2/\alpha_k}y^{2/\hat{\alpha}_k}\mathcal{F}[\beta(z),\gamma(w),\alpha_k]\right), \quad (4.35)
$$

where the functional $\mathcal{F}[a,b,c]$ is defined as

$$
\mathcal{F}[a,b,c]\triangleq\frac{a\,\Psi(a,c)}{a-b}-\frac{b\,\Psi(b,c)}{a-b}, \quad (4.36)
$$

and

$$
\Psi(p,q)\triangleq\int_1^\infty\frac{p}{p+t^{q/2}}\mathrm{d}t. \quad (4.37)
$$

Combining (4.30), (4.31) and (4.34)–(4.37) yields the result.

5

Conclusion

Interference correlation across Rx branches due to common locations of interferers has a detrimental effect on diversity schemes. As discussed in this thesis, analyzing this effect is challenging due to the mathematical nature of the underlying problem resulting from the complicated correlation structure of the interference. A clearer view on this effect would however help assessing the performance of diversity schemes more accurately and allow for balancing performance-complexity trade-offs more properly. This thesis addressed this challenge by developing stochastic models that enable a mathematical analysis using tools from stochastic geometry. The models, which are tailored to the essential characteristics of wireless *ad hoc* networks and HCNs, are fairly realistic while still tractable. Focus was put on multi-antenna receivers with MRC, in particular IA-MRC, as the considered diversity-combining scheme, since this scheme is widely used though its performance under interference correlation is not well understood. Generally speaking, this thesis spans two areas of contribution. First, theoretical expressions for key performance metrics were derived, which releases system designers from the necessity of founding decisions exclusively on non-intuitive results obtained from time-consuming simulations. Second, using the theoretical framework many practical design guidelines for diversity combining under interference correlation were obtained and discussed.

5.1 Summary

The findings obtained in Chapter 2 showed that the performance of IA-MRC may be strongly affected by interference correlation in SIMO wireless *ad hoc* networks. Ignoring this type of correlation significantly overestimates the true diversity that can be exploited and hence, the performance is overestimated as well. In particular, in the case of weak channel fluctuations and/or strong path loss, interference correlation should not be ignored. For the same case, assuming full interference correlation across Rx antennas yields a reasonably close performance characterization for IA-MRC. Moreover, it was mathematically shown that in the limiting case, when channel fluctuations on the interfering links due to fading vanish, IA-MRC and IB-MRC are equivalent in terms of post-combiner SINR. This result suggests that IB-MRC may be more favorable than IA-MRC when fading is not severe given the smaller complexity of IB-MRC. A comparison with IA-SC and MMSE combining showed that the path loss law matters for the relative performances and should therefore be taken into account when comparing the performance-complexity trade-offs of different diversity-combining schemes.

Some of the above findings extend to downlink HCNs as well, which were treated in detail in Chapter 3. In contrast to wireless *ad hoc* networks, however, HCNs exhibit a cell-association mechanism and typically have multi-antenna BSs, which leads to distinct interference statistics also discussed in this chapter. With OSTBC-based Tx diversity using multiple Tx antennas, the gain of IA-MRC over IB-MRC becomes less pronounced. The reason is that Tx diversity reduces the fluctuations on the interfering channels and hence, it increases the interference correlation across Rx antennas. Thus, similarly to the SIMO case with weak fading, IB-MRC may be the better choice in systems with Tx diversity.

While the first two chapters mainly focused on MRC in multi-antenna receivers, Chapter 4 looked at the influence of interference correlation on other forms of diversity schemes. One example, which was studied in Section 4.1, is cooperative relaying, where a relay assists a source node in conveying information to the destination. In such a setting, the interference experienced at the relay and destination is correlated, which disperses the diversity order gains known for the interference-free case. However, in the absence of fading and with a perfect relay-destination

link, a diversity order gain can be obtained if the relay and destination are sufficiently apart. This suggests that only distributed Rx-diversity systems are desirable from a diversity order perspective in the presence of interference, albeit cooperative relaying can still improve performance in terms of outage probability compared to non-cooperative transmissions. Frequency diversity is another form of diversity exploitation and is commonly used in cellular systems with flexible resource allocation. In Section 4.2, the data rate offered to a user under frequency diversity in a HCN was studied. It was shown that the gains from this type of diversity suffer from interference correlation across the allocated spectrum. Depending on the degree of spectrum diversification, ignoring this type of correlation may yield a significantly optimistic performance prediction.

5.2 Outlook

This thesis focused on the widely-used PPP to model the locations of transmitters. Other and more sophisticated point processes that are capable of modeling also repulsion and/or clustering between transmitters could be considered as well. For instance, in wireless *ad hoc* networks, more complex geometries of interferers around a given receiver arising from, e.g., CSMA, can be incorporated using a Poisson-Hardcore mixture model [118–120]. Besides, very recent work presented new models based on determinantal point processes for characterizing the spatial distribution of BSs in cellular systems more accurately [121, 122]. Although the main insights and performance trends obtained in this thesis are not expected to change when considering other point processes, such extensions may be useful when performance nuances and hard numbers becomes of interest, though at the cost of loosing mathematical tractability. Since for IA-MRC, theoretical results for only the dual-antenna case were obtained, another promising research direction could be to find a possibly different approach that allows a performance characterization for the general case with $N > 2$ Rx antennas. The same holds for the two-block fading model in Section 4.2 for the analysis of frequency-diversity reception in HCNs. Here, an extension to a more general N-block fading model could be of interest.

Given the challenging nature of the underlying mathematical problem, practical impairments such as fading correlation or imperfect CSI were

left aside throughout this thesis. Fading correlation due to, e.g., suboptimal antenna-array design, would certainly contribute to the interference correlation across Rx antennas, thereby further reducing the gains of IA diversity-combing schemes over their IB counterparts. Complementing this work by incorporating such practical aspects in the model could further contribute to a better understanding of diversity combining in wireless networks with interference.

Chapters 2 and 3 focused on relatively simple open-loop diversity schemes for different MIMO settings. Going beyond open-loop MIMO diversity and developing models for more sophisticated (closed-loop) multi-antenna schemes could be of strong interest as well. Some recent work in this direction using stochastic geometry tools are [94, 95]. In particular, comparing the performance of such more powerful multi-antenna schemes under realistic assumptions, e.g., unreliable CSI-Tx and/or imperfect interference-channel estimation in interference-canceling receivers, to the ones considered in this thesis, could help balancing performance-complexity trade-offs and/or finding optimal switching points between different multi-antenna schemes.

A

Selected Topics on Probability Theory and Stochastic Geometry

This appendix reviews some probability theory and stochastic geometry concepts of special relevance to this work. The interested reader is referred to the references accompanying this appendix for further discussions.

Probability Theory

Let $(\Omega, \mathcal{F}, P)$ be a probability space with set Ω describing the possible "outcomes" of the underlying experiment, the σ-algebra $\mathcal{F}$ on Ω describing the set of "events", and P being a probability measure defined on $\mathcal{F}$. A real-valued random variable z is a measurable function on the sample space Ω to $\mathbb{R}$, i.e., $\mathsf{z} : (\Omega, \mathcal{F}) \mapsto (\mathbb{R}, \mathcal{B})$, where $\mathcal{B}$ is the Borel σ-algebra on $\mathbb{R}$. The probability of observing a certain event $B \in \mathcal{B}$ through the random variable z is then given by

$$\mathbb{P}(\mathsf{z} \in B) \triangleq P\left(\mathsf{z}^{-1}(B)\right) = P\left(\{\omega \in \Omega \,|\, \mathsf{z}(\omega) \in B\}\right) \quad \text{for all } B \in \mathcal{B}. \text{ (A.1)}$$

Here, $\mathbb{P}(\mathsf{z} \in \cdot)$ is the induced probability measure associated with the random variable z. The CDF is a special case of $\mathbb{P}(\mathsf{z} \in \cdot)$ and is defined as $F_\mathsf{z}(z) \triangleq \mathbb{P}(\mathsf{z} \leq z)$ for $z \in \mathbb{R}$. The corresponding PDF $f_\mathsf{z}(z)$ is defined by the relation $F_\mathsf{z}(z_2) - F_\mathsf{z}(z_1) = \int_{z_1}^{z_2} f_\mathsf{z}(z)\,\mathrm{d}z$. The reader is referred to [81, 123] for further details.

Definition A.1 (Gamma, Erlang, and Exponential Distribution [80])**.** *Let $a, b > 0$. A non-negative random variable z with PDF*

$$f_\mathsf{z}(z) = \frac{b^a}{\Gamma(a)} z^{a-1} e^{-bz}, \quad z \geq 0, \tag{A.2}$$

is called

- *Gamma distributed,*

- *Erlang distributed if $a \in \mathbb{N}$,*

- *exponentially distributed if $a = 1$.*

The CDF of z is given by

$$F_\mathsf{z}(z) = \frac{\gamma(a, bz)}{\Gamma(a)} \overset{a \in \mathbb{N}}{=} 1 - e^{-bz} \sum_{i=0}^{a-1} \frac{(bz)^i}{i!}, \tag{A.3}$$

where $\gamma(\nu, x) \triangleq \int_0^x t^{\nu-1} e^{-\nu t}\,\mathrm{d}t$ is the lower incomplete Gamma function.

The parameters a and b are the *shape* and *rate* of the Gamma distribution, respectively.

Lemma A.1 (*p*-th moment of a Gamma random variable)**.** *The p-th moment of a Gamma distributed random variable z with shape a and rate b is given by*

$$\mathbb{E}\left[\mathsf{z}^p\right] = \frac{\Gamma(a+p)}{b^p\,\Gamma(a)}, \quad p > -a. \tag{A.4}$$

The distribution of a non-negative random variable z can be entirely characterized by its Laplace transform $\mathcal{L}_\mathsf{z}(s) \triangleq \mathbb{E}[\exp(-s\mathsf{z})]$ for $s \geq 0$. The case when z is Gamma distributed is of special interest in this thesis.

Lemma A.2 (Laplace transform of a Gamma random variable)**.** *Let* z *be Gamma distributed with shape a and rate b. Then, the Laplace transform of z is given by*

$$\mathcal{L}_z(s) = \left(1 + \frac{s}{b}\right)^{-a}, \quad s \geq 0. \tag{A.5}$$

Let $\{z_k\}$ be a finite collection of independent Gamma distributed random variables, each with shape a_k and rate $b_k = b \ \forall k$. By Lemma A.2, it then follows that $\sum_k z_k$ is again Gamma distributed with shape $\sum_k a_k$ and rate b.

The squared Frobenius norm of a matrix $\mathbf{X} \in \mathbb{C}^{U \times V}$ is given by $\|\mathbf{X}\|_F^2 = \sum_{u=1}^{U} \sum_{v=1}^{V} |x_{uv}|^2$. The following Lemma, characterizes the distribution of $\|\mathbf{X}\|_F^2$ with circular-symmetric complex Gaussian entries.

Lemma A.3 (Gaussian matrices)**.** *Let* $\mathbf{X}(u) \in \mathbb{C}^{v \times w}$ *have $u \leq vw$* $\mathcal{CN}(0,1)$ *distributed entries and $vw - u$ zeros. Then, $\|\mathbf{X}(u)\|_F^2$ is Erlang distributed with shape u and rate 1.*

The next result is useful when computing fractional moments of random variables for which their Laplace transform is known.

Lemma A.4 (Fractional moments of a non-negative random variable [124])**.** *Let* z *be a non-negative random variable with PDF $f_z(z)$ and Laplace transform $\mathcal{L}_z(s)$. Then, the p-th moment of z satisfies*

$$\mathbb{E}\left[z^p\right] = \begin{cases} \dfrac{p}{\Gamma(1-p)} \displaystyle\int_0^\infty \frac{1 - \mathcal{L}_z(s)}{s^{1+p}} \, \mathrm{d}s, & 0 < p < 1, \quad (\text{A.6}) \\[4mm] \dfrac{1}{\Gamma(-p)} \displaystyle\int_0^\infty \frac{\mathcal{L}_z(s)}{s^{1+p}} \, \mathrm{d}s, & p < 0. \quad\quad (\text{A.7}) \end{cases}$$

Stochastic Geometry

The following section presents a concise introduction to the theory of point processes based on the monographs [34, 35, 49]. Emphasis is put on the PPP and its properties, which are of main interest in this thesis.

Let again $(\Omega, \mathcal{F}, P)$ be a probability space. Define a measurable space $(\mathbb{M}, \mathcal{M})$, where $\mathbb{M}$ is a set of sequences $\varphi = \{x_i\}$ of points in $\mathbb{R}^d$ and

$\mathcal{M}$ is the smallest σ-algebra on $\mathbb{M}$ to make all mappings $\varphi \mapsto \varphi(B)$ measurable for bounded Borel sets $B \subset \mathbb{R}^d$. Here, $\varphi(\cdot)$ is the *point counting* formulation of the sequence φ, i.e., $\varphi(B) \triangleq \sum_{x_i \in \varphi} \mathbb{1}(x_i \in B)$. The sequences φ are assumed to satisfy the following conditions:

(i) they are *locally finite*, i.e., $\varphi(B) < \infty$ for each bounded $B \subset \mathbb{R}^d$.

(ii) they are *simple*, i.e., $x_i \neq x_j$ if $i \neq j$.

Then, a point process Φ is a measurable mapping from the space $(\Omega, \mathcal{F})$ to the space of sequences $(\mathbb{M}, \mathcal{M})$, i.e., $\Phi : (\Omega, \mathcal{F}) \mapsto (\mathbb{M}, \mathcal{M})$. The distribution of Φ on $\mathbb{M}$ is defined as $\mathbb{P}(\Phi \in A) = P\left(\Phi^{-1}(A)\right) = P(\{\omega \in \Omega \mid \Phi(\omega) \in A\})$ for all $A \in \mathcal{M}$. Note that Φ can be seen as a *random closed set* $\Phi = \{x_i\}$, or as a *random counting measure* $\Phi(B) \triangleq \sum_{x_i \in \Phi} \mathbb{1}(x_i \in B)$ for bounded Borel sets $B \subset \mathbb{R}^d$. This thesis focuses on the former notion.

Definition A.2 (PPP [34, 35, 49]). *A point process Φ on $\mathbb{R}^d$ is called a PPP with intensity measure Λ if*

(i) *the number of points falling into any bounded Borel set $B \subset \mathbb{R}^d$ is Poisson distributed with mean $\Lambda(B)$, i.e.,*

$$\mathbb{P}\left(\Phi(B) = k\right) = \frac{\Lambda(B)^k}{k!} \exp\left(-\Lambda(B)\right). \tag{A.8}$$

(ii) *the number of points falling into mutually disjoints Borel sets $B_n \subset \mathbb{R}^d$ are independent random variables, i.e.,*

$$\mathbb{P}\left(\bigcap_n \{\Phi(B_n) = k_n\}\right) = \prod_n \mathbb{P}\left(\Phi(B_n) = k_n\right). \tag{A.9}$$

The intensity measure Λ satisfies the relation $\Lambda(B) = \int_B \lambda(x)\,\mathrm{d}x$, where $\lambda(x)$ is called the *intensity* (function) of the PPP Φ. Note that $\mathbb{E}[\Phi(B)] = \Lambda(B)$. This thesis will be mainly concerned with stationary PPPs, which are introduced next.

Definition A.3 (Stationary PPP [34]). *A PPP Φ is stationary if $\mathbb{P}(\Phi_r \in A) = \mathbb{P}(\Phi \in A)$, for all $A \in \mathcal{M}$, where $\Phi_r = \{x_i + r\}$ and all $r \in \mathbb{R}^d$.*

For a PPP defined on $\mathbb{R}^d$, *stationarity* is equivalent to *homogeneity*, in which case the intensity function becomes location-invariant, i.e., $\lambda(x) = \lambda$ $\forall x \in \mathbb{R}^d$ and hence, $\Lambda(B) = \lambda \int_B \mathrm{d}x = \lambda|B|$ for all Borel sets $B \subset \mathbb{R}^d$.

The PPP has a number of interesting properties, of which two are of particular interest in this thesis.

Lemma A.5 (Independent thinning [35]). *Let Φ be a PPP with intensity measure Λ. Independently retaining each point x of Φ with probability $p(x)$ yields another PPP with intensity measure $\Lambda(B) = \int_B \lambda(x)p(x)\,\mathrm{d}x$.*

Lemma A.6 (Independent superposition [35]). *Let $\{\Phi_k\}$ be a finite collection of independent PPPs on the same space with intensity functions $\{\lambda_k\}$. Then, the superposition $\cup_k \Phi_k$ yields another PPP with intensity function $\lambda(x) = \sum_k \lambda_k(x)$.*

In some cases, the distribution of Φ, *conditioned* on a given point at $x \in \mathbb{R}^d$ without counting it, will be of interest. To make the notion of conditional probability work also for point processes, one has to resort to the reduced Palm distribution $\mathbb{P}_x^!$ of Φ. Here, $\mathbb{P}_x^!(\cdot)$ may be viewed as the conditional probability $\mathbb{P}\left(\Phi \setminus \{x\} \in \cdot \mid x \in \mathbb{R}^d\right)$. The following striking result specializes this concept to PPPs.

Theorem A.1 (Slivnyak's Theorem [34]). *Let Φ be a PPP. Then,*

$$\mathbb{P}_x^!(A) = \mathbb{P}\left(\Phi \in A\right) \tag{A.10}$$

holds for all $A \in \mathcal{M}$ and $x \in \mathbb{R}^d$.

The intuition behind Theorem A.1 is that the presence of a particular point at x does not affect the statistics of the remaining points. This result is in line with property (ii) in Definition A.2.

Taking expectations over sums and products of functions of Φ is another frequently recurring task in this thesis. The following results provide the required tools for this purpose.

Theorem A.2 (Campbell-Mecke Theorem for PPPs [34, 49]). *Let Φ be a PPP with intensity measure Λ and let $f(x, \varphi)$ be any non-negative measurable function on $\mathbb{R}^d \times \mathcal{M}$. Then,*

$$\mathbb{E}\left[\sum_{\mathsf{x}_i \in \Phi} f\left(\mathsf{x}_i, \Phi \setminus \{\mathsf{x}_i\}\right)\right] = \int_{\mathbb{R}^d} \mathbb{E}\left[f(x, \Phi)\right] \lambda(x)\,\mathrm{d}x. \tag{A.11}$$

Note that Theorem A.2 can be stated for general point processes, see for instance [49].

Theorem A.3 (PGFL for PPPs [34, 49]). *Let Φ be a PPP with intensity measure Λ and let $v(x)$ be any non-negative measurable function on $\mathbb{R}^d$. Then,*

$$\mathbb{E}\left[\prod_{\mathsf{x}_i \in \Phi} v(\mathsf{x}_i)\right] = \exp\left(-\int_{\mathbb{R}^d}(1 - v(x))\lambda(x)\,\mathrm{d}x\right). \qquad (\text{A.12})$$

Note that by Slivnyak's theorem, see Theorem A.1, the right-hand side of (A.12) holds for the *conditional* PGFL as well, see for instance [49].

B

Post-Combiner SINR for IA-MRC

In this appendix, the post-combiner SINR for IA-MRC is derived based on the system model introduced in Section 2.3. The derivation covers the $1 \times N$ SIMO case. A corresponding expression for the MIMO case with additional Tx diversity can be found in Chapter 3.

For a given realization of interferer locations $\varphi = \{x_i\}$ and channel fading gains $\{g_{o,n}\}$ and $\{g_{i,n}\}$, the interference-plus-noise corrupted time-discrete baseband signal at the n-th Rx antenna can be expressed as

$$\mathsf{r}_n = h_{o,n}\mathsf{s}_o + y^{\alpha/2} \sum_{x_i \in \varphi} \frac{h_{i,n}}{\|x_i\|^{\alpha/2}}\mathsf{s}_i + \mathsf{w}_n, \tag{B.1}$$

where $\mathsf{s}_o \in \mathbb{C}$ is the desired signal, $\mathsf{s}_i \in \mathbb{C}$ is the signal transmitted by the i-th interferer, and $\mathsf{w}_n \sim \mathcal{CN}(0, 1/\mathtt{SNR})$ is the Rx noise, which is assumed AWGN. The fading gains $h_{o,n}$ follow the relation $h_{o,n} \triangleq \sqrt{g_{o,n}}e^{j\theta_{o,n}}$, where $\theta_{o,n} \in [-\pi, \pi)$ is the phase of $h_{o,n}$. Similarly, $h_{i,n} \triangleq \sqrt{g_{i,n}}e^{j\theta_{i,n}}$ with $\theta_{i,n} \in [-\pi, \pi)$.

Furthermore, within the duration of one transmission slot, the following assumptions are reasonable:

i) $\mathbb{E}[\mathsf{s}_i] = 0$ and $\mathbb{E}[|\mathsf{s}_i|^2] = 1 \ \forall i \in \mathbb{N} \cup \{o\}$, e.g., Phase Shift Keying (PSK).

ii) $\mathbb{E}[\mathsf{s}_i\mathsf{s}_k^*] = 0 \ \forall i \neq k, \ i, k \in \mathbb{N} \cup \{o\}$, i.e., transmitted symbols are independent across transmitters.

iii) $\mathbb{E}[\mathsf{w}_n\mathsf{w}_m^*] = 0 \; \forall m,n \in \{1,\ldots,N\}$. Furthermore, $\mathbb{E}\left[\mathsf{w}_n\mathsf{s}_i^*\right] = 0 \; \forall i \in \mathbb{N} \cup \{o\}$.

Since the receiver is assumed to be interference-aware, it knows not only the instantaneous fading gains $\{h_{o,n}\}$, but also the current interference-plus-noise signal variance (or equivalently, interference-plus-noise power) in one block/frame at Rx antenna n, which is given by

$$
\mathrm{Var}_{\{\mathsf{s}_i\},\mathsf{w}_n}\left[y^{\alpha/2}\sum_{x_i\in\varphi}\frac{h_{i,n}}{\|x_i\|^{\alpha/2}}\mathsf{s}_i + \mathsf{w}_n\right]
$$

$$
= \mathbb{E}_{\{\mathsf{s}_i\},\mathsf{w}_n}\left[\left|y^{\alpha/2}\sum_{x_i\in\varphi}\frac{h_{i,n}}{\|x_i\|^{\alpha/2}}\mathsf{s}_i + \mathsf{w}_n\right|^2\right]
$$

$$
= y^\alpha\sum_{x_i\in\varphi}\frac{g_{i,n}}{\|x_i\|^\alpha}\mathbb{E}[|\mathsf{s}_i|^2] + y^\alpha\sum_{\substack{x_i,x_k\in\varphi \\ i\neq k}}\frac{h_{i,n}h_{k,n}^*\mathbb{E}[\mathsf{s}_i\mathsf{s}_k^*]}{\|x_i\|^{\alpha/2}\|x_k\|^{\alpha/2}}
$$

$$
+ y^{\alpha/2}2\Re\left\{\sum_{x_i\in\varphi}\frac{h_{i,n}}{\|x_i\|^{\alpha/2}}\mathbb{E}[\mathsf{s}_i\mathsf{w}_n^*]\right\} + \mathbb{E}\left[|\mathsf{w}_n|^2\right]
$$

$$
= \underbrace{y^\alpha\sum_{i=1}^{\infty}\frac{g_{i,n}}{\|x_i\|^\alpha}}_{\triangleq\, I_n} + \frac{1}{\mathtt{SNR}}, \qquad (\mathrm{B.2})
$$

where the steps in (B.2) follow from i) – iii) above. Estimating the interference-plus-noise power $I_n + \frac{1}{\mathtt{SNR}}$ can be realized, e.g., using techniques similar to those proposed in [87, 88].

Recall that interference is treated as white noise. Under this assumption, the post-combiner SINR is maximized by IA-MRC. According to [12], the MRC weight a_n for the n-th Rx antenna is then chosen as $a_n = h_{o,n}^*/(I_n + \mathtt{SNR}^{-1})$. The post-combiner SINR then becomes

$$
\mathtt{SINR}_\Sigma = \frac{\mathbb{E}\left[|\mathsf{s}_o|^2\right]\left|\sum_{n=1}^{N}a_n h_{o,n}\right|^2}{\mathrm{Var}\left[\sum_{n=1}^{N}a_n\left(y^{\alpha/2}\sum_{x_i\in\varphi}\frac{h_{i,n}}{\|x_i\|^{\alpha/2}}\mathsf{s}_i + \mathsf{w}_n\right)\right]}. \qquad (\mathrm{B.3})
$$

The numerator in (B.3) can be computed as

$$
\mathbb{E}\left[|\mathsf{s}_o|^2\right]\left|\sum_{n=1}^{N}a_n h_{o,n}\right|^2 = \left(\sum_{n=1}^{N}\frac{g_{o,n}}{I_n + \mathtt{SNR}^{-1}}\right)^2. \qquad (\mathrm{B.4})
$$

Define $\mathbf{i}'_n = \sum_{x_i \in \varphi} h_{i,n} \|x_i\|^{-\alpha/2} \mathbf{s}_i$ for short-hand notation. The denominator in (B.3) then becomes

$$\mathrm{Var}_{\{\mathbf{s}_i\},\{\mathbf{w}_n\}}\left[\sum_{n=1}^{N} a_n\left(y^{\alpha/2}\mathbf{i}'_n + \mathbf{w}_n\right)\right]$$

$$= \sum_{n=1}^{N} \mathrm{Var}_{\{\mathbf{s}_i\},\{\mathbf{w}_n\}}\left[a_n\left(y^{\alpha/2}\mathbf{i}'_n + \mathbf{w}_n\right)\right]$$

$$+ \sum_{\substack{n,m=1 \\ n \neq m}}^{N} \mathrm{Cov}_{\{\mathbf{s}_i\},\{\mathbf{w}_n\}}\left[a_n\left(y^{\alpha/2}\mathbf{i}'_n + \mathbf{w}_n\right), a_m\left(y^{\alpha/2}\mathbf{i}'_m + \mathbf{w}_m\right)\right]$$

$$\overset{(a)}{=} \sum_{n=1}^{N} |a_n|^2(I_n + \mathrm{SNR}^{-1}) + y^\alpha \sum_{\substack{n,m=1 \\ n<m}}^{N} \sum_{x_i \in \varphi} \underbrace{2\Re\left\{a_n a_m^* \frac{h_{i,n} h_{i,m}^*}{\|x_i\|^\alpha}\right\}}_{\triangleq \, Z_{i,nm}}$$

$$= \sum_{n=1}^{N} \frac{g_{o,n}}{I_n + \mathrm{SNR}^{-1}} + y^\alpha \sum_{\substack{n,m=1 \\ n<m}}^{N} \sum_{x_i \in \varphi} Z_{i,nm}, \tag{B.5}$$

where (a) follows from the same line of reasoning as in (B.2). Inserting (B.4) and (B.5) into (B.3) yields

$$\mathrm{SINR}_\Sigma = \frac{\sum_{n=1}^{N} \frac{g_{o,n}}{I_n + \mathrm{SNR}^{-1}}}{1 + \frac{y^\alpha \sum_{n,m=1,n<m}^{N} \sum_{x_i \in \varphi} Z_{i,nm}}{\sum_{n=1}^{N} \frac{g_{o,n}}{I_n + \mathrm{SNR}^{-1}}}}. \tag{B.6}$$

Unfortunately, the mathematical structure in (B.6) is difficult to work with directly due to the covariance terms $\{Z_{i,nm}\}$. However, in NLoS environments with rich scattering, e.g., Rayleigh fading, the channel phases $\{\theta_{i,n}\}$ can be assumed independent across Rx antennas, i.e., $\mathrm{Cov}[\theta_{i,n}, \theta_{i,m}] = 0$ $\forall m,n \in \{1, \ldots, N\}$ and $i \in \mathbb{N} \cup \{o\}$. When the fading channel has a dominant LoS path plus some medium-strong reflections (Nakagami with $m > 1$), this assumption is still reasonable as long as mobility causes the transmitter-receiver geometry to change frequently, see [20, Sec. 7.2.1]. In this case, one has $\mathrm{Cov}[\theta_{i,n}, \theta_{i,m}] = 0$ $\forall n,m \in \{1, \ldots, N\}$ and $i \in \mathbb{N} \cup \{o\}$ and it is easy to verify that the latter then implies $\mathbb{E}_{\theta_{i,n},\theta_{i,m}}[Z_{i,nm}] = 0$ $\forall n,m \in \{1, \ldots, N\}$ and $i \in \mathbb{N} \cup \{o\}$. This means that, if one would average over the channel phases $\{\theta_{i,n}\}$, the covariance terms $\{Z_{i,nm}\}$
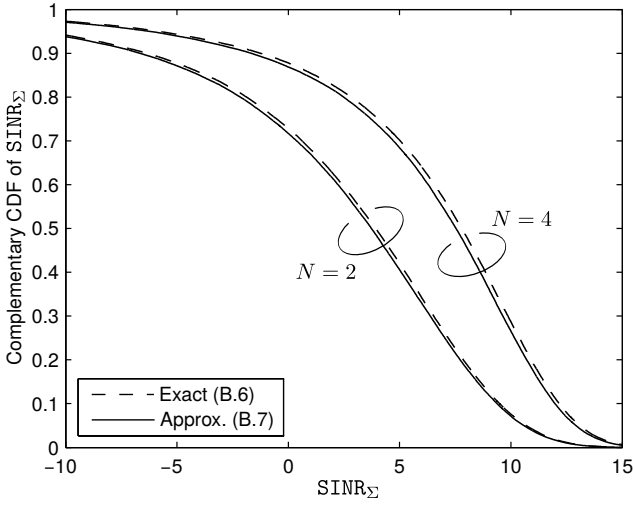
Figure B.1: Simulated complementary CDF of exact and approximate $\mathtt{SINR}_\Sigma$ for different number of Rx antennas N. Parameters: $\lambda = 10^{-3}$, $\alpha = 3.5$, $y = 10$, $\mathtt{SNR} = 7$ dB.

vanish. It is therefore reasonable to ignore the covariance terms and approximate the true post-combiner SINR by the *simplified* expression

$$\mathtt{SINR}_\Sigma = \sum_{n=1}^{N} \frac{g_{o,n}}{I_n + \mathtt{SNR}^{-1}}. \tag{B.7}$$

Obviously, (B.7) is analytically more tractable than (B.6). By Jensen's inequality [81],

$$\mathbb{E}_{\{\theta_{i,n}\}}\left[\mathtt{SINR}_\Sigma\right] = \mathbb{E}_{\{\theta_{i,n}\}}\left[\frac{\sum_{n=1}^{N} \frac{g_{o,n}}{I_n + \mathtt{SNR}^{-1}}}{1 + \frac{y^\alpha \sum_{n,m=1,n<m}^{N} \mathsf{Z}_{i,nm}}{\sum_{n=1}^{N} \frac{g_{o,n}}{I_n + \mathtt{SNR}^{-1}}}}\right]$$

$$\geq \frac{\sum_{n=1}^{N} \frac{g_{o,n}}{I_n + \mathtt{SNR}^{-1}}}{1 + \frac{y^\alpha \sum_{n,m=1,n<m}^{N} \mathbb{E}[\mathsf{Z}_{i,nm}]}{\sum_{n=1}^{N} \frac{g_{o,n}}{I_n + \mathtt{SNR}^{-1}}}}$$

$$= \sum_{n=1}^{N} \frac{g_{o,n}}{I_n + \mathtt{SNR}^{-1}}, \tag{B.8}$$

135

which means that the simple expression in (B.7) tends to underestimate the true post-combiner SINR. The resulting approximation error, however, is barely noticeable as illustrated in Fig. B.1 through detailed simulations assuming the *ad hoc* network model from Chapter 2. The approximation is verified for HCNs with MIMO diversity in Chapter 3.

Acronyms, Abbreviations, and Notation

Acronyms

3GPP	3rd Generation Partnership Project
4G	4th Generation
5G	5th Generation
ASEP	Average Symbol Error Probability
AWGN	Additive White Gaussian Noise
BC	Broadcast
BS	Base Station
CDF	Cumulative Distribution Function
CDMA	Code Division Multiple Access
CoMP	Coordinated Multi-Point
CSI	Channel State Information
CSMA	Carrier Sense Multiple Access
D2D	Device-to-Device
DVRB	Distributed Virtual Resource Block
FC	Full Correlation
FDD	Frequency Division Duplexing
HCN	Heterogeneous Cellular Network

IA	Interference-Aware
IB	Interference-Blind
IEEE	Institute of Electrical and Electronics Engineers
IRC	Interference Rejection Combining
LoS	Line-of-Sight
LTE	Long Term Evolution
MAC	Multiple Access Channel
MIMO	Multiple-Input Multiple-Output
MISO	Multiple-Input Single-Output
MMSE	Minimum Mean Square Error
MRC	Maximal-Ratio Combining
MTC	Machine-Type Communications
NC	No Correlation
NLoS	None-Line-of-Sight
OFDM	Orthogonal Frequency Division Multiplexing
OSTBC	Orthogonal Space-Time Blockcode
PDF	Probability Density Function
PGFL	Probability Generating Functional
PPP	Poisson Point Process
PSK	Phase Shift Keying
RRH	Radio Remote Head
SC	Selection Combining
SDF	Selection Decode-and-Forward
SDO	Spatial Diversity Order
SFBC	Space-Frequency Blockcode
SIMO	Single-Input Multiple-Output
SINR	Signal-to-Interference-plus-Noise Ratio
SIR	Signal-to-Interference Ratio
SISO	Single-Input Single-Output
SNR	Signal-to-Noise Ratio

Abbreviations

e.g.	exempli gratia
i.e.	id est
i.i.d.	independent and identically distributed
Rx	Receive
Tx	Transmit

Notation

In this thesis, random variables are expressed in sans-serif font (z) and their realizations in *italic font* (z). Vectors are denoted by **lower-case bold** symbols ($\mathbf{z}$) and matrices by **upper-case bold** symbols ($\mathbf{Z}$).

$\lvert\,\cdot\,\rvert$	Volume of $\cdot$
$\lVert\cdot\rVert$	Euclidean norm of $\cdot$
$\lVert\cdot\rVert_F$	Frobenius norm of $\cdot$
$(\cdot)^+$	$\max\{0,\cdot\}$
$\mathbf{Z}^H;\mathbf{z}^H$	Hermitian transpose of $\mathbf{Z}$; of $\mathbf{z}$
$\mathbf{Z}^T;\mathbf{z}^T$	Transpose of $\mathbf{Z}$; of $\mathbf{z}$
$B(\cdot,\cdot)$	Beta function
$b(x,r)$	Ball with radius r centered at x
$\mathrm{Cov}[\mathsf{z}_1,\mathsf{z}_1]$	Covariance between z_1 and z_2
$\csc(\cdot)$	Cosecant, i.e., $\csc(\cdot)=1/\sin(\cdot)$
$\Delta_C^{\text{A-B}}$	Relative gain of scheme A over scheme B in terms of C
δ_C^{A}	Relative C-deviation between model A and exact model
δ_{ij}	$\delta_{ij}=1$ if $i=j$ and zero otherwise
$\mathrm{diag}(\cdot)$	Diagonal matrix with diagonal entries $\cdot$
$\mathbb{E}[\mathsf{z}]$	Expected value of z
$f_{\mathsf{z}}(\cdot)$	Probability density function of z
$F_{\mathsf{z}}(\cdot)$	Cumulative distribution function of z
${}_2F_1(\cdot,\cdot,\cdot;\cdot)$	Gaussian hypergeometric function
${}_2\mathbf{F}_1(\cdot,\cdot,\cdot;\cdot)$	Regularized Gaussian hypergeometric function
$\Gamma(\cdot)$	Gamma function
$\Gamma(a,z)$	Upper incomplete Gamma function
$\gamma(a,z)$	Lower incomplete Gamma function
$\mathbf{I}_N$	Identity matrix of dimension $N\times N$
$\mathcal{L}_{\mathsf{z}}(s)$	Laplace transform $\mathbb{E}[e^{-s\mathsf{z}}]$ of z
o	Origin of the plane $\mathbb{R}^2$
$\mathbb{P}(\cdot)$	Probability of event $\cdot$
$T_n(\cdot)$	Chebyshev polynomial of degree n
$U(\cdot,\cdot,\cdot)$	Confluent hypergeometric function (Kummer's U-function)
$\mathrm{Var}[\mathsf{z}]$	Variance of z
$\mathbf{0}_N$	Zero matrix of dimension $N\times N$

Bibliography

[1] Cisco, "Cisco visual networking index: Global mobile data traffic forecast update, 2013–2018," Tech. Rep., 2014.

[2] Qualcomm, "Rising to meet the 1000x mobile data challenge," Tech. Rep., Sep. 2013.

[3] G. Wu *et al.*, "M2M: from mobile to embedded internet," *IEEE Commun. Mag.*, vol. 49, no. 4, pp. 36–43, Apr. 2011.

[4] Ericsson, "Ericsson mobility report," Tech. Rep., Nov. 2014.

[5] J. G. Andrews *et al.*, "What will 5G be?" *IEEE J. Sel. Areas Commun.*, vol. 32, no. 6, pp. 1065–1082, Jun. 2014.

[6] A. Ghosh *et al.*, "Heterogeneous cellular networks: From theory to practice," *IEEE Commun. Mag.*, vol. 50, no. 6, pp. 54–64, Jun. 2012.

[7] K. Doppler *et al.*, "Device-to-device communication as an underlay to LTE-advanced networks," *IEEE Commun. Mag.*, vol. 47, no. 12, pp. 42–49, Dec. 2009.

[8] R. Tanbourgi, H. Jäkel, and F. K. Jondral, "Cooperative interference cancellation using device-to-device communications," *IEEE Commun. Mag.*, vol. 52, no. 6, pp. 118–124, Jun. 2014.

[9] M. Conti and S. Giordano, "Mobile ad hoc networking: milestones, challenges, and new research directions," *IEEE Commun. Mag.*, vol. 52, no. 1, pp. 85–96, Jan. 2014.

[10] GSA. (2015) GSA confirms 360 LTE networks commercially launched by end 2014, strong growth in LTE-Advanced and VoLTE deployments. [Online]. Available: http://www.gsacom.com/news

[11] Z. Pi and F. Khan, "An introduction to millimeter-wave mobile broadband systems," *IEEE Commun. Mag.*, vol. 49, no. 6, pp. 101–107, Jun. 2011.

[12] D. G. Brennan, "Linear diversity combining techniques," *Proceedings of the IRE*, vol. 47, no. 6, pp. 1075–1102, Jun. 1959.

[13] J. H. Winters, "Optimum combining in digital mobile radio with cochannel interference," *IEEE J. Sel. Areas Commun.*, vol. 2, no. 4, pp. 528–539, Jul. 1984.

[14] J. H. Winters, "On the capacity of radio communication systems with diversity in a Rayleigh fading environment," *IEEE J. Sel. Areas Commun.*, vol. 5, no. 5, pp. 871–878, Jun. 1987.

[15] G. J. Foschini, "Layered space-time architecture for wireless communication in a fading environment when using multi-element antennas," *Bell Labs Technical Journal*, vol. 1, no. 2, pp. 41–59, Autumn 1996.

[16] V. Tarokh, H. Jafarkhani, and A. Calderbank, "Space-time block coding for wireless communications: performance results," *IEEE J. Sel. Areas Commun.*, vol. 17, no. 3, pp. 451–460, Mar. 1999.

[17] V. Tarokh, H. Jafarkhani, and A. Calderbank, "Space-time block codes from orthogonal designs," *IEEE Trans. Inf. Theory*, vol. 45, no. 5, pp. 1456–1467, Jul. 1999.

[18] E. Telatar, "Capacity of multi-antenna Gaussian channels," *European Transactions on Telecommunications*, vol. 10, no. 6, pp. 585–595, 1999.

[19] A. Goldsmith, *Wireless Communications*. Cambridge University Press, 2005.

[20] D. Tse and P. Viswanath, *Fundamentals of Wireless Communication.* Cambridge University Press, 2005.

[21] A. Paulraj, R. Nabar, and D. Gore, *Introduction to Space-Time Wireless Communications*, 1st ed. Cambridge University Press, 2003.

[22] M. K. Simon and M.-S. Alouini, *Digital Communication over Fading Channels*, 2nd ed., ser. Wiley series in telecommunications and signal processing. Wiley-Interscience, 2005.

[23] T. Sälzer *et al.*, "Multiple antenna techniques," in *LTE - The UMTS Long Term Evolution: From Theory to Practice*, 2nd ed., S. Sesia, I. Toufik, and M. Baker, Eds. Wiley, Sep. 2011.

[24] J. Andrews, "Interference cancellation for cellular systems: a contemporary overview," *IEEE Wireless Commun.*, vol. 12, no. 2, pp. 19–29, Apr. 2005.

[25] L. Thiele, M. Schellmann, T. Wirth, and V. Jungnickel, "On the value of synchronous downlink MIMO-OFDMA systems with linear equalizers," in *IEEE International Symposium on Wireless Communication Systems*, Oct. 2008, pp. 428–432.

[26] V. H. Mac Donald, "Advanced mobile phone service: The cellular concept," *Bell System Technical Journal, The*, vol. 58, no. 1, pp. 15–41, Jan. 1979.

[27] T. S. Rappaport, *Wireless Communications: Principles and Practice*, 1st ed. IEEE Press, 1996.

[28] Cisco, "White paper: Cisco clientlink: Optimized device performance with 802.11n," Tech. Rep., May 2009.

[29] Qualcomm, "AR9462: single-chip, 2.4/5 GHz, 2-stream 802.11a/b/g/n and BT 4.0 + HS SoC solution with SST technology," Tech. Rep., 2013.

[30] J. Cui and A. U. H. Sheikh, "Outage probability of cellular radio systems using maximal ratio combining in the presence of multiple interferers," *IEEE Trans. Commun.*, vol. 47, no. 8, pp. 1121–1124, Aug. 1999.

[31] V. A. Aalo and C. Chayawan, "Outage probability of cellular radio systems using maximal ratio combining in Rayleigh fading channel with multiple interferers," *Electronics Lett.*, vol. 36, no. 15, pp. 1314–1315, Jul. 2000.

[32] X. Cui, Q. Zhang, and Z. Feng, "Outage performance for maximal ratio combiner in the presence of unequal-power co-channel interferers," *IEEE Commun. Lett.*, vol. 8, no. 5, pp. 289–291, May 2004.

[33] Renesas Mobile Europe Ltd., "Link level performance evaluation of MMSE-IRC receiver," *3GPP TSG-RAN WG4 Meeting #62*, Feb. 2012.

[34] D. Stoyan, W. Kendall, and J. Mecke, *Stochastic Geometry and its Applications*, 2nd ed.   Wiley, 1995.

[35] F. Baccelli and B. Błaszczyszyn, "Stochastic geometry and wireless networks, Volume 1: Theory," *Foundations and Trends in Networking*, vol. 3, no. 3-4, pp. 249–449, Jan. 2010.

[36] F. Baccelli and B. Błaszczyszyn, "Stochastic geometry and wireless networks, Volume 2: Applications," *Foundations and Trends in Networking*, vol. 4, no. 1-2, pp. 1–312, Jan. 2010.

[37] J. G. Andrews *et al.*, "A primer on spatial modeling and analysis in wireless networks," *IEEE Commun. Mag.*, vol. 48, no. 11, pp. 156 –163, Nov. 2010.

[38] M. Haenggi, *Stochastic Geometry for Wireless Networks.*   Cambridge University Press, 2012.

[39] J. G. Andrews, F. Baccelli, and R. K. Ganti, "A tractable approach to coverage and rate in cellular networks," *IEEE Trans. Commun.*, vol. 59, no. 11, pp. 3122 –3134, Nov. 2011.

[40] V. A. Aalo, "Performance of maximal-ratio diversity systems in a correlated Nakagami-fading environment," *IEEE Trans. Commun.*, vol. 43, no. 8, pp. 2360–2369, Aug. 1995.

[41] C. S. R. Murthy and B. S. Manoj, *Ad Hoc Wireless Networks: Architectures and Protocols.*   Prentice Hall Communications Engineering and Emerging Technologies Series, 2004.

[42] S. Weber, J. G. Andrews, and N. Jindal, "An overview of the transmission capacity of wireless networks," *IEEE Trans. Wireless Commun.*, vol. 58, no. 12, pp. 3593 –3604, Dec. 2010.

[43] C. Biao and M. J. Gans, "MIMO communications in ad hoc networks," *IEEE Trans. Signal Process.*, vol. 54, no. 7, pp. 2773–2783, Jul. 2006.

[44] N. Jindal, J. G. Andrews, and S. Weber, "Multi-antenna communication in ad hoc networks: Achieving MIMO gains with SIMO transmission," *IEEE Trans. Commun.*, vol. 59, no. 2, pp. 529–540, Feb. 2011.

[45] S. W. Halpern, "The effect of having unequal branch gains practical predetection diversity systems for mobile radio," *IEEE Trans. Veh. Technol.*, vol. 26, no. 1, pp. 94–105, Feb. 1977.

[46] S. Weber and J. G. Andrews, "Transmission capacity of wireless networks," *Foundations and Trends in Networking*, vol. 5, no. 2-3, pp. 109–281, Jan. 2012.

[47] Z. Sheng, Z. Ding, and K. Leung, "Transmission capacity of decode-and-forward cooperation in overlaid wireless networks," in *IEEE Intl. Conf. on Commun. (ICC)*, May 2010.

[48] A. Rajan and C. Tepedelenlioglu, "Diversity combining over Rayleigh fading channels with symmetric alpha-stable noise," *IEEE Trans. Wireless Commun.*, vol. 9, no. 9, pp. 2968–2976, Sep. 2010.

[49] M. Haenggi and R. K. Ganti, "Interference in large wireless networks," *Foundations and Trends in Networking*, vol. 3, pp. 127–248, Feb. 2009.

[50] A. M. Hunter, J. G. Andrews, and S. Weber, "Transmission capacity of ad hoc networks with spatial diversity," *IEEE Trans. Wireless Commun.*, vol. 7, no. 12, pp. 5058–5071, Dec. 2008.

[51] A. Chopra, "Modeling and mitigation of interference in wireless receivers with multiple antennae," Ph.D. dissertation, The University of Texas at Austin, Dec. 2011.

[52] A. Chopra and B. L. Evans, "Joint statistics of radio frequency interference in multiantenna receivers," *IEEE Trans. Signal Process.*, vol. 60, no. 7, pp. 3588–3603, Jul. 2012.

[53] R. K. Ganti and M. Haenggi, "Spatial and temporal correlation of the interference in Aloha ad hoc networks," *IEEE Commun. Lett.*, vol. 13, no. 9, pp. 631–633, Sep. 2009.

[54] M. Haenggi and R. Smarandache, "Diversity polynomials for the analysis of temporal correlations in wireless networks," *IEEE Trans. Wireless Commun.*, vol. 12, no. 11, pp. 5940–5951, Nov. 2013.

[55] M. Haenggi, "Diversity loss due to interference correlation," *IEEE Commun. Lett.*, vol. 16, no. 10, pp. 1600–1603, Oct. 2012.

[56] A. Crismani *et al.*, "Cooperative relaying under spatially and temporally correlated interference," *IEEE Trans. Veh. Technol.*, vol. PP, no. 99, pp. 1–1, 2014.

[57] X. Zhang and N. C. Beaulieu, "Explicit analytical expressions for outage and error rate of diversity cellular systems in the presence of multiple interferers and correlated Rayleigh fading," *IEEE Trans. Commun.*, vol. 55, no. 12, pp. 2303–2315, Dec. 2007.

[58] K.-S. Ahn and R. W. Heath Jr., "Performance analysis of maximum ratio combining with imperfect channel estimation in the presence of cochannel interferences," *IEEE Trans. Wireless Commun.*, vol. 8, no. 3, pp. 1080–1085, Mar. 2009.

[59] M. Di Renzo *et al.*, "Error performance of multi-antenna receivers in a Poisson field of interferers: A stochastic geometry approach," *IEEE Trans. Commun.*, vol. 61, no. 5, pp. 2025–2047, May 2013.

[60] A. Chopra and B. L. Evans, "Outage probability for diversity combining in interference-limited channels," *IEEE Trans. Wireless Commun.*, vol. 12, no. 2, pp. 550–560, Feb. 2013.

[61] B. Błaszczyszyn and M. K. Karray, "Linear-regression estimation of the propagation-loss parameters using mobiles' measurements in wireless cellular network," in *International Symposium on Modeling and Optimization in Mobile, Ad Hoc and Wireless Networks (WiOpt)*, 2012.

[62] H. P. Keeler, B. Błaszczyszyn, and M. K. Karray, "SINR-based k-coverage probability in cellular networks with arbitrary shadowing," in *IEEE Intl. Symposium on Information Theory (ISIT)*, Jul. 2013.

[63] H. S. Dhillon and J. G. Andrews, "Downlink rate distribution in heterogeneous cellular networks under generalized cell selection," *IEEE Wireless Commun. Lett.*, vol. 3, no. 1, pp. 42–45, Feb. 2014.

[64] R. Tanbourgi, S. Singh, J. G. Andrews, and F. K. Jondral, "A tractable model for non-coherent joint transmission base station cooperation," *IEEE Trans. Wireless Commun.*, vol. 13, no. 9, pp. 4959–4973, Sep. 2014.

[65] R. Tanbourgi, S. Singh, J. G. Andrews, and F. K. Jondral, "Analysis of non-coherent joint-transmission cooperation in heterogeneous cellular networks," in *IEEE Intl. Conf. on Commun. (ICC)*, Jun. 2014.

[66] F. W. Olver, D. W. Lozier, R. F. Boisvert, and C. W. Clark, *NIST Handbook of Mathematical Functions*, 1st ed. Cambridge University Press, 2010.

[67] M. Abramowitz and I. A. Stegun, *Handbook of Mathematical Functions with Formulas, Graphs, and Mathematical Tables.* Dover Publications, Inc., 1964.

[68] Wolfram. Gauss Hypergeometric Function. [Online]. Available: http://functions.wolfram.com/HypergeometricFunctions/Hypergeometric2F1/

[69] R. K. Ganti, J. G. Andrews, and M. Haenggi, "High-SIR transmission capacity of wireless networks with general fading and node distribution," *IEEE Trans. Inf. Theory*, vol. 57, no. 5, pp. 3100–3116, May 2011.

[70] D. B. H. Cline and G. Samorodnitsky, "Subexponentiality of the product of independent random variables," *Stochastic Processes and their Applications*, vol. 49, no. 1, pp. 75 – 98, 1994.

[71] S. Foss, D. Korshunov, and S. Zachary, *An Introduction to Heavy-Tailed and Subexponential Distributions*, 2nd ed., ser. Springer Series in Operations Research and Financial Engineering. Springer, 2013.

[72] F. di Bruno, "Note sur un nouvelle formule de calcul differentiel," in *Quarterly Journal of Pure and Applied Mathematics 1*, 1857.

[73] W. P. Johnson, "The curious history of Faà di Bruno's formula," available online: http://www.maa.org/news/monthly217-234.pdf.

[74] V. F. Ivanoff, "Problem 4782," *Amer. Math. Monthly*, vol. 65, 1958.

[75] W. H. Press, S. A. Teukolsky, W. T. Vetterling, and B. P. Flannery, Eds., *Numerical Recipes : The Art of Scientific Computing*, 3rd ed. Cambridge University Press, 2007.

[76] S. Lin and D. J. Costello, *Error Control Coding*, 2nd ed. Prentice-Hall, Inc., 2004.

[77] T. Richardson and R. Urbanke, *Modern Coding Theory*. Cambridge University Press, 2008.

[78] F. Baccelli, B. Błaszczyszyn, and P. Muhlethaler, "An Aloha protocol for multihop mobile wireless networks," *IEEE Trans. Inf. Theory*, vol. 52, no. 2, pp. 421–436, Feb. 2006.

[79] O. Ali, C. Cardinal, and F. Gagnon, "Performance of optimum combining in a Poisson field of interferers and Rayleigh fading channels," *IEEE Trans. Wireless Commun.*, vol. 9, no. 8, pp. 2461–2467, Aug. 2010.

[80] W. Feller, *An Introduction to Probability Theory and its Applications*, 2nd ed. Wiley, 1971, vol. 2.

[81] A. Gut, *Probability: A Graduate Course*, ser. Springer texts in statistics. Springer, 2005.

[82] C. A. Coelho and J. T. Mexia, "On the distribution of the product and ratio of independent generalized gamma-ratio random variables," *Sankhya : The Indian Journal of Statistics*, vol. 69, no. 2, pp. 221–255, 2007.

[83] D. Gesbert *et al.*, "Shifting the MIMO paradigm," *IEEE Signal Process. Mag.*, vol. 24, no. 5, pp. 36–46, Sep. 2007.

[84] Q. H. Spencer, C. B. Peel, A. L. Swindlehurst, and M. Haardt, "An introduction to the multi-user MIMO downlink," *IEEE Commun. Mag.*, vol. 42, no. 10, pp. 60–67, Oct. 2004.

[85] 3GPP, "Further advancements for E-UTRA," TR 36.213, Tech. Rep., Mar. 2008.

[86] A. Ghosh, J. Zhang, J. G. Andrews, and R. Muhamed, *Fundamentals of LTE*, 1st ed. Prentice Hall Press, 2010.

[87] T. Benedict and T. Soong, "The joint estimation of signal and noise from the sum envelope," *IEEE Trans. Inf. Theory*, vol. 13, no. 3, pp. 447–454, Jul. 1967.

[88] D. R. Pauluzzi and N. C. Beaulieu, "A comparison of SNR estimation techniques for the AWGN channel," *IEEE Trans. Commun.*, vol. 48, no. 10, pp. 1681–1691, Oct. 2000.

[89] H.-S. Jo, Y. J. Sang, P. Xia, and J. G. Andrews, "Heterogeneous cellular networks with flexible cell association: A comprehensive downlink SINR analysis," *IEEE Trans. Wireless Commun.*, vol. 11, no. 10, pp. 3484–3495, Oct. 2012.

[90] H. S. Dhillon, R. K. Ganti, F. Baccelli, and J. G. Andrews, "Modeling and analysis of K-tier downlink heterogeneous cellular networks," *IEEE J. Sel. Areas Commun.*, vol. 30, no. 3, pp. 550–560, Apr. 2012.

[91] M. Di Renzo and P. Guan, "A mathematical framework to the computation of the error probability of downlink MIMO cellular networks by using stochastic geometry," *IEEE Trans. Commun.*, vol. 62, no. 8, pp. 2860–2879, Aug. 2014.

[92] M. Di Renzo and W. Lu, "Stochastic geometry modeling and performance evaluation of MIMO cellular networks by using the Equivalent-in-Distribution (EiD)-based approach," *IEEE Trans. Commun.*, vol. 63, no. 3, pp. 977–996, Mar. 2015.

[93] C. Li, J. Zhang, and K. Letaief, "Throughput and energy efficiency analysis of small cell networks with multi-antenna base stations," vol. 13, no. 5, pp. 2505–2517, May 2014.

[94] H. S. Dhillon, M. Kountouris, and J. G. Andrews, "Downlink MIMO hetnets: Modeling, ordering results and performance analysis," *IEEE Trans. Wireless Commun.*, vol. 12, no. 10, pp. 5208–5222, Oct. 2013.

[95] A. K. Gupta, H. S. Dhillon, S. Vishwanath, and J. G. Andrews, "Downlink multi-antenna heterogeneous cellular network with load balancing," *IEEE Trans. Commun.*, vol. 62, no. 11, pp. 4052–4067, Nov. 2014.

[96] A. Shah and A. Haimovich, "Performance analysis of maximal ratio combining and comparison with optimum combining for mobile radio communications with cochannel interference," *IEEE Trans. Veh. Technol.*, vol. 49, no. 4, pp. 1454–1463, Jul 2000.

[97] E. G. Larsson and P. Stoica, *Space-Time Block Coding for Wireless Communications*, 1st ed.   Cambridge University Press, 2008.

[98] H. El Gamal and A. Hammons, "On the design of algebraic space-time codes for MIMO block-fading channels," *IEEE Trans. Inf. Theory*, vol. 49, no. 1, pp. 151–163, Jan. 2003.

[99] 3GPP, "Further advancements for E-UTRA," TR 36.814, Tech. Rep., Mar. 2009.

[100] B. Hochwald, T. Marzetta, and V. Tarokh, "Multiple-antenna channel hardening and its implications for rate feedback and scheduling," *IEEE Trans. Inf. Theory*, vol. 50, no. 9, pp. 1893–1909, Sep. 2004.

[101] Y. Shang, "Space-time code designs and fast decoding for MIMO and cooperative communication systems," Ph.D. dissertation, University of Delaware, 2008.

[102] C. E. Shannon, "Communication in the presence of noise," *Proceedings of the IRE*, vol. 37, no. 1, pp. 10–21, Jan 1949.

[103] X. Zhang and M. Haenggi, "A stochastic geometry analysis of inter-cell interference coordination and intra-cell diversity," *IEEE Trans. Wireless Commun.*, vol. 13, no. 12, pp. 6655–6669, Dec. 2014.

[104] C. Hoymann *et al.*, "Relaying operation in 3GPP LTE: Challenges and solutions," *IEEE Commun. Mag.*, vol. 50, no. 2, pp. 156 –162, Feb. 2012.

[105] T. Cover and A. E. Gamal, "Capacity theorems for the relay channel," *IEEE Trans. Inf. Theory*, vol. 25, no. 5, pp. 572 – 584, Sep. 1979.

[106] R. K. Ganti and M. Haenggi, "Spatial analysis of opportunistic downlink relaying in a two-hop cellular system," *IEEE Trans. Commun.*, vol. 60, no. 5, pp. 1443–1450, 2012.

[107] A. Altieri, L. R. Vega, P. Piantanida, and C. G. Galarza, "Analysis of a cooperative strategy for a large decentralized wireless network," *IEEE/ACM Trans. Netw.*, vol. 22, no. 4, pp. 1039–1051, Aug. 2014.

[108] J. Laneman, D. Tse, and G. Wornell, "Cooperative diversity in wireless networks: Efficient protocols and outage behavior," *IEEE Trans. Inf. Theory*, vol. 50, no. 12, pp. 3062 – 3080, Dec. 2004.

[109] J. G. Andrews, "Seven ways that HetNets are a cellular paradigm shift," *IEEE Commun. Mag.*, vol. 51, no. 3, pp. 136–144, Mar. 2013.

[110] M. Sawahashi *et al.*, "Coordinated multipoint transmission/reception techniques for LTE-advanced [coordinated and distributed MIMO]," *IEEE Wireless Commun.*, vol. 17, no. 3, pp. 26–34, Jun. 2010.

[111] D. Lee *et al.*, "Coordinated multipoint transmission and reception in LTE-advanced: deployment scenarios and operational challenges," *IEEE Commun. Mag.*, vol. 50, no. 2, pp. 148–155, Feb. 2012.

[112] S. Weber, X. Yang, J. G. Andrews, and G. de Veciana, "Transmission capacity of wireless ad hoc networks with outage constraints," *IEEE Trans. Inf. Theory*, vol. 51, no. 12, pp. 4091–4102, Dec. 2005.

[113] J. G. Andrews, S. Weber, and M. Haenggi, "Ad hoc networks: To spread or not to spread? [ad hoc and sensor networks]," *IEEE Commun. Mag.*, vol. 45, no. 12, pp. 84–91, Dec. 2007.

[114] J. Montojo and J. Damnjanovic, "Carrier aggregation," in *LTE - The UMTS Long Term Evolution: From Theory to Practice*, 2nd ed., S. Sesia, I. Toufik, and M. Baker, Eds.   Wiley, Sep. 2011.

[115] S. Singh, H. S. Dhillon, and J. G. Andrews, "Offloading in heterogeneous networks: Modeling, analysis, and design insights," *IEEE Trans. Wireless Commun.*, vol. 12, no. 5, pp. 2484–2497, Dec. 2013.

[116] X. Lin, J. G. Andrews, and A. Ghosh, "Modeling, analysis and design for carrier aggregation in heterogeneous cellular networks," *IEEE Trans. Commun.*, vol. 61, no. 9, pp. 4002–4015, Sep. 2013.

[117] G. D. Forney Jr. and G. Ungerboeck, "Modulation and coding for linear gaussian channels," *IEEE Trans. Inf. Theory*, vol. 44, no. 6, pp. 2384–2415, Oct. 1998.

[118] A. M. Hunter, R. K. Ganti, and J. G. Andrews, "Transmission capacity of multi-antenna ad hoc networks with CSMA," in *Asilomar Conf. on Signals, Systems and Computers (ASILOMAR)*, Nov. 2010.

[119] R. Tanbourgi, J. P. Elsner, H. Jäkel, and F. K. Jondral, "Adaptive frequency hopping in ad hoc networks with Rayleigh fading and imperfect sensing," *IEEE Wireless Commun. Lett.*, vol. 1, no. 3, pp. 185–188, Jun. 2012.

[120] H. ElSawy and E. Hossain, "A modified hard core point process for analysis of random CSMA wireless networks in general fading environments," *IEEE Trans. Commun.*, vol. 61, no. 4, pp. 1520–1534, Apr. 2013.

[121] Y. Li, F. Baccelli, H. Dhillon, and J. Andrews, "Fitting determinantal point processes to macro base station deployments," in *IEEE Global Communications Conference (GLOBECOM)*, Dec. 2014, pp. 3641–3646.

[122] N. Deng, W. Zhou, and M. Haenggi, "The Ginibre point process as a model for wireless networks with repulsion," vol. 14, no. 1, pp. 107–121, Jan 2015.

[123] W. Feller, *An Introduction to Probability Theory and its Applications*, 3rd ed., ser. Wiley series in probability and mathematical statistics.   Wiley, 1968, vol. 1.

[124] S. J. Wolfe, "On moments of probability distribution functions," in *Fractional Calculus and Its Applications*, ser. Lecture Notes in Mathematics, B. Ross, Ed.   Springer, 1975, vol. 457, pp. 306–316.

Index

Related Publications

This thesis contains material from the following publications [T1-T6, T8], ©2013-2015 IEEE. Reprinted, with permission.

This thesis contains material that will appear in publication [T7].

[T1] R. Tanbourgi, H. S. Dhillon, J. G. Andrews, and F. K. Jondral, "Effect of spatial interference correlation on the performance of maximum ratio combining," *IEEE Trans. Wireless Commun.*, vol. 13, no. 6, pp. 3307–3316, Jun. 2014.

[T2] R. Tanbourgi, H. S. Dhillon, J. G. Andrews, and F. K. Jondral, "Dual-branch MRC receivers under spatial interference correlation and Nakagami fading," *IEEE Trans. Commun.*, vol. 62, no. 6, pp. 1830–1844, Jun. 2014.

[T3] R. Tanbourgi, H. S. Dhillon, J. G. Andrews, and F. K. Jondral, "Dual-branch MRC receivers in the cellular downlink under spatial interference correlation," in *20th European Wireless Conference*, May 2014, **(Invited, Best Student Paper)**.

[T4] R. Tanbourgi and F. K. Jondral, "Downlink MIMO diversity with maximal-ratio combining in heterogeneous cellular networks," in *IEEE International Conference on Commun. (ICC)*, 2015.

[T5] R. Tanbourgi, H. S. Dhillon, and F. K. Jondral, "Analysis of joint transmit-receive diversity in downlink MIMO heterogeneous cellular networks," *IEEE Trans. Wireless Commun.*, to appear.

[T6] R. Tanbourgi, H. Jäkel, and F. K. Jondral, "Cooperative relaying in a Poisson field of interferers: A diversity order analysis," in *IEEE International Symposium on Information Theory (ISIT)*, Jul. 2013.

[T7] R. Tanbourgi, H. Jäkel, and F. K. Jondral, "Cooperative diversity under spatial interference correlation in wireless networks," in *Signals and Communication Technology*. Springer, 2015.

[T8] R. Tanbourgi and F. K. Jondral, "Analysis of heterogeneous cellular networks under frequency diversity and interference correlation," *IEEE Wireless Commun. Lett.*, vol. 4, no. 1, pp. 2–5, Feb. 2015.

Sponsorship

Biography

Ralph Tanbourgi (* September 11, 1983) received a Diploma degree (Dipl.-Ing.) in Electrical Engineering from the Karlsruhe Institute of Technology (KIT), Germany, in 2010. Since 2010, he has been a research associate with the Communications Engineering Lab, KIT. He has held a research intern at the German Aerospace Center (DLR) in Oberpfaffenhofen, Germany, in 2010, and was a visiting researcher to the Wireless Networking and Communications Group (WNCG), The University of Texas at Austin, TX, USA, in 2013.

Ralph Tanbourgi received the EADS Argus Award in 2009 and the European Wireless Conference Best Student Paper Award 2014. His research interests include cooperative and heterogeneous cellular networks, device-to-device communications, multi-antenna communications, and stochastic geometry. He is an IEEE Student Member and a VDE Member.